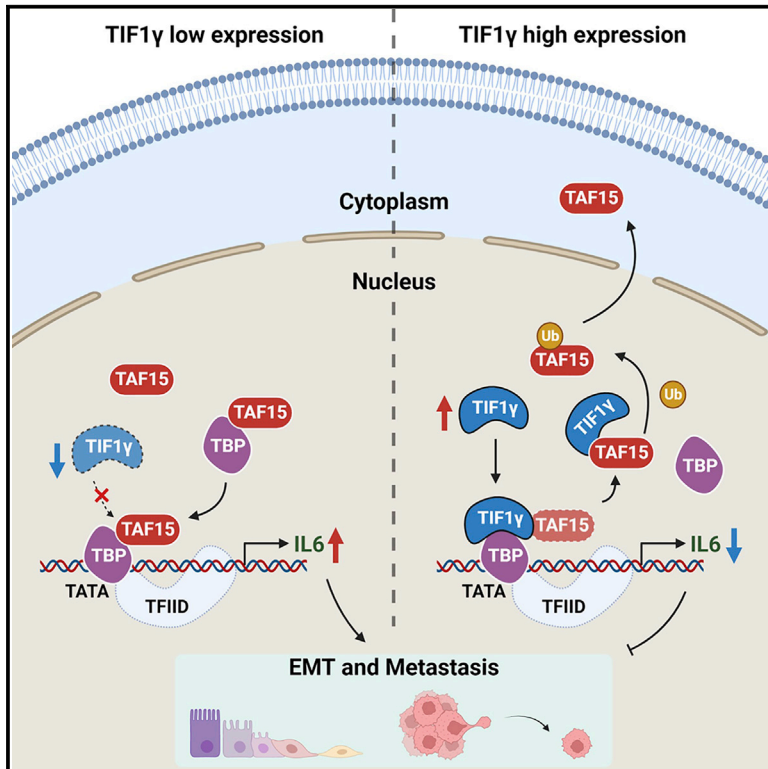


# TIF1 $\gamma$ inhibits lung adenocarcinoma EMT and metastasis by interacting with the TAF15/TBP complex

## Graphical abstract



## Authors

Zhiyue Su, Zelong Sun, Zhao Wang, ..., Xia Liu, Zhe Lei, Hong-Tao Zhang

## Correspondence

leizhe@suda.edu.cn (Z.L.),  
htzhang@suda.edu.cn (H.-T.Z.)

## In brief

Su et al. demonstrate that TIF1 $\gamma$  inhibits EMT and metastasis of LUAD cells by interfering with TAF15/TBP-mediated IL-6 transactivation. TIF1 $\gamma$  binds to TBP in competition with TAF15 via its M-containing domains. TIF1 $\gamma$  multi-mono-ubiquitylates TAF15 through its RBCC domain and drives TAF15 nuclear export.

## Highlights

- TIF1 $\gamma$  inhibits TAF15-promoted EMT and metastasis in LUAD
- TIF1 $\gamma$  competes with TAF15 for interacting with TBP
- TIF1 $\gamma$  multi-mono-ubiquitylates TAF15 and promotes nuclear export of TAF15
- TIF1 $\gamma$  impedes TAF15/TBP complex-dependent IL-6 transcription initiation



## Article

# TIF1 $\gamma$ inhibits lung adenocarcinoma EMT and metastasis by interacting with the TAF15/TBP complex

Zhiyue Su,<sup>1,2,8</sup> Zelong Sun,<sup>1,2,8</sup> Zhao Wang,<sup>1,2,8</sup> Shengjie Wang,<sup>3,8</sup> Yuxin Wang,<sup>1,2</sup> Ersuo Jin,<sup>1,2</sup> Chang Li,<sup>4</sup> Jun Zhao,<sup>4</sup> Zeyi Liu,<sup>5</sup> Zhengyu Zhou,<sup>6</sup> Yong Wang,<sup>1,2</sup> Xiaoyan Chen,<sup>1,2</sup> Xia Liu,<sup>1,2</sup> Zhe Lei,<sup>1,2,\*</sup> and Hong-Tao Zhang<sup>1,2,7,9,\*</sup>

<sup>1</sup>Soochow University Laboratory of Cancer Molecular Genetics, Suzhou Medical College of Soochow University, Suzhou, Jiangsu 215123, China

<sup>2</sup>Department of Genetics, School of Biology and Basic Medical Sciences, Suzhou Medical College of Soochow University, Suzhou, Jiangsu 215123, China

<sup>3</sup>Department of Basic Medicine, Kangda College of Nanjing Medical University, Lianyungang 222000, China

<sup>4</sup>Department of Thoracic Surgery, First Affiliated Hospital of Soochow University, Suzhou Medical College of Soochow University, Suzhou, Jiangsu 215006, China

<sup>5</sup>Department of Pulmonary and Critical Care Medicine, First Affiliated Hospital of Soochow University, Suzhou Medical College of Soochow University, Suzhou, Jiangsu 215006, China

<sup>6</sup>Laboratory Animal Center, Suzhou Medical College of Soochow University, Suzhou, Jiangsu 215123, China

<sup>7</sup>Suzhou Key Laboratory for Molecular Cancer Genetics, Suzhou, Jiangsu 215123, China

<sup>8</sup>These authors contributed equally

<sup>9</sup>Lead contact

\*Correspondence: [leizhe@suda.edu.cn](mailto:leizhe@suda.edu.cn) (Z.L.), [htzhang@suda.edu.cn](mailto:htzhang@suda.edu.cn) (H.-T.Z.)

<https://doi.org/10.1016/j.celrep.2022.111513>

## SUMMARY

The molecular underpinnings of lung adenocarcinoma (LUAD) metastasis remain poorly defined. Here, using human LUAD cell lines, we find that transcriptional intermediary factor 1  $\gamma$  (TIF1 $\gamma$ ) binds to TATA box binding protein (TBP) in competition with TBP-associated factor 15 (TAF15) and impedes TAF15/TBP-mediated interleukin 6 (IL-6) transactivation. TIF1 $\gamma$  modifies TAF15 through multi-mono-ubiquitylation and drives nuclear export of TAF15. Functionally, TAF15 accelerates epithelial-mesenchymal transition (EMT) and metastasis of LUAD cells, acting in just the opposite way as TIF1 $\gamma$ . Low TIF1 $\gamma$  or high TAF15 expression levels are shown in metastatic LUAD specimens and correlate with poor survival of individuals with LUAD. Our findings suggest that the TAF15/TBP complex is required for IL-6 activation-induced EMT and invasion, which are inhibited by TIF1 $\gamma$ . This study highlights the crucial interaction between TIF1 $\gamma$  and the TAF15/TBP complex for regulating EMT and metastasis in LUAD.

## INTRODUCTION

Lung cancer is the leading cause of cancer mortality globally, and the proportion of individuals with non-small cell lung cancer (NSCLC) in all lung cancer cases is approximately 85% (Chen et al., 2016; Siegel et al., 2016). Lung adenocarcinoma (LUAD) represents the largest subtype of NSCLC and has the most aggressive features (Kuhn et al., 2018). Despite introduction of new medical treatments in recent years, the prognosis of individuals with LUAD remains poor. This is mainly due to the high metastasis potential of cancer cells (Gupta and Massague, 2006). Therefore, it is of great urgency to decipher the specific mechanisms behind metastasis of LUAD.

Epithelial-mesenchymal transition (EMT) is a cellular biological process that triggers polarized and immotile epithelial cells to acquire a mesenchymal cell phenotype, playing a critical role in embryogenesis, wound healing, and tumor metastasis. There is extensive evidence that EMT is related to tumor cell migration

and invasion, affecting tumor metastasis (Chaffer et al., 2016; Nieto et al., 2016; Williams et al., 2019). Besides cell morphology changes in EMT, epithelial cells undergo alterations of multiple molecules, including downregulation of epithelial markers (e.g., E-cadherin) and upregulation of mesenchymal markers (e.g., N-cadherin), leading them to differentiate into mesenchymal cells (Babaei et al., 2021). Abnormal changes in the stability, sub-cellular localization, post-translational modification, and functionality of EMT-associated transcription factors are the driving forces of EMT in tumor cells (De Craene and Berx, 2013).

Transcriptional intermediary factor 1  $\gamma$  (TIF1 $\gamma$ ), also known as TRIM33/Ectoderm, is a member of the TIF1 family, which mainly comprises three proteins: TIF1 $\alpha$ /TRIM24, TIF1 $\beta$ /TRIM28, and TIF1 $\gamma$ /TRIM33. TIF1 $\gamma$  structurally resembles other TIF1 members that share an N-terminal RING finger-B box-coiled-coil (RBCC) domain (Venturini et al., 1999), and this domain endows them with E3 ubiquitin ligase function (McAvera and Crawford, 2020). TIF1 $\gamma$  may inhibit transcription by interacting



with molecular partners (Venturini et al., 1999). TIF1 $\gamma$  has been reported to regulate transforming growth factor  $\beta$  receptor 1 (TGF- $\beta$ R1), SMAD4, and  $\beta$ -catenin through ubiquitylation (Dupont et al., 2009; Quere et al., 2014; Xue et al., 2015). TIF1 $\gamma$  expression is frequently reduced in human glioblastoma, NSCLC, pancreatic cancer, hepatocellular carcinoma, and clear renal cell carcinoma (Ding et al., 2014; Vincent et al., 2009; Wang et al., 2016, 2018; Xu et al., 2020; Xue et al., 2015). Recently, we have demonstrated that repression of TIF1 $\gamma$  by SOX2 overexpression or circPTK2 knockdown promotes TGF- $\beta$ -induced EMT and invasion of NSCLC cells (Wang et al., 2016, 2018). In fact, more attention has been paid to the role of TIF1 $\gamma$  in TGF- $\beta$ /SMAD signaling-mediated EMT and tumor cell invasiveness (Jingushi et al., 2015; Ligr et al., 2014; Wang et al., 2016; Xue et al., 2014). TIF1 $\gamma$  has been shown to regulate TGF- $\beta$ /SMAD signaling by monoubiquitinating or competing with SMAD4 to undermine formation of R-SMAD/SMAD4 transcriptional complexes (Dupont et al., 2009; He et al., 2006; Xue et al., 2014). However, to date, there are very few mechanisms other than the ones mentioned above to explain how TIF1 $\gamma$  regulates EMT and metastasis independent of TGF- $\beta$ /SMAD signaling in cancers, especially in LUAD.

Thus, we initially performed mass spectrometry (MS)-based proteomics analysis to explore what could be downstream targets of TIF1 $\gamma$  in TGF- $\beta$ -untreated LUAD cells. Among the TIF1 $\gamma$ -interacting proteins we found, TATA box binding protein (TBP)-associated factor 15 (TAF15) attracted our interest. From view of their nuclear-cytoplasmic distribution, it is not surprising because TIF1 $\gamma$  shows nuclear localization in NSCLC cells (Wang et al., 2016) and TAF15 may be expressed in the nucleus and cytoplasm of lung epithelial cells (Andersson et al., 2008). However, to the best of our knowledge, very little is known mechanistically about the connection between TIF1 $\gamma$  and TAF15. Thus, we deduced that TIF1 $\gamma$  might post-translationally regulate TAF15 in NSCLC cells. TAF15 (also known as TAFII68) has been identified as a specific TAF distinct from the other 13 best-known TAFs constituting the transcriptional factor IID (TFIID) complex (Bertolotti et al., 1996). Usually, TAF15 is involved in forming the TFIID multi-subunit complex with TBP to initiate gene transcription with participation of RNA polymerase II (Bell and Tora, 1999; Chen et al., 2021; He et al., 2013). Besides a specialization of binding onto the core promoter of genes, TAF15 may interact not only with RNA but also single-strand DNA because it contains an RNA-binding domain (Bell and Tora, 1999). TAF15 also functions in coupling transcription with RNA processing by associating with the spliceosomal U1 small nuclear ribonucleoprotein particle (snRNP) complex (Leichter et al., 2011). The N-terminal domain of TAF15 has transactivation and oncogenic properties (Bertolotti et al., 1999). For example, TAF15 can be recruited by the long non-coding RNA (lncRNA) PITPNA-AS1 to stabilize HMGB3 mRNA and promote proliferation and migration of lung squamous cell carcinoma (LUSC) cells (Ren et al., 2020). Although high-level expression of TAF15 was significantly correlated with poor survival of individuals with LUAD (Singh et al., 2020), it has been unclear how TAF15 transcriptionally affects its downstream target genes and controls TIF1 $\gamma$ -associated EMT and metastasis of LUAD cells.

Given that TIF1 $\gamma$  and TAF15 are inactivated and activated, respectively, in multiple cancers, including LUAD, we investigated potential interaction of TIF1 $\gamma$  with formation of the TAF15/TBP transcriptional complex to control EMT and metastasis of LUAD cells. Based on RNA sequencing (RNA-seq) analysis and computational algorithm prediction, we explored the role of TAF15/TBP-mediated interleukin 6 (IL-6) transactivation in facilitating EMT and metastasis of LUAD cells. This study suggests that TIF1 $\gamma$  is essential for restraining TAF15/TBP complex-dependent overactivation of transcription initiation during metastasis.

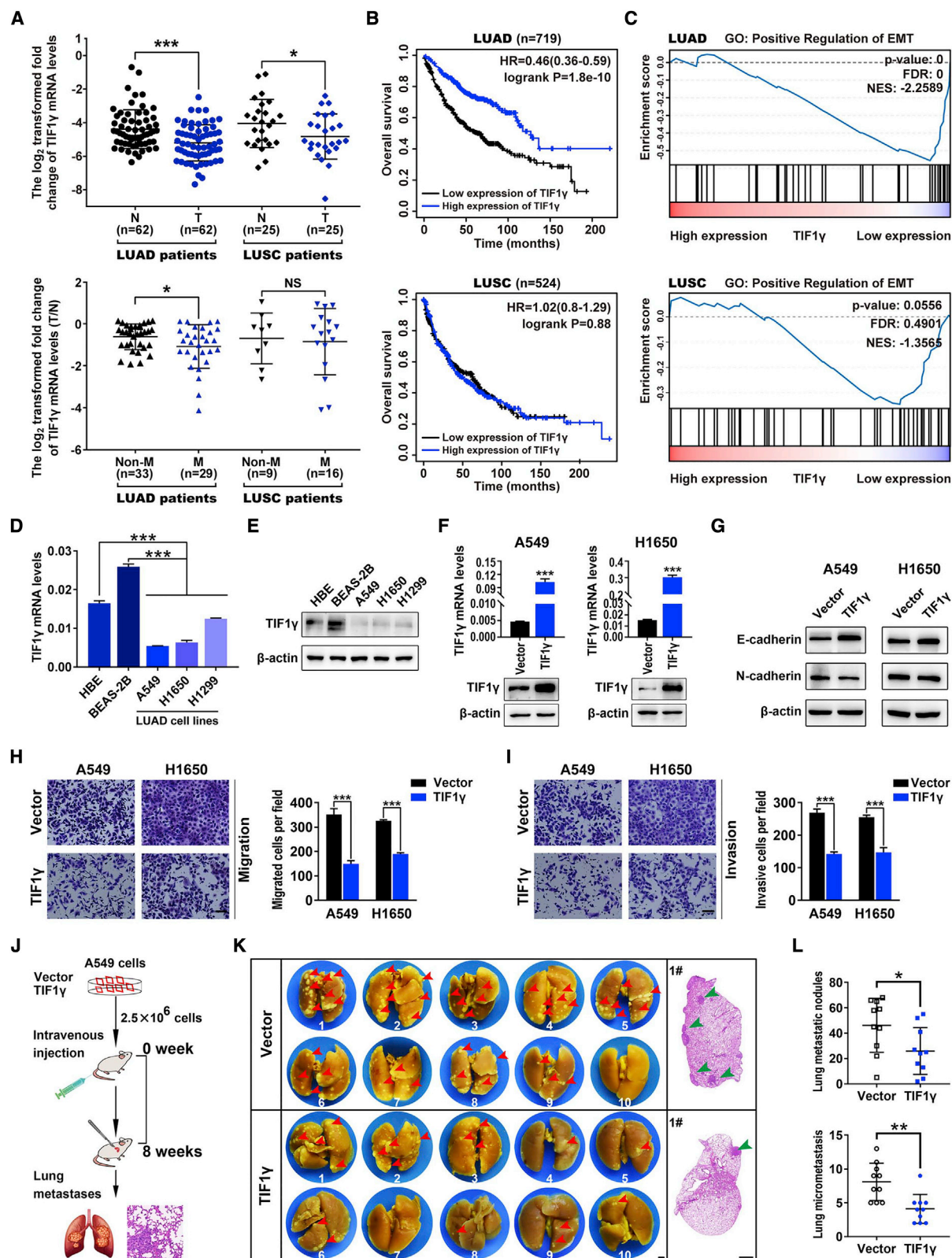
## RESULTS

### TIF1 $\gamma$ expression is positively associated with good prognosis of individuals with LUAD and inhibits EMT and metastasis of LUAD cells

We have reported previously that TIF1 $\gamma$  expression was frequently reduced in NSCLC tissue (Wang et al., 2016). To test this, we examined TIF1 $\gamma$  expression in 87 paired NSCLC tissues, including 62 LUAD and 25 LUSC tissues, and found that TIF1 $\gamma$  expression was significantly lower in LUAD and LUSC tissues than in paired adjacent noncancerous tissue (Figure 1A, top panel). Relative TIF1 $\gamma$  expression (tumor tissue [T]/noncancerous tissue [N]) showed a significant reduction in metastatic LUAD tissue (n = 29) compared with non-metastatic counterparts (n = 33), but there was no difference between metastatic (n = 16) and non-metastatic (n = 9) LUSC tissue (Figure 1A, bottom panel; Tables S1 and S2). Kaplan-Meier Plotter (<http://kmplot.com/analysis/>) indicated that individuals with LUAD with low expression of TIF1 $\gamma$  had poor survival, whereas TIF1 $\gamma$  expression was not associated with survival in individuals with LUSC (Figure 1B). Using GSE29016 from the Gene Expression Omnibus (GEO) database, we performed gene set enrichment analysis (GSEA) and identified that the EMT gene set was significantly enriched in LUAD but not in LUSC samples with low TIF1 $\gamma$  expression (Figure 1C). These results suggest that TIF1 $\gamma$  is negatively associated with EMT and metastasis in LUAD.

Downregulation of TIF1 $\gamma$  in tumor tissues from individuals with LUAD was reproduced in 3 LUAD cell lines (A549, H1650, and H1299), which presented dramatically decreased levels of TIF1 $\gamma$  mRNA and protein compared with 2 human bronchial epithelial cell lines, HBE and BEAS-2B (Figures 1D and 1E). Thus, we successfully overexpressed TIF1 $\gamma$  in A549 and H1650 cells using a lentiviral system (Figure 1F). Subsequently, TIF1 $\gamma$ -overexpressing A549 and H1650 cells displayed increased E-cadherin and decreased N-cadherin (Figure 1G), suggesting an inhibitory role of TIF1 $\gamma$  in EMT. Transwell assays showed that TIF1 $\gamma$  overexpression significantly attenuated the migration and invasion capabilities of A549 and H1650 cells (Figures 1H and 1I).

To evaluate the function of TIF1 $\gamma$  in LUAD cell metastasis *in vivo*, we intravenously (i.v.) injected TIF1 $\gamma$ -overexpressing and empty vector-transfected A549 cells into BALB/c nude mice (Figure 1J). Two groups of mice were killed without pain 8 weeks after inoculation, and their lungs were surgically excised and subjected to detection of metastatic lung lesions (Figure 1J). After treatment with Bouin's solution and hematoxylin and eosin (H&E), we



(legend on next page)



observed that the mice injected with TIF1 $\gamma$ -overexpressing A549 cells developed fewer metastatic lung nodules and micrometastatic foci in lung tissue compared with those injected with control A549 cells (Figures 1K and 1L). These results indicate that TIF1 $\gamma$  correlates with a favorable prognosis in LUAD and suppresses EMT and metastasis of LUAD cells.

### TIF1 $\gamma$ not only interacts with TAF15 but also competes with TAF15 for binding to TBP in LUAD cells

To discover unknown TIF1 $\gamma$ -interacting molecules, we firstly employed an anti-hemagglutinin (HA) immunoprecipitation (IP) assay followed by MS-based analysis in HEK293T cells transfected with an HA-tagged TIF1 $\gamma$  expression vector. One hundred and seventy-eight candidate TIF1 $\gamma$ -interacted proteins were identified (Figure 2A and Table S3). Considering our previous report that TIF1 $\gamma$  predominantly localizes in the LUAD cell nucleus (Wang et al., 2016) and probably interacts with several specific TFs that function in the nucleus, we intersected 2,690 TFs from the AnimalTFDB database (<http://bioinfo.life.hust.edu.cn/AnimalTFDB/>) with the aforementioned candidate proteins. In total, we found 25 potential TFs or cofactors that interacted with TIF1 $\gamma$  (Figure 2A). In support of our findings, TRIM24, TRIM28, and SSRP1 have been shown to interact with TIF1 $\gamma$  (Ferri et al., 2019; Herquel et al., 2011), and they were included in our MS data. However, TAF15 garnered more attention in the present study, which was confirmed by silver staining analysis (Figure 2B).

Then we confirmed whether TIF1 $\gamma$  interacts with TAF15. In HEK293T cells co-transfected with HA-tagged TIF1 $\gamma$  and FLAG-tagged TAF15 expression vectors, TAF15 was successfully co-immunoprecipitated with TIF1 $\gamma$  (Figure 2C). Endogenous TAF15 was coprecipitated with TIF1 $\gamma$  in HEK293T and A549 cells (Figures 2D and 2E) and vice versa in A549 cells (Figure 2F). By using immunofluorescence staining in A549 cells, we found

that TIF1 $\gamma$  and TAF15 were co-localized in the nucleoplasm (Figure 2G), supporting the interaction between TIF1 $\gamma$  and TAF15 in LUAD cells. Because of the established fact that TAF15 is a TBP-associated factor and closely related to TFIID (Bertolotti et al., 1996), we speculate that TIF1 $\gamma$  could participate in the interplay of TAF15 with TBP. CoIP experiments showed that TBP was co-precipitated with TAF15 in HEK293T cells co-transfected with FLAG-tagged TAF15 and HA-tagged TBP expression vectors and in A549 cells (Figures 2H and 2I), underpinning an interaction of TAF15 with TBP.

Based on these findings, TAF15 seems to link TIF1 $\gamma$  to TBP in A549 cells. In fact, when TAF15 expression was silenced in A549 cells (Figure 2J), not only did TIF1 $\gamma$  coprecipitate with TBP, but TIF1 $\gamma$  had an increased binding activity to TBP (Figure 2K). TBP was coprecipitated with TIF1 $\gamma$  in HEK293T cells co-transfected with FLAG-tagged TIF1 $\gamma$  and HA-tagged TBP vectors (Figure 2L). In contrast, when TIF1 $\gamma$  was overexpressed in A549 cells, the amount of TBP coprecipitated with TAF15 was dramatically decreased (Figure 2M). These results demonstrate that TIF1 $\gamma$  competes with TAF15 for interaction with TBP.

### Identification of domains of TIF1 $\gamma$ interacting with TAF15 and TBP

Given the facts that TIF1 $\gamma$  is an E3 ubiquitin ligase (McAvera and Crawford, 2020) and our aforementioned findings, we hypothesized that TIF1 $\gamma$  might modify TAF15 and/or TBP via a ubiquitylation machinery. Thus, we first generated four various constructs with HA/FLAG tags, which contain a full-length (FL) coding sequence (CDS) of TIF1 $\gamma$  and three truncated CDSs (i.e., a combination of RBCC with a middle region [RBCC + M], an N-terminal RBCC unit [RBCC], and a combination of the middle region with a C-terminal PHD finger-bromodomain [M + PB]) (Figure 3A). Subsequently, different constructs were co-transfected

### Figure 1. TIF1 $\gamma$ expression is positively associated with good prognosis of individuals with LUAD and inhibits EMT and metastasis of LUAD cells

(A) Top panel: qRT-PCR analysis of TIF1 $\gamma$  mRNA levels in 62 LUAD tissues, 25 LUSC tissues, and their matched adjacent noncancerous tissue. N, noncancerous tissue; T, tumor tissue. Bottom panel: relative mRNA expression (T/N) of TIF1 $\gamma$  in non-metastatic (n = 33) and metastatic (n = 29) LUAD tissue and non-metastatic (n = 9) and metastatic (n = 16) LUSC tissue. T were categorized into non-metastatic and metastatic tissues as described in STAR Methods. Non-M and M represent non-metastatic and metastatic T, respectively. Data are shown as the mean  $\pm$  SD (n = 2). NS, not significant. \*p < 0.05, \*\*\*p < 0.001 by paired Student's t test (top panel) or unpaired Student's t test (bottom panel).

(B) Kaplan-Meier survival curves (<http://kmplot.com/analysis/>) of individuals with LUAD (n = 719) and LUSC (n = 524) with low or high TIF1 $\gamma$  expression. Log rank test was used to compare the differences between two groups.

(C) GSEA was performed based on GSE29016 from the GEO database. The gene set "Positive Regulation of EMT" was enriched in TIF1 $\gamma$  low-expression LUAD samples. FDR, false discovery rate; NES, normalized enrichment score. GSEA was considered to be significant at predefined values of p < 0.05, FDR < 0.25, and |NES| > 1.

(D and E) qRT-PCR and western blot analyses of TIF1 $\gamma$  expression levels in human bronchial epithelial cell lines (HBE and BEAS-2B) and LUAD cell lines (A549, H1650, and H1299).  $\beta$ -Actin was used as an internal control. Data are shown as the mean  $\pm$  SD (n = 3). \*\*\*p < 0.001 by unpaired Student's t test.

(F) TIF1 $\gamma$  expression levels in A549 and H1650 cells stably overexpressing TIF1 $\gamma$ . Data are shown as the mean  $\pm$  SD (n = 3). \*\*\*p < 0.001 by unpaired Student's t test.

(G) Western blot analysis of the EMT markers E-cadherin and N-cadherin expressed in TIF1 $\gamma$ -overexpressing A549 and H1650 cells.

(H and I) TIF1 $\gamma$ -overexpressing A549 and H1650 cells were allowed to migrate through an 8- $\mu$ m pore membrane (H) or invade through a Matrigel-coated membrane in Transwells (I). After 30 h, migrated and invasive cells were stained, photographed, and counted in at least three microscopic fields. Scale bar, 100  $\mu$ m. Data are shown as the mean  $\pm$  SD (n = 3). \*\*\*p < 0.001 by unpaired Student's t test.

(J) Schematic flowchart of the LUAD cell *in vivo* metastasis model. TIF1 $\gamma$ -overexpressing and control vector A549 cells ( $2.5 \times 10^6$  cells/mouse) were i.v. injected into BALB/c nude mice (10 mice per group).

(K) Representative photographs of lung metastatic nodules and micrometastatic foci developed in mice 8 weeks after injection of TIF1 $\gamma$ -overexpressing or control vector A549 cells. The surgically resected lungs were fixed and stained and histologically examined as described in STAR Methods. Red arrowheads denote metastatic nodules established in lungs. Scale bar, 3 mm (left part). Green arrowheads indicate micrometastatic foci. Scale bar, 1 mm (right part).

(L) Plots showing the difference in lung metastatic nodules or micrometastasis counts between the TIF1 $\gamma$ -overexpressing group and vector control group (n = 10 mice per group). Data are shown as the mean  $\pm$  SD. \*p < 0.05, \*\*p < 0.01 by unpaired Student's t test.

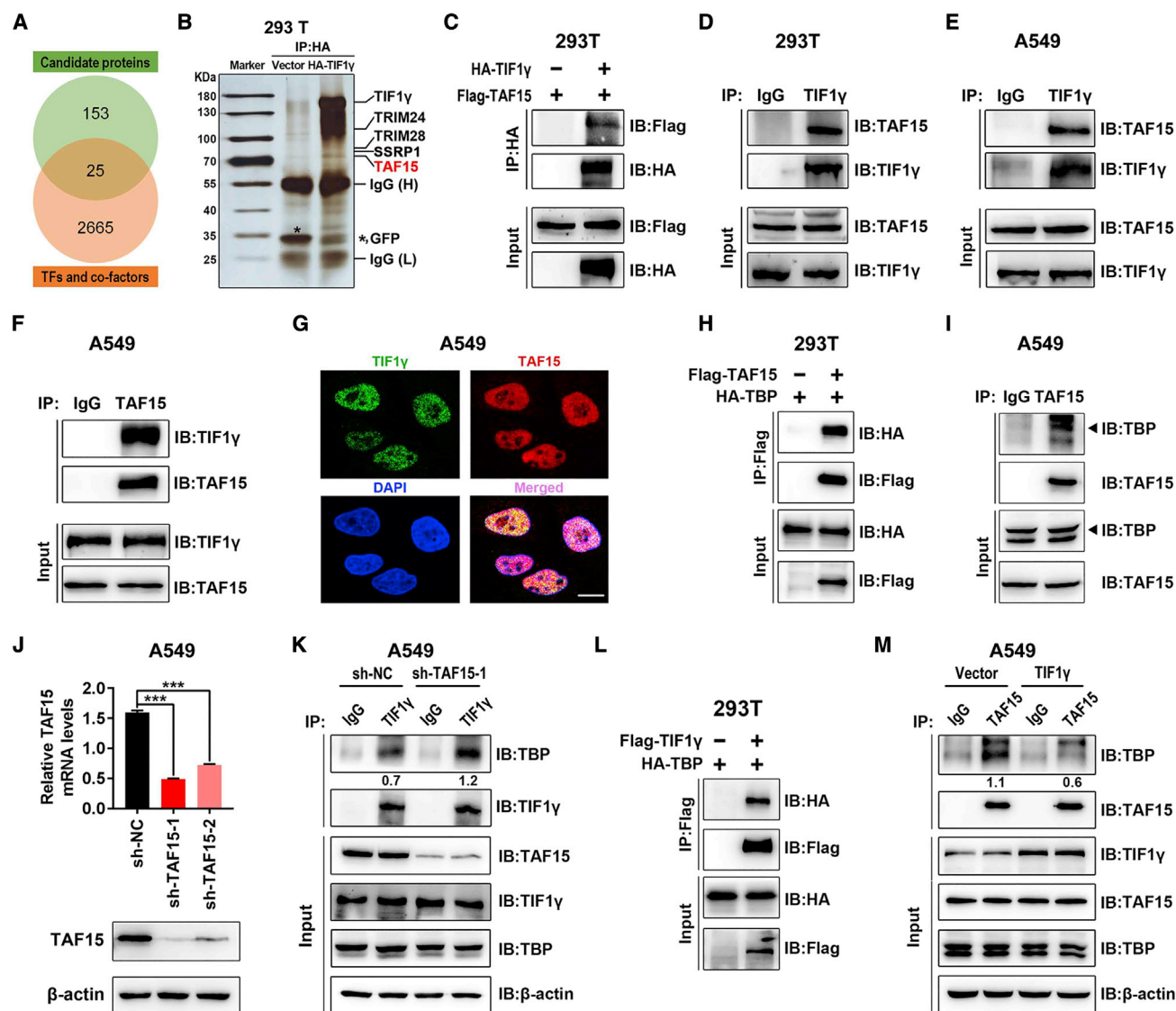


**Figure 2. TIF1γ not only interacts with TAF15 but also competes with TAF15 for binding to TBP in LUAD cells**

(A and B) HEK293T cells were transfected with HA-tagged TIF1γ expression or control vectors for 48 h, and cell lysates were immunoprecipitated with anti-HA antibody. Bound proteins were eluted and subjected to MS-based analysis. Subsequently, 178 candidate proteins interacting with TIF1γ were overlapped with 2,690 TFs and co-factors from the AnimalTFDB database (<http://bioinfo.life.hust.edu.cn/AnimalTFDB/>) (A). Eluted proteins were separated on SDS-PAGE gel and visualized by silver staining (B). IP, immunoprecipitation.

(C) HEK293T cells co-expressing HA-tagged TIF1γ and FLAG-tagged TAF15 were subjected to coIP analysis. HA-tagged TIF1γ protein was immunoprecipitated using anti-HA antibodies. Binding of TAF15 to TIF1γ was detected by immunoblot (IB) with an anti-FLAG antibody.

(D) CoIP was performed in HEK293T cells. Endogenous TIF1γ was immunoprecipitated with an anti-TIF1γ antibody. Binding of TAF15 to TIF1γ was determined by IB with an anti-TAF15 antibody. An anti-immunoglobulin G (IgG) antibody was used as a negative control.

(E and F) CoIP was conducted by anti-TIF1γ or anti-TAF15 antibodies in the lysate of A549 cells.

(G) A549 cells were co-incubated with a mouse anti-TIF1γ antibody and a rabbit anti-TAF15 antibody and then stained with fluorescein isothiocyanate (FITC)-conjugated anti-mouse IgG (green, for TIF1γ) and Cy3-conjugated anti-rabbit IgG (red, for TAF15). Cell nuclei were counterstained and visualized with DAPI (blue). Scale bar, 10 μm.

(H) HEK293T cells were co-transfected with FLAG-tagged TAF15 and HA-tagged TBP expression vectors for 48 h and subjected to coIP analysis. FLAG-tagged TAF15 protein in the cell lysate was immunoprecipitated with anti-FLAG antibodies. Binding of TBP to TAF15 was examined by IB using an anti-HA antibody.

(I) A549 cell lysates were immunoprecipitated with anti-TAF15 antibody and then immunoblotted with anti-TBP antibodies. An anti-IgG antibody served as a negative control.

(J) qRT-PCR and western blot analyses of TAF15 expression in TAF15-silenced or control A549 cells, which were transfected with short hairpin RNA (shRNA; sh-TAF15) or a scrambled sequence (sh-NC). β-Actin was used as an internal control. Data are shown as the mean ± SD (n = 3). \*\*\*p < 0.001 by unpaired Student's t test.

(legend continued on next page)

into HEK293T cells with FLAG-tagged TAF15 or HA-tagged TBP expression vectors. CoIP analysis showed that TAF15 coprecipitated with RBCC and RBCC-containing domains rather than M + PB of TIF1 $\gamma$  (Figure 3B), indicating that only the RBCC domain of TIF1 $\gamma$  interacts with TAF15. However, the M domain of TIF1 $\gamma$  was able to bind with TBP (Figure 3C). These results demonstrate that TIF1 $\gamma$  can bind to TAF15 or TBP by utilizing diverse domains. In terms of these, we examined whether TIF1 $\gamma$  regulates TAF15 or TBP ubiquitylation. In HEK293T cells transfected with expression plasmids encoding FLAG-tagged TIF1 $\gamma$  and HA-tagged ubiquitin, endogenous TAF15 ubiquitylation was significantly enhanced upon TIF1 $\gamma$  overexpression (Figure 3D), whereas TBP ubiquitylation was not affected by TIF1 $\gamma$  (Figure 3E). These results indicate that TIF1 $\gamma$  regulates TAF15 ubiquitylation through its RBCC domain. In contrast to RBCC domain, M-containing domains of TIF1 $\gamma$  attenuated the binding capability of TAF15 with TBP (Figure 3F), strengthening the aforementioned notion that TIF1 $\gamma$  competes with TAF15 for interaction with TBP.

#### TIF1 $\gamma$ modifies TAF15 through multi-mono-ubiquitylation and promotes nuclear export of TAF15

Ubiquitylation modification has been documented to cause degradation of target proteins (Hershko and Ciechanover, 1998). Although TIF1 $\gamma$  is required for TAF15 ubiquitylation, overexpression of TIF1 $\gamma$  failed to suppress TAF15 mRNA and protein expression levels in the LUAD cell lines A549 and H1650 (Figure 4A). TIF1 $\gamma$  overexpression altered the nuclear-cytoplasmic distribution of TAF15 protein, leading to a decrease of TAF15 in the nucleus concomitant with an increase in the cytoplasm (Figure 4B). The promotion of nuclear export of TAF15 by TIF1 $\gamma$  overexpression was visualized upon immunofluorescence staining of A549 and H1650 cells (Figure 4C). In light of the evidence showing that modification with monoubiquitin or multi-mono-ubiquitin regulates protein subcellular localization (Fulda et al., 2012), we assumed that TIF1 $\gamma$  might modify TAF15 by mono/multi-mono-ubiquitylation. To test this, we performed coIP analyses in HEK293T cells co-transfected with FLAG-tagged TIF1 $\gamma$  and HA-tagged ubiquitin or HA-tagged mutant ubiquitin (all 7 lysines mutated to arginines) expression vectors and found that TIF1 $\gamma$  overexpression increased the binding ability of wild-type/mutant ubiquitin to TAF15 (Figure 4D). Lysine-less mutant ubiquitin (K0-Ub) is unable to form Ub chains but modifies protein in the presence of E3 ligase (Oshikawa et al., 2012). Therefore, our findings suggest that TIF1 $\gamma$  regulates TAF15 via mono-ubiquitylation.

Upon TIF1 $\gamma$  overexpression, more ubiquitinated TAF15 was immunoprecipitated with Ub, regardless of whether Ub was wild type or mutant (Figure 4E, top panel). By extending exposure time, we detected TAF15 bands of higher molecular weights corresponding to TAF15 with multiple mono-Ub (molecular weight [MW] of a single Ub: 8.5 kDa) in whole lysates (Figure 4E,

bottom panel), indicating that TAF15 was modified at more than one lysine residue in a mono-ubiquitylation manner. We determined whether the RBCC domain of TIF1 $\gamma$  directly affects TAF15 mono-ubiquitylation. Depletion of the RBCC domain decreased accumulation of ubiquitinated TAF15 that was coprecipitated with Ub (Figure 4F). TIF1 $\gamma$  overexpression significantly increased cytoplasmic localization of TAF15 in A549 and H1650 cells transfected with HA-tagged Ub (K0) expression vectors (Figures 4G and 4H), suggesting that TIF1 $\gamma$  promotes nuclear export of TAF15 by mono-ubiquitylation modification. These results demonstrate that TIF1 $\gamma$  modifies TAF15 through multi-mono-ubiquitylation and facilitates nuclear export of TAF15.

#### TAF15 knockdown suppresses EMT and LUAD cell invasion and metastasis

TAF15 upregulation is associated with worse survival of individuals with LUAD (Singh et al., 2020). However, it is unclear whether TAF15 contributes to EMT and invasion of LUAD cells. Knockdown of TAF15 significantly increased expression of the epithelial marker E-cadherin and decreased expression of the mesenchymal marker N-cadherin in A549 and H1650 cells (Figures 5A and S1A), indicating that TAF15 expression is positively correlated with EMT in LUAD cells. TAF15 knockdown effectively delayed wound healing of A549 and H1650 cells (Figures 5B and S1B) and attenuated the migration and invasion abilities of A549 and H1650 cells (Figures 5C and S1C). In contrast, TAF15-overexpressing A549 and H1650 cells exhibited the opposite effects in terms of EMT marker expression, wound healing, and invasion abilities (Figures S1D–S1F).

Next we assessed the effect of TAF15 on LUAD cell metastasis in an *in vivo* model as established above (Figure 1J). 8 weeks after inoculation, injection of TAF15-silenced A549 cells into mice significantly prevented development of metastatic lung nodules and formation of micrometastatic foci in lung/liver tissue compared with the negative control group (Figures 5D and 5E). In clinical tissue, TAF15 expression was higher in LUAD tissue than matched noncancerous tissue (Figure 5F, top panel; Table S1). Importantly, metastatic LUAD tissue showed an increase in relative TAF15 expression (T/N) compared with non-metastatic tissue (Figure 5F, bottom panel; Table S1). Kaplan-Meier Plotter showed that high expression of TAF15 was significantly correlated with poor survival rate of individuals with LUAD (Figure 5G) but not LUSC (data not shown). These data reveal a metastasis-promoting function of TAF15 in LUAD progression.

#### TIF1 $\gamma$ overexpression inhibits TAF15-promoted EMT and invasion in LUAD cells

Based on these findings, we tested whether TIF1 $\gamma$  may antagonize enhancement of TAF15 on EMT and invasion of LUAD cells.

(K) Anti-TIF1 $\gamma$  coIP analysis was performed in A549 cells transfected with sh-TAF15 or sh-NC. The amount of TBP bound to TIF1 $\gamma$  was determined by IB with anti-TBP antibodies, which was quantified by densitometry. Densitometry values of TBP protein were normalized to those of immunoprecipitated TIF1 $\gamma$  and are shown below the corresponding bands.

(L) HEK293T cells co-expressing FLAG-tagged TIF1 $\gamma$  and HA-tagged TBP were used for coIP analysis. FLAG-tagged TIF1 $\gamma$  protein in cell lysates was immunoprecipitated with anti-FLAG antibodies. The indicated proteins were detected by western blot.

(M) Anti-TAF15 coIP analysis was done in TIF1 $\gamma$ -overexpressing or control vector A549 cells. The amount of TBP bound to TAF15 was detected by IB with anti-TBP antibodies. The densitometric values of TBP relative to those of the immunoprecipitated TAF15 are presented below the corresponding bands.

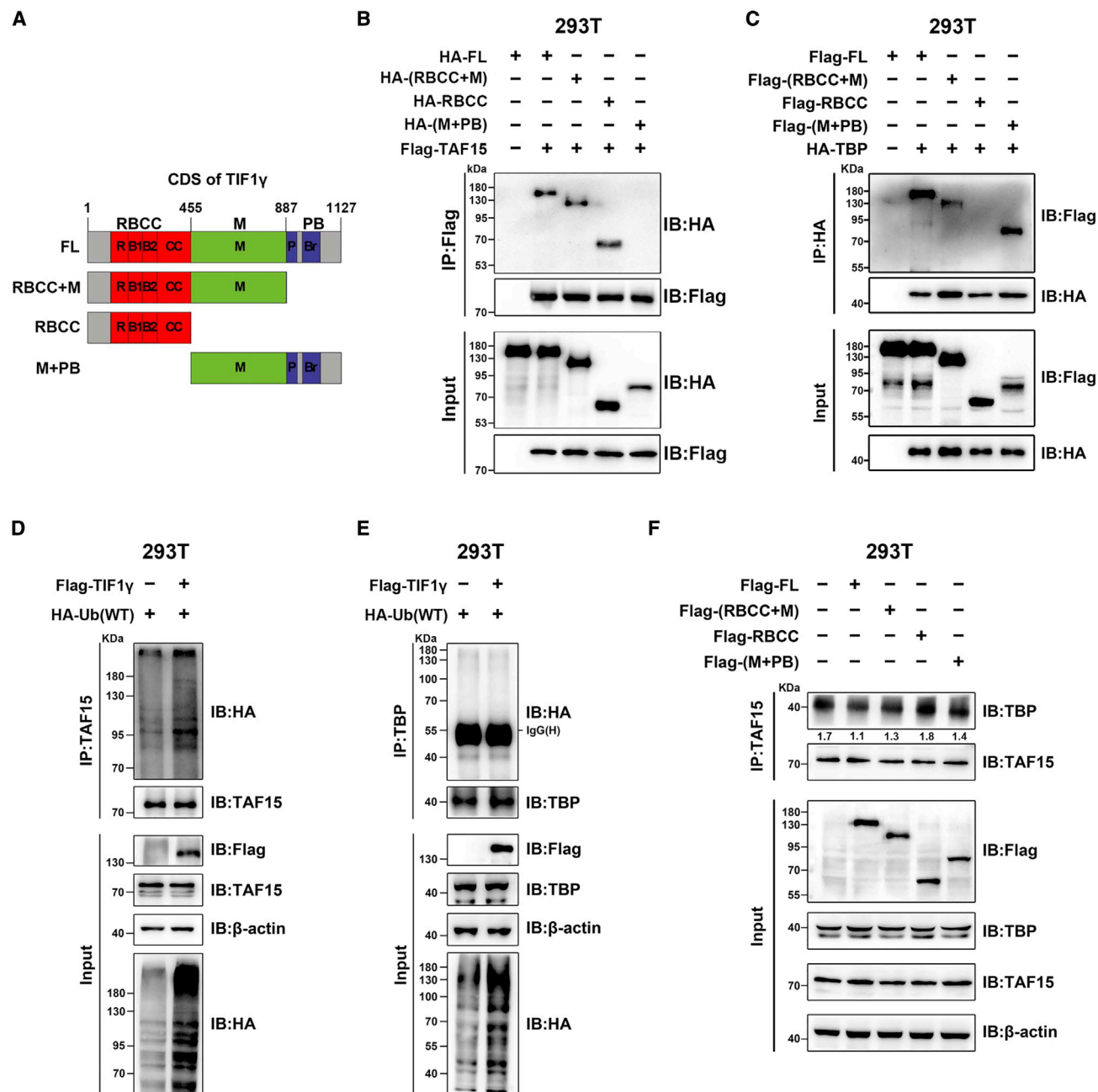


**Figure 3. Identification of domains of TIF1 $\gamma$  interacted with TAF15 and TBP**

(A) A FL and three truncated CDSs of TIF1 $\gamma$  (denoted FL, RBCC + M, RBCC, and M + PB) were used for construction of HA/FLAG-tagged TIF1 $\gamma$  expression vectors. (B and C) The abovementioned HA/FLAG-tagged TIF1 $\gamma$  vectors and FLAG-tagged TAF15/HA-tagged TBP vectors were co-transfected into HEK293T cells as indicated for 48 h, and then cells were subjected to coIP analysis for detection of domains of TIF1 $\gamma$  interacting with TAF15/TBP.

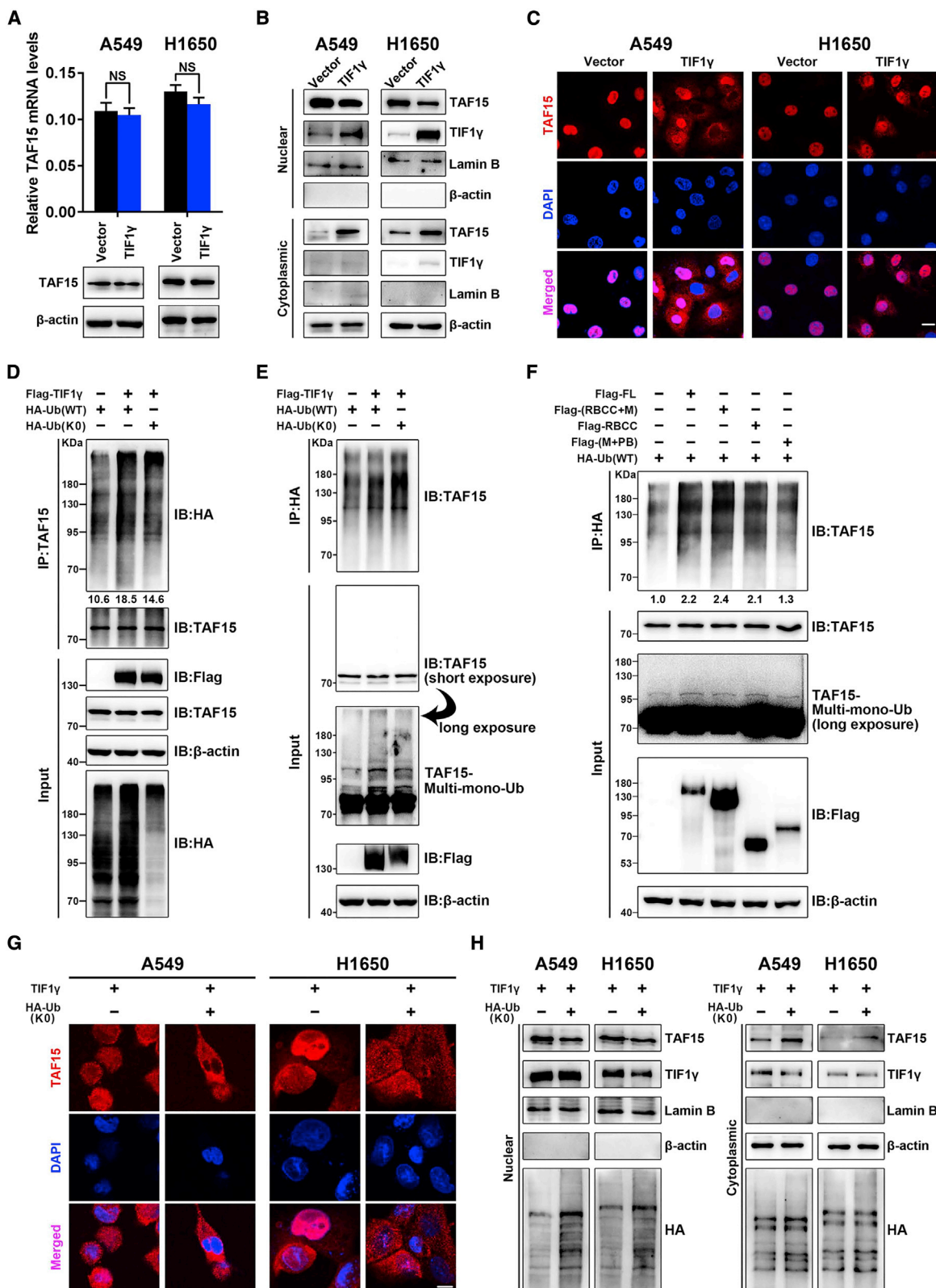
(D and E) HEK293T cells were co-transfected with FLAG-tagged TIF1 $\gamma$  and HA-tagged Ub (wild type [WT]) for 48 h, and cell lysates were immunoprecipitated with anti-TAF15 antibodies (D) or TBP antibodies (E). HA antibodies were used to monitor the ubiquitylation status of TAF15 and TBP. Ub, ubiquitin.

(F) Anti-TAF15 coIP analysis was performed in HEK293T cells expressing FL and three truncated CDSs of TIF1 $\gamma$ . The amount of TBP bound to TAF15 was detected by IB with TBP antibodies, which was quantified by densitometry. Densitometry values of TBP relative to those of immunoprecipitated TAF15 are shown below the corresponding bands.

Downregulation of E-cadherin and upregulation of N-cadherin in A549 and H1650 cells upon TAF15 overexpression was reversed by TIF1 $\gamma$  overexpression, and EMT marker expression was

similar to that in control cells without TAF15 and TIF1 $\gamma$  overexpression (Figure S2A). TIF1 $\gamma$  overexpression significantly repressed the migration- and invasion-promoting abilities





(legend on next page)

caused by TAF15 overexpression (Figure S2B). When TAF15 was knocked down in A549 and H1650 cells, the inhibitory effects of TIF1 $\gamma$  on EMT and invasion were partially or completely abrogated, respectively (Figures S2C–S2E). These results indicate that TIF1 $\gamma$  inhibits TAF15-promoted EMT and invasion and suggest that the EMT- and invasion-inhibiting roles of TIF1 $\gamma$  depend on TAF15 in LUAD cells.

Combined with our aforementioned findings that the M + PB domain of TIF1 $\gamma$  failed to interact with TAF15 (Figure 3B), we assessed whether M + PB can inhibit EMT and invasion of LUAD cells. Compared with the empty vector control, M + PB overexpression significantly suppressed EMT, as evidenced by upregulation of E-cadherin and downregulation of N-cadherin (Figure S3A). M + PB attenuated the migration and invasion abilities of LUAD cells (Figure S3B). This role of M + PB largely mirrored that of TIF1 $\gamma$ -FL overexpression (Figure S3).

### TIF1 $\gamma$ impedes TAF15-dependent expression of IL-6, and IL-6 promotes EMT and invasion in LUAD cells

To screen for downstream target genes regulated by the interplay between TIF1 $\gamma$  and TAF15, we first performed RNA-seq analysis using total RNA from TIF1 $\gamma$ -overexpressing and TAF15-silenced A549 cells and the corresponding control cells. We identified 4,702 differentially expressed genes (DEGs), including 2,683 up-regulated and 2,019 down-regulated mRNAs, in TIF1 $\gamma$ -overexpressing A549 cells (Figures 6A and 6B; Table S4). We found 3,895 DEGs, including 2,115 up-regulated and 1,780 down-regulated mRNAs, in TAF15-silenced A549 cells (Figures 6A and 6B; Table S5). To discover TIF1 $\gamma$ -inactivated and TAF15-activated target genes, 2,019 and 1,780 mRNAs down-regulated in TIF1 $\gamma$ -overexpressing and TAF15-silenced A549 cells, respectively, were intersected to yield 679 mRNAs (Figure 6B). Next, 679 selected mRNAs were subjected to Gene Ontology (GO) enrichment analysis (<https://metascape.org>), and they were enriched in multiple biological processes (BPs), including the top 20 significant BPs (Figure 6C, left panel). Among these 20 BPs, only one process, “locomotion,” was related to cell migration, which consists of multiple sub-processes (Figure 6C, right panel). Thirty-six genes enriched in

“locomotion” were arranged in descending order by their fold change expressed in TAF15-silenced A549 cells, and IL-6 ranks first among 36 down-regulated genes (Figure 6D, left panel; Table S5). Because of the fact that TBP is positioned approximately 30 bp upstream of the transcription start site (TSS) of mammalian genes (Chen et al., 2021; O’Shea-Greenfield and Smale, 1992), we predicted that most of these 36 genes had TATA box motifs within 1,000 bp upstream of the TSS using the Eukaryotic Promoter Database (<https://epd.epfl.ch/index.php>). Seven genes, including IL-6, harbor one TATA box element at the –30 bp position relative to the TSS (Figure 6D, right panel). To verify the RNA-seq results, we examined IL-6 expression using qRT-PCR, immunoblotting, and so forth. As a result, TAF15-silenced A549 and H1650 cells showed a significant reduction in IL-6 mRNA, protein, and protein secretion levels (Figures 6E–6G), whereas TAF15 overexpression led to the opposite results (Figures S4A–S4C). In contrast, TIF1 $\gamma$  overexpression inhibited IL-6 expression in A549 and H1650 cells (Figures S4D and S4E). TIF1 $\gamma$  overexpression repressed TAF15-promoted IL-6 expression (Figure S4F). When TAF15 was knocked down in A549 and H1650 cells, the inhibitory effect of TIF1 $\gamma$  on IL-6 expression was partially abolished (Figure S4G), suggesting that TIF1 $\gamma$  regulates IL-6 expression in a TAF15-dependent manner.

Kaplan-Meier survival analysis showed that individuals with LUAD with high expression of IL-6 had a significantly poor survival (Figure S4H). We reported previously that IL-6 was involved in promoting EMT and invasion of LUAD cells (Liu et al., 2014). In this study, after being treated with IL-6 for 24 h, A549 and H1650 cells underwent EMT (Figure S4I). IL-6 stimulation accelerated cell wound-healing, migration, and invasion (Figures S4J and S4K).

### Transactivation of IL-6 by TAF15 depends on TBP

We used Actinomycin D (Act-D), a widely accepted mRNA synthesis inhibitor, to examine whether TAF15 affects IL-6 mRNA stability in LUAD cells. After being treated with Act-D, neither TAF15-overexpressing nor TAF15-silenced A549 and H1650 cells showed a time-dependent alteration of IL-6 mRNA

### Figure 4. TIF1 $\gamma$ modifies TAF15 through multi-mono-ubiquitylation and promotes nuclear export of TAF15

- (A) qRT-PCR and western blot analyses of TAF15 expression in A549 and H1650 cells overexpressing TIF1 $\gamma$ . Data are shown as the mean  $\pm$  SD (n = 3). Statistical analysis was conducted by unpaired Student’s t test.
- (B) Western blot analysis of TAF15 expression in nuclear and cytoplasmic fractions extracted from TIF1 $\gamma$ -overexpressing A549 and H1650 cells. Lamin B and  $\beta$ -actin served as loading controls for nuclear and cytoplasmic extracts, respectively.
- (C) Immunofluorescence analysis of TAF15 subcellular localization in A549 and H1650 cells overexpressing TIF1 $\gamma$ . Immunostaining was performed as described in Figure 2G. Scale bar, 10  $\mu$ m.
- (D and E) FLAG-tagged TIF1 $\gamma$  and/or HA-tagged Ub (WT or K0) vectors were co-transfected into HEK293T cells as indicated for 48 h. Then cell lysates were immunoprecipitated with anti-HA antibodies (D) or HA antibodies (E) and immunoblotted with antibodies against HA or TAF15, respectively. Total lysates were immunoblotted with the indicated antibodies, and  $\beta$ -actin served as a loading control. K0, all 7 lysines of Ub were mutated to arginines. In the TAF15-immunoprecipitated fractions (D), the amount of HA-tagged ubiquitination was quantified by densitometry values, which were normalized to TAF15 and are shown below the corresponding bands.
- (F) Lysates of HEK293T cells transfected with FLAG-tagged TIF1 $\gamma$  FL, truncated CDS, and HA-tagged Ub (WT) expression vectors as indicated were immunoprecipitated with anti-HA antibodies and then immunoblotted with TAF15 antibodies. The amount of TAF15 in the HA-immunoprecipitated fractions was quantified by densitometry. The densitometry values of TAF15 under different transfection conditions were compared with the first lane, whose densitometry value was set to 1. All values are shown below the corresponding bands.
- (G) TIF1 $\gamma$ -overexpressing A549 and H1650 cells were transiently transfected with or without HA-tagged Ub (K0) expression vectors for 48 h and subjected to immunofluorescence analysis of TAF15 subcellular localization. Immunostaining was performed as described in Figure 2G. Scale bar, 10  $\mu$ m.
- (H) Western blot analysis of TAF15 expression in nuclear and cytoplasmic fractions extracted from the treated A549 and H1650 cells (G). Lamin B and  $\beta$ -actin served as loading controls for nuclear and cytoplasmic extracts, respectively.

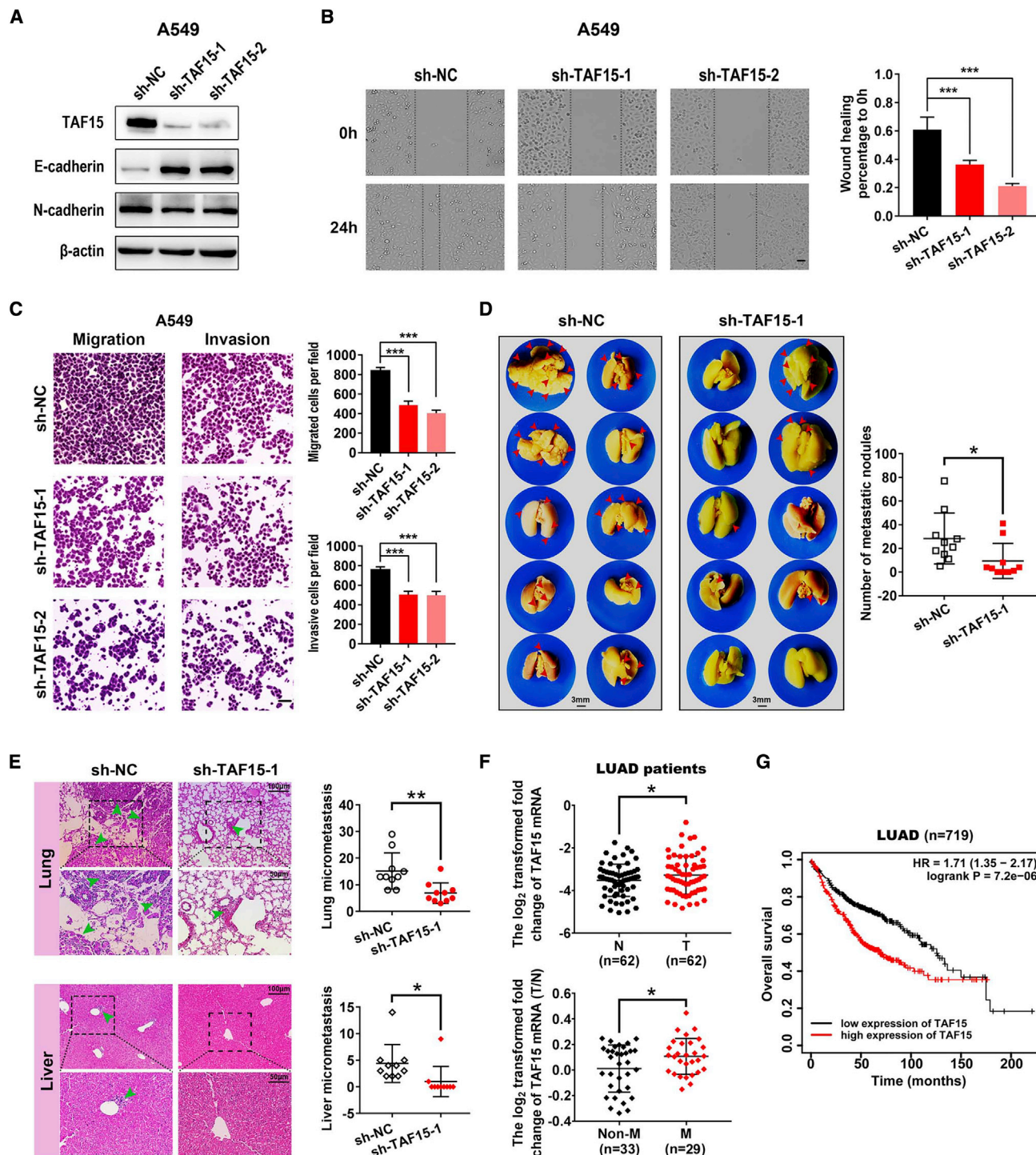


**Figure 5. TAF15 knockdown suppresses EMT and LUAD cell invasion and metastasis**

(A) Western blot analysis of TAF15, E-cadherin, and N-cadherin expression in TAF15-silenced A549 cells.  $\beta$ -Actin served as an internal control.

(B) Wound healing assays of cell migration in TAF15-silenced or control A549 cells. Wound healing was recorded and quantitated for at least three microscopic fields. Scale bar, 100  $\mu$ m. Data are shown as the mean  $\pm$  SD (n = 3). \*\*\*p < 0.001 by unpaired Student's t test.

(C) Migration and invasion abilities of TAF15-silenced A549 cells were determined by Transwell assays as described in Figures 1H and 1I. Migrated or invasive cells were stained and counted under a light microscope. Scale bar, 100  $\mu$ m. Data are shown as the mean  $\pm$  SD (n = 3). \*\*\*p < 0.001 by unpaired Student's t test.

(D) The *in vivo* metastasis model was established in BALB/c nude mice as described in Figure 1J. Metastatic nodules in surgically resected lungs of mice (n = 10 mice per group) injected with TAF15-silenced or control A549 cells are presented. Red arrowheads indicate metastatic nodules developed in lungs. Scale bar,

(legend continued on next page)



expression (Figures 7A, 7B, and S5A). Combined with the aforementioned results (Figures 6E and S4A), we suggested that TAF15 promotes IL-6 mRNA expression through transcriptional rather than post-transcriptional mechanisms.

Therefore, we next explored whether TAF15 transcriptionally regulates IL-6 expression through TAF15-interacting TBP, a TF binding to the TATA box element. First, small interfering RNA (siRNA)-mediated knockdown of TBP in A549 and H1650 cells (Figure S5B) resulted in a decrease in IL-6 mRNA and protein levels (Figure S5C), similar to the results obtained in TAF15-silenced A549 and H1650 cells (Figures 6E and 6F). Second, we looked for specific regions on the IL-6 promoter interacting with TAF15 or TBP. Before doing so, we overexpressed TBP in A549 cells (Figure S5D) and designed four pairs of primers for amplification of different regions within 2,000 bp upstream of the TSS of the IL-6 promoter (IP1/2/3/4) (Figure 7C). Then chromatin IP (ChIP) experiments were performed in A549 cells transfected with HA-tagged TBP or FLAG-tagged TAF15 expression vectors. ChIP revealed that a DNA fragment containing IP4 was enriched in the corresponding IP fractions using anti-HA or anti-FLAG antibodies (Figure 7D). In support of this, a luciferase reporter assay showed that the luciferase activity of pGL3-IP1~4 was significantly higher in TBP- or TAF15-overexpressing A549 cells than that in vector control cells, whereas the luciferase activity of pGL3-IP1~3 was not changed (Figures 7E and 7F). These results demonstrate that TBP and TAF15 regulate IL-6 transcription through its IP4 promoter region (approximately -497 to +1 bp). Third, to define specific functional site in IP4, we predicted three potential TATA box sites (-446, -272, and -30 bp) located in the IP4 region (Figures 7G and 6D, right panel). Thus, we generated pGL3-IP4 luciferase reporter plasmids containing the wild type or mutants of three putative TATA elements and transfected them into TBP- or TAF15-overexpressing A549 cells. The results of the luciferase reporter assay indicated that TBP- or TAF15-promoted pGL3-IP4 activity was abrogated only when the -30 bp TATA box site was mutated (Figures 7H and 7I), suggesting that -30 bp is a functional site of the IL-6 promoter. Fourth, we investigated whether TAF15 is involved in TBP-mediated IL-6 transcriptional initiation when endogenous TAF15 was knocked down in TBP-overexpressing A549 cells. Using a luciferase reporter assay, we found that TBP-promoted pGL3-IP1~4 activity was partially repressed by TAF15 knockdown (Figure 7J).

We determined whether TBP is indispensable for TAF15 to activate IL-6 transcription when endogenous TBP was knocked down in TAF15-overexpressing A549 cells. A ChIP assay showed that TAF15 was unable to precipitate any IL-6 promoter fragments, including IP4, in the absence of TBP (Figure 7K).

TAF15-involved increased pGL3-IP1~4 activity was significantly inhibited by TBP knockdown (Figure 7L). TBP knockdown abolished the promotive effect of TAF15 overexpression on IL-6 protein expression in A549 and H1650 cells (Figures 7M and S5E). These results suggest that TAF15 promotes IL-6 transcription in dependence on TBP.

## DISCUSSION

TIF1 $\gamma$  functions in various kinds of processes, including hematopoiesis, inflammation response, pulmonary fibrosis, and tumorigenesis (Bai et al., 2010; Boutanquoi et al., 2020; He et al., 2006; Kassem et al., 2015; Petit et al., 2019), most of which are regulated by TIF1 $\gamma$  via TGF- $\beta$ /SMAD signaling. We reported previously that TIF1 $\gamma$  was negatively involved in TGF- $\beta$ /SMAD signaling-induced EMT and metastasis of NSCLC cells (Wang et al., 2016, 2018). In support of this, TIF1 $\gamma$  inhibits TGF- $\beta$ /SMAD-induced EMT in other types of human cancers, diminishing cancer metastasis (Ding et al., 2014; Jingushi et al., 2015; Qi et al., 2019; Xue et al., 2014). However, it is widely accepted that cancer metastasis is an extremely complex process involving multiple steps and factors that regulate diverse signaling pathways (Bakir et al., 2020; Suhail et al., 2019). Therefore, as a tumor suppressor implicated in ubiquitination modification (Xue et al., 2015; Yu et al., 2019), it is highly probable that TIF1 $\gamma$  regulates EMT and cancer metastasis by interacting with factors other than SMADs. In this report, we demonstrate that the TIF1 $\gamma$ -TAF15/TBP interaction is an important mechanism for regulating IL-6 transcription and LUAD cell EMT, invasion, and metastasis. TIF1 $\gamma$  not only competes with TAF15 for interacting with TBP but also modifies TAF15 via multi-mono-ubiquitylation and drives nuclear export of TAF15. This prevents TAF15/TBP-mediated IL6 transactivation.

As one of the TIF1 family members with N-terminal RING fingers, TIF1 $\gamma$ 's RBCC domain confers E3 Ub ligase activity (McAvera and Crawford, 2020). It has been reported that TIF1 $\gamma$  promotes TGF- $\beta$ R1 and  $\beta$ -catenin degradation through poly-ubiquitination (Quere et al., 2014; Xue et al., 2015). Although TIF1 $\gamma$  does not affect SMAD4 protein stability, it regulates nuclear transport of SMAD4 by multi-mono-ubiquitination (Dupont et al., 2009; Xue et al., 2014). Here we show that the RBCC domain of TIF1 $\gamma$  interacts with and multi-mono-ubiquitylates TAF15 (Figures 3B and 4F), whose modification promotes nuclear export of TAF15 without affecting protein stability (Figures 4G and 4H). In fact, Agricola et al. (2011) reported that PB of TIF1 $\gamma$  can specifically bind to histone H3 tails, and ubiquitination of SMAD4 by TIF1 $\gamma$  requires PB (Agricola et al., 2011). However, in this study, we found that PB had a weak effect on

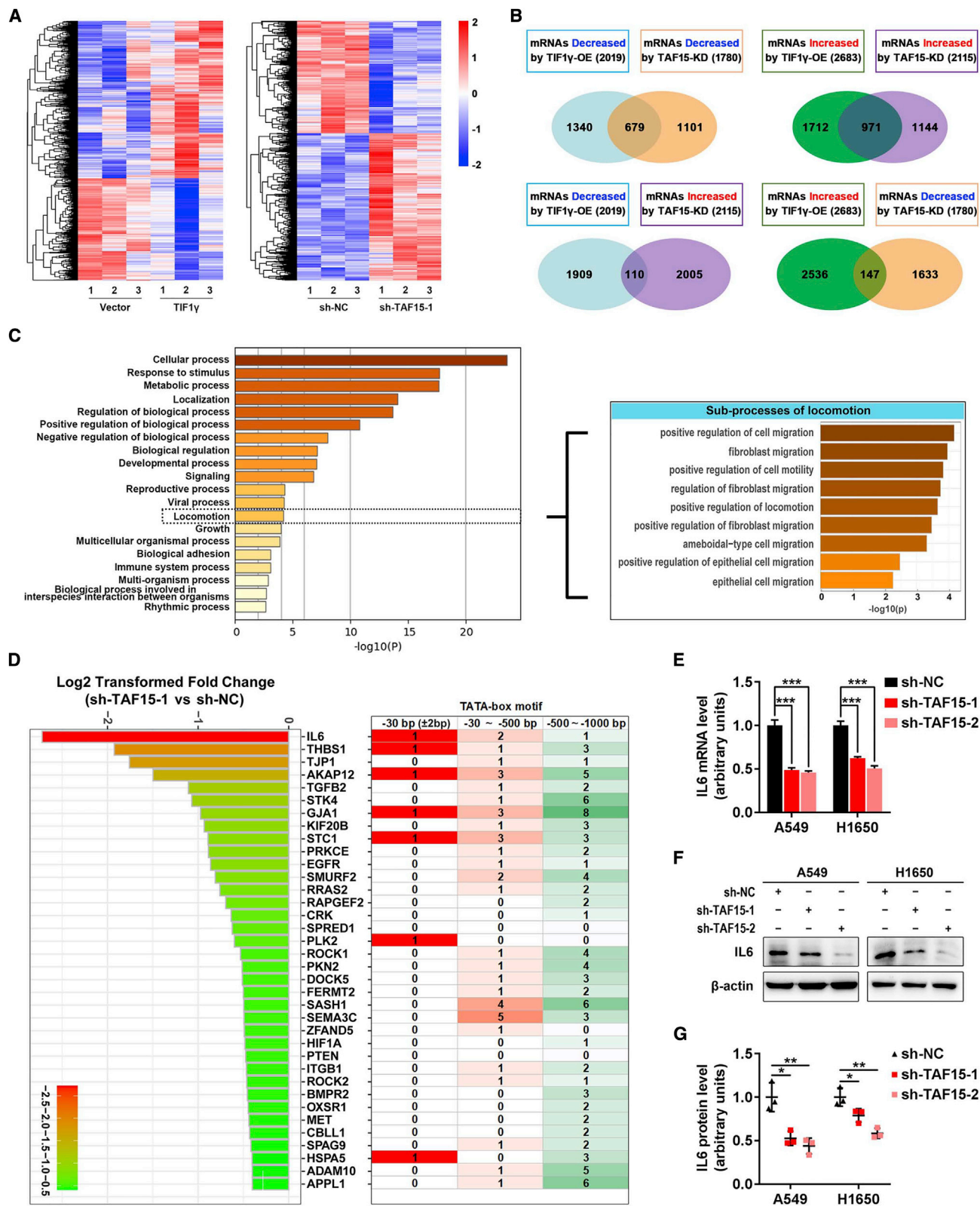
3 mm (left panel). Also shown is a comparison of lung metastatic nodules between the TAF15-silenced group and control group (right panel). Data are shown as the mean  $\pm$  SD. \* $p$  < 0.05 by unpaired Student's  $t$  test.

(E) Lung or liver micrometastases were histologically evaluated using H&E staining. Green arrowheads denote the corresponding micrometastases (left panel). The difference in micrometastasis counts in lung or liver tissues between the TAF15-silenced group and control group ( $n$  = 10 mice per group) was analyzed by unpaired Student's  $t$  test (right panel). Data are shown as the mean  $\pm$  SD. \* $p$  < 0.05, \*\* $p$  < 0.01.

(F) qRT-PCR analysis of TAF15 mRNA levels in 62 LUAD tissues and matched adjacent N (top panel). Relative mRNA expression (T/N) of TAF15 in non-metastatic ( $n$  = 33) and metastatic ( $n$  = 29) LUAD tissue (bottom panel). Data are shown as the mean  $\pm$  SD ( $n$  = 2). \* $p$  < 0.05 by paired Student's  $t$  test (top panel) or unpaired Student's  $t$  test (bottom panel).

(G) Kaplan-Meier survival curves (<http://kmplot.com/analysis/>) of individuals with LUAD ( $n$  = 719) with TAF15 high or low expression. Log rank test was used to compare differences between two groups.





(legend on next page)

ubiquitination of TAF15 compared with the RBCC domain (Figure 4F), suggesting a predominant role of TIF1 $\gamma$ 's RBCC in TAF15 ubiquitination. We also identified that the M-containing domain of TIF1 $\gamma$  was able to interact with TBP (Figure 3C), but TIF1 $\gamma$  failed to ubiquitylate TBP (Figure 3E). M-containing domains of TIF1 $\gamma$  diminished the binding capability of TAF15 with TBP (Figure 3F), supporting our findings that TIF1 $\gamma$  binds TBP in competition with TAF15 (Figures 2K and 2M). He et al. (2006) found previously that the M domain of TIF1 $\gamma$  inhibited SMAD4-SMAD2/3 interaction, suggesting that TIF1 $\gamma$  and SMAD4 competitively share SMAD2/3 (He et al., 2006). Prior to this report, it was unknown whether TIF1 $\gamma$  can competitively interact with other proteins in the nucleus. Therefore, TIF1 $\gamma$  acts as a competitor to different TFs or cofactors.

The structural mechanisms of stepwise TFIID-based preinitiation complex (PIC) assembly and specific loading of TBP by TFIID onto core promoters have been well elucidated (Chen et al., 2021; He et al., 2013; Patel et al., 2018). However, as a specific TBP-associated factor, TAF15 is different from the 13 best-known TAFs that constitute TFIID. TAF15 shares extensive sequence similarity with the pro-oncoproteins TLS/FUS and EWS, associated with TFIID and RNA polymerase II (Bertolotti et al., 1996, 1998). Particularly, the N terminus of TAF15 was identified to exhibit transactivation and oncogenic properties (Bertolotti et al., 1999). Our present study indicates that TAF15 significantly promotes EMT and metastasis of LUAD cells (Figure 5 and S1), highlighting the oncogenic role of TAF15 in cancer progression. TAF15-promoted EMT and cell invasion of LUAD cells were reversed by TIF1 $\gamma$  overexpression, and depletion of TAF15 abolished the inhibitory effects of TIF1 $\gamma$  on EMT and invasion (Figure S2). This indicates that TAF15 is required for TIF1 $\gamma$ 's function in LUAD cells.

Although we discovered the novel mechanism whereby TIF1 $\gamma$  competes with TAF15 for binding to TBP, it needs to be addressed how TIF1 $\gamma$ -TAF15/TBP interaction regulates downstream target genes associated with EMT and invasion of LUAD cells. We identified that IL-6 was controlled by this interplay in LUAD cells (Figure 6). IL-6, a pleiotropic cytokine, is of high importance in cancer development and progression (Jin, 2020; Taniguchi and Karin, 2014). We found previously that IL-6 synergistically promotes TGF- $\beta$ -induced EMT and invasion in LUAD cells (Liu et al., 2014). Here we verified the

crucial roles of IL-6 in promoting EMT and invasion of LUAD cells (Figures S4I–S4K). More importantly, we found that TIF1 $\gamma$  inhibited TAF15-dependent expression of IL-6 (Figures S4F and S4G) and that promotion of IL-6 transcriptional activity by TAF15 requires TBP (Figures 7 and S5). Our findings suggest that TAF15 functions as a transactivation factor not by directly recognizing specific TATA box elements (position –30) of the IL-6 gene promoter but by indirectly interacting with the TATA box binding protein (i.e., TBP). However, we could not exclude the possibility that TAF15 may enhance the association between TFIID-based PIC and multiple transcriptional factors binding to distinct *cis*-regulatory elements of the IL-6 gene, including nuclear factor  $\kappa$ B (NF- $\kappa$ B) and C/EBP (Dendorfer et al., 1994; Faggioli et al., 2004; Libermann and Baltimore, 1990). In fact, the TATA box has been confirmed to be located approximately 30 bp upstream of the TSS in various human core promoters, including the IL-6 promoter (Faggioli et al., 2004; O'Shea-Greenfield and Smale, 1992). Although two additional potential TATA box elements (positions –446 and –272) on the IL-6 promoter were analyzed in our study, they were not able to affect the transcriptional activity of the IL-6 promoter in the presence of TBP or TAF15.

EMT has long been considered a binary conversion process involving two types of cells (i.e., epithelial and mesenchymal cells). Recently, increasing evidence indicates that a hybrid EMT state is common in various cancer cell lines and presents the highest metastatic potential (George et al., 2017; Jolly et al., 2015; Pastushenko and Blanpain, 2019). Here we found that E-cadherin and N-cadherin were present in all situations rather than one of them being completely absent or present. However, it is unknown whether there are distinct cell populations with multiple EMT statuses for each cell line. We performed confocal microscopy to detect E-cadherin and N-cadherin in A549 and H1650 cells and observed that both proteins were co-expressed in most of the cells, exhibiting high homogeneity (Figure S6A). By analyzing RNA-seq data from a public database, we found that the E-cadherin mRNA level was lower than that of N-cadherin in A549 cells, suggesting that A549 cells are more predisposed to the mesenchymal state (Figure S6B). By collecting MS-based data from a published study, we summarized that H1650 cells exhibit an epithelial status with higher E-cadherin expression (Figure S6C; Schliekelman et al., 2015). Therefore, it is a possibility that

#### Figure 6. IL-6 is a potential downstream target gene regulated by TIF1 $\gamma$ -TAF15 interaction

(A) Total RNA isolated from TIF1 $\gamma$ -overexpressing or TAF15-silenced A549 cells was subjected to RNA-seq analysis as described in STAR Methods. Hierarchical cluster analysis (heatmap) was employed to show DEGs with a fold change of 1.3 or greater and a *q* value of less than 0.05. Three independent samples were tested in each group. Each column and row indicates a test sample and a mRNA, respectively. Red and blue denote high and low mRNA expression, respectively. (B) Venn diagrams were used to depict the overlap between two datasets. Light blue and green circles represent decreased and increased mRNAs in TIF1 $\gamma$ -overexpressing A549 cells, respectively. Orange and purple represent decreased and increased mRNAs in TAF15-silenced A549 cells, respectively. The numbers of DEGs are indicated in rectangles. (C) GO enrichment analysis (<https://metascape.org>) showing the top 20 significant biological processes (BPs) where 679 candidate mRNAs simultaneously inactivated by TIF1 $\gamma$  overexpression and TAF15 silencing (B) were enriched (left panel). Multiple sub-processes included in one BP, "locomotion," were associated with cell migration (right panel). (D) Schematic presenting 36 genes enriched in the BP "locomotion" and listed according to the log2-transformed fold change. IL-6 ranks first among 36 down-regulated genes in TAF15-silenced A549 cells (left panel). The Eukaryotic Promoter Database (<https://epd.epfl.ch/index.php>) was utilized to predict the TATA box motif within 1,000 bp upstream of the TSS of the indicated genes (right panel). (E–G) qRT-PCR, western blot, and ELISA assays were performed to examine the expression of IL-6 mRNA, protein, and protein secretion levels in TAF15-silenced A549 and H1650 cells. Data are shown as the mean  $\pm$  SD (*n* = 3). \**p* < 0.05, \*\**p* < 0.01, \*\*\**p* < 0.001 by unpaired Student's *t* test.

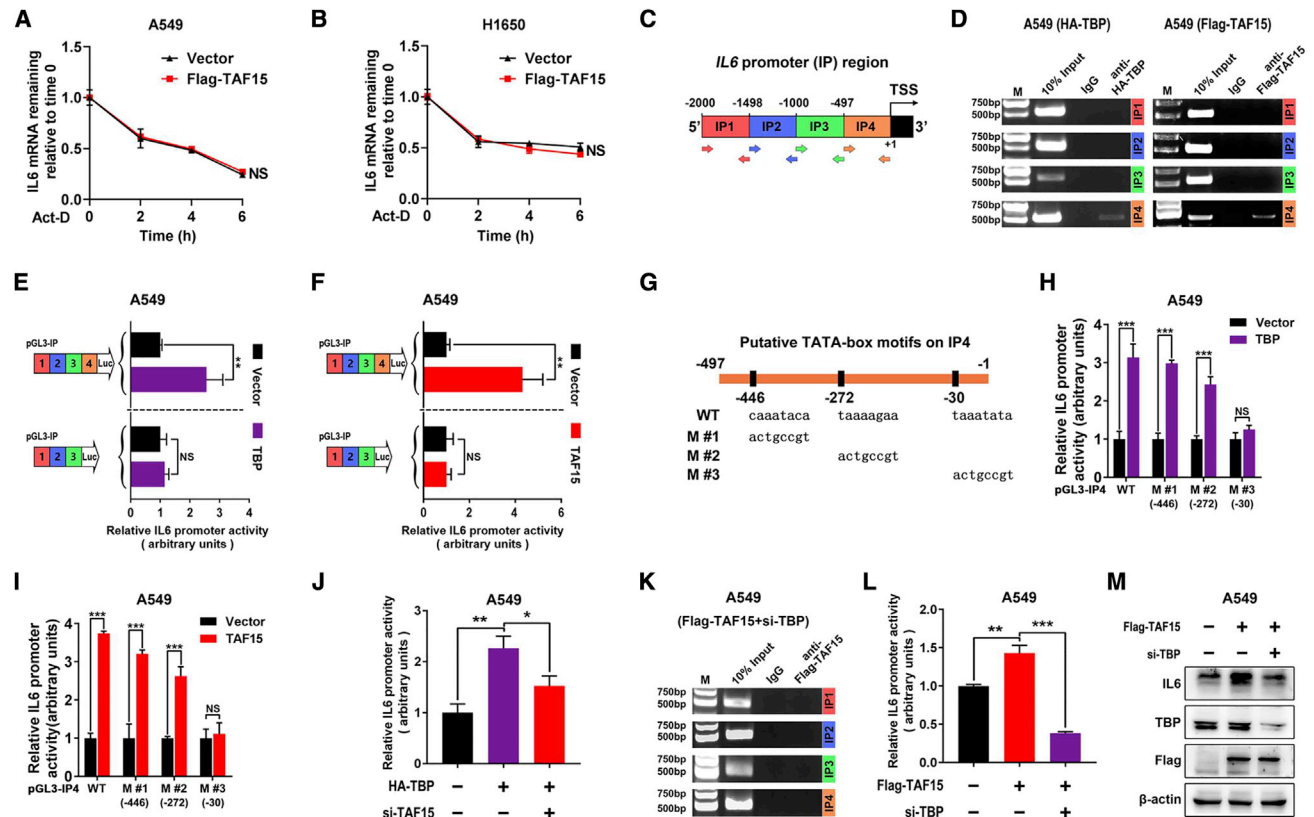


**Figure 7. Transactivation of IL-6 by TAF15 depends on TBP**

(A and B) IL-6 mRNA stability was evaluated in A549 and H1650 cells transfected with FLAG-tagged TAF15 or control expression vectors. Cells were treated with Act-D (10  $\mu$ g/mL) for 0, 2, 4, or 6 h, and IL-6 mRNA levels were determined by qRT-PCR. The quantity value of qRT-PCR at 0 h was set to 1. Statistical analysis was conducted using unpaired Student's t test ( $n = 3$ ).

(C) Schematic of the IL-6 promoter region (position -2,000 to +1). Locations of each pair of primers for amplification of the IP1, IP2, IP3, and IP4 regions are indicated below. TSS, transcription start site; IP, IL-6 promoter.

(D) HA-tagged TBP- or FLAG-tagged TAF15-overexpressing A549 cells were subjected to ChIP analysis, in which anti-HA or anti-FLAG antibodies were used. Before IP, 10% input was used as a positive control to confirm the fragments containing the IP1, IP2, IP3, or IP4 regions. Anti-IgG antibody served as a negative control. The immunoprecipitated DNA fragments were subjected to PCR and gel staining analyses to detect the enrichment of IP1, IP2, IP3, or IP4 regions.

(E and F) Two different pGL3 luciferase reporter constructs (pGL3-IP1~4 and pGL3-IP1~3) were transiently transfected into HA-tagged TBP- or FLAG-tagged TAF15-overexpressing and control A549 cells for 48 h, and then their luciferase activity was measured as described in STAR Methods. Data are shown as the mean  $\pm$  SD ( $n = 3$ ). \*\* $p < 0.01$  compared with empty vector by unpaired Student's t test.

(G) Schematic showing the locations of three potential TATA box sites (positions -446, -272, and -30) in the IP4 region. The WT and mutant of each putative TATA box sequence are indicated below. M, mutant.

(H and I) Four pGL3-IP4 luciferase reporter plasmids containing the abovementioned TATA box motifs (G) were transfected into A549 cell lines overexpressing HA-tagged TBP or FLAG-tagged TAF15 for 48 h, and then their luciferase activity was determined. Data are shown as the mean  $\pm$  SD ( $n = 3$ ). \*\*\* $p < 0.001$  by unpaired Student's t test.

(J) The luciferase reporter plasmids (pGL3-IP1~4) were transfected into HA-tagged TBP-overexpressing A549 cells, which were then co-transfected with si-TAF15 as indicated. The luciferase activity of pGL3-IP1~4 was measured as above. Data are shown as the mean  $\pm$  SD ( $n = 3$ ). \* $p < 0.05$ , \*\* $p < 0.01$  by unpaired Student's t test.

(K) Anti-FLAG ChIP analysis was performed in FLAG-tagged TAF15-overexpressing A549 cells transfected with si-TBP. The assessment of IL-6 promoter fragments (IP1, IP2, IP3, and IP4) enrichment was performed as described above.

(L) The luciferase reporter plasmids (pGL3-IP1~4) were transfected into FLAG-TAF15-overexpressing A549 cells, which were then co-transfected with si-TBP as indicated. The luciferase activity was determined as above. Data are shown as the mean  $\pm$  SD ( $n = 3$ ). \*\* $p < 0.01$ , \*\*\* $p < 0.001$  by unpaired Student's t test.

(M) Western blot analysis of IL-6, TBP, and FLAG protein levels in FLAG-tagged TAF15-overexpressing A549 cells co-transfected with si-TBP.  $\beta$ -Actin served as an internal control.

TIF1 $\gamma$  overexpression or TAF15 deficiency drives A549 cells to enter a hybrid or even an epithelial state while enhancing the epithelial phenotype of H1650 cells.

Our findings reveal a novel mechanism by which TIF1 $\gamma$  interacts with TAF15/TBP-IL-6 to repress EMT and metastasis of LUAD

cells, and improve our understanding of the function of TIF1 $\gamma$  in restricting TAF15/TBP complex-dependent transcription initiation. The regulatory mechanisms of different functional domains of TIF1 $\gamma$  strategically provide potential clues for treatment of metastatic LUADs.

## Limitations of the study

In this study, although our findings show that TIF1 $\gamma$  interacts with TAF15, the interaction will be strengthened when several assays, such as glutathione S-transferase (GST) pull-down, are performed *in vitro*. Nevertheless, we believe that TIF1 $\gamma$  can directly interact with TAF15 because our results reveal a direct interaction between the RBCC domain of TIF1 $\gamma$  and TAF15, leading to TAF15 multi-mono-ubiquitylation. On the other hand, we cannot be sure whether TAF15 interacts directly with TBP or indirectly with TBP via other TAFs that comprise the TFIID complex, which is definitely worth further investigation.

## STAR★METHODS

Detailed methods are provided in the online version of this paper and include the following:

- KEY RESOURCES TABLE
- RESOURCE AVAILABILITY
  - Lead contact
  - Materials availability
  - Data and code availability
- EXPERIMENTAL MODEL AND SUBJECT DETAILS
  - Cell culture
  - *In vivo* metastasis assays
  - Human LUAD and LUSC tissue specimens
- METHOD DETAILS
  - Gene set enrichment analysis (GSEA)
  - Mass spectrometry assay
  - Construction of vectors
  - Generation of stable cell lines
  - RNA interference
  - Western blot analysis
  - Protein silver-staining assay
  - Real-time quantitative reverse transcriptase PCR (qRT-PCR) and mRNA half-life assays
  - Co-immunoprecipitation (Co-IP)
  - Immunofluorescence analysis
  - Chromatin immunoprecipitation (ChIP)
  - Transwell migration and invasion assays
  - Wound-healing migration assay
  - RNA-seq analysis
  - Enzyme-linked immunosorbent assay (ELISA)
  - Luciferase reporter assay
  - Gene ontology (GO) analysis
- QUANTIFICATION AND STATISTICAL ANALYSIS

## SUPPLEMENTAL INFORMATION

Supplemental information can be found online at <https://doi.org/10.1016/j.celrep.2022.111513>.

## ACKNOWLEDGMENTS

We are grateful for participation and cooperation from individuals with NSCLC. This work was supported in part by the National Natural Science Foundation of China (82273372, 82073198, 81872343, and 81972174), the Suzhou Key Laboratory for Molecular Cancer Genetics (SZS201209), and the Project funded by the Priority Academic Program Development of Jiangsu Higher Education Institutions (PAPD).

## AUTHOR CONTRIBUTIONS

Z. Su, Z. Sun, Z.W., S.W., Z. Lei, and H.-T.Z. designed the research. Z. Su, Z. Sun, Z.W., S.W., Yuxin Wang, and E.J. performed the majority of experiments and analyzed data. C.L., J.Z., and Z. Liu contributed to clinical samples and reagents. Z.Z., E.J., Yong Wang, X.C., and X.L. conducted several experiments. Z. Su, Z. Lei, and H.-T.Z. wrote and edited the manuscript. H.-T.Z. supervised the study.

## DECLARATION OF INTERESTS

The authors declare no competing interests.

Received: April 25, 2022

Revised: August 24, 2022

Accepted: September 26, 2022

Published: October 18, 2022

## REFERENCES

- Agricola, E., Randall, R.A., Gaarenstroom, T., Dupont, S., and Hill, C.S. (2011). Recruitment of TIF1gamma to chromatin via its PHD finger-bromodomain activates its ubiquitin ligase and transcriptional repressor activities. *Mol. Cell* 43, 85–96. <https://doi.org/10.1016/j.molcel.2011.05.020>.
- Andersson, M.K., Ståhlberg, A., Arvidsson, Y., Olofsson, A., Semb, H., Stenman, G., Nilsson, O., and Aman, P. (2008). The multifunctional FUS, EWS and TAF15 proto-oncoproteins show cell type-specific expression patterns and involvement in cell spreading and stress response. *BMC Cell Biol.* 9, 37. <https://doi.org/10.1186/1471-2121-9-37>.
- Babaei, G., Aziz, S.G.G., and Jaghi, N.Z.Z. (2021). EMT, cancer stem cells and autophagy; the three main axes of metastasis. *Biomed. Pharmacother.* 133, 110909. <https://doi.org/10.1016/j.biopha.2020.110909>.
- Bai, X., Kim, J., Yang, Z., Jurynek, M.J., Akie, T.E., Lee, J., LeBlanc, J., Sessa, A., Jiang, H., DiBiase, A., et al. (2010). TIF1gamma controls erythroid cell fate by regulating transcription elongation. *Cell* 142, 133–143. <https://doi.org/10.1016/j.cell.2010.05.028>.
- Bakir, B., Chiarella, A.M., Pitarresi, J.R., and Rustgi, A.K. (2020). EMT, MET, plasticity, and tumor metastasis. *Trends Cell Biol.* 30, 764–776. <https://doi.org/10.1016/j.tcb.2020.07.003>.
- Bell, B., and Tora, L. (1999). Regulation of gene expression by multiple forms of TFIID and other novel TAFII-containing complexes. *Exp. Cell Res.* 246, 11–19. <https://doi.org/10.1006/excr.1998.4294>.
- Bertolotti, A., Bell, B., and Tora, L. (1999). The N-terminal domain of human TAFII68 displays transactivation and oncogenic properties. *Oncogene* 18, 8000–8010. <https://doi.org/10.1038/sj.onc.1203207>.
- Bertolotti, A., Lutz, Y., Heard, D.J., Chambon, P., and Tora, L. (1996). hTAF(II) 68, a novel RNA/ssDNA-binding protein with homology to the pro-oncoproteins TLS/FUS and EWS is associated with both TFIID and RNA polymerase II. *EMBO J.* 15, 5022–5031.
- Bertolotti, A., Melot, T., Acker, J., Vigneron, M., Delattre, O., and Tora, L. (1998). EWS, but not EWS-FLI-1, is associated with both TFIID and RNA polymerase II: interactions between two members of the TET family, EWS and hTAFII68, and subunits of TFIID and RNA polymerase II complexes. *Mol. Cell Biol.* 18, 1489–1497. <https://doi.org/10.1128/MCB.18.3.1489>.
- Boutanquoi, P.M., Burgy, O., Beltramo, G., Bellaye, P.S., Dondaine, L., Marcion, G., Pommerolle, L., Vadel, A., Spanjaard, M., Demidov, O., et al. (2020). TRIM33 prevents pulmonary fibrosis by impairing TGF-beta1 signaling. *Eur. Respir. J.* 55, 1901346. <https://doi.org/10.1183/13993003.01346-2019>.
- Chaffer, C.L., San Juan, B.P., Lim, E., and Weinberg, R.A. (2016). EMT, cell plasticity and metastasis. *Cancer Metastasis Rev.* 35, 645–654. <https://doi.org/10.1007/s10555-016-9648-7>.



- Chen, W., Zheng, R., Baade, P.D., Zhang, S., Zeng, H., Bray, F., Jemal, A., Yu, X.Q., and He, J. (2016). Cancer statistics in China, 2015. *CA. Cancer J. Clin.* 66, 115–132. <https://doi.org/10.3322/caac.21338>.
- Chen, X., Qi, Y., Wu, Z., Wang, X., Li, J., Zhao, D., Hou, H., Li, Y., Yu, Z., Liu, W., et al. (2021). Structural insights into preinitiation complex assembly on core promoters. *Science* 372, eaba8490. <https://doi.org/10.1126/science.aba8490>.
- De Craene, B., and Berx, G. (2013). Regulatory networks defining EMT during cancer initiation and progression. *Nat. Rev. Cancer* 13, 97–110. <https://doi.org/10.1038/nrc3447>.
- Dendorfer, U., Oettgen, P., and Libermann, T.A. (1994). Multiple regulatory elements in the interleukin-6 gene mediate induction by prostaglandins, cyclic AMP, and lipopolysaccharide. *Mol. Cell Biol.* 14, 4443–4454. <https://doi.org/10.1128/mcb.14.7.4443-4454.1994>.
- Ding, Z.Y., Jin, G.N., Wang, W., Chen, W.X., Wu, Y.H., Ai, X., Chen, L., Zhang, W.G., Liang, H.F., Laurence, A., et al. (2014). Reduced expression of transcriptional intermediary factor 1 gamma promotes metastasis and indicates poor prognosis of hepatocellular carcinoma. *Hepatology* 60, 1620–1636. <https://doi.org/10.1002/hep.27273>.
- Dreos, R., Ambrosini, G., Périer, R.C., and Bucher, P. (2015). The Eukaryotic Promoter Database: expansion of EPDnew and new promoter analysis tools. *Nucleic Acids Res.* 43, D92–D96. <https://doi.org/10.1093/nar/gku1111>.
- Dupont, S., Mamidi, A., Cordenonsi, M., Montagner, M., Zacchigna, L., Adorno, M., Martello, G., Stinchfield, M.J., Soligo, S., Morsut, L., et al. (2009). FAM/USP9x, a deubiquitinating enzyme essential for TGFbeta signaling, controls Smad4 monoubiquitination. *Cell* 136, 123–135. <https://doi.org/10.1016/j.cell.2008.10.051>.
- Faggioli, L., Costanzo, C., Donadelli, M., and Palmieri, M. (2004). Activation of the Interleukin-6 promoter by a dominant negative mutant of c-Jun. *Biochim. Biophys. Acta* 1692, 17–24. <https://doi.org/10.1016/j.bbamcr.2004.03.001>.
- Ferri, F., Petit, V., Barroca, V., and Romeo, P.H. (2019). Interplay between FACT subunit SPT16 and TRIM33 can remodel chromatin at macrophage distal regulatory elements. *Epigenet. Chromatin* 12, 46. <https://doi.org/10.1186/s13072-019-0288-3>.
- Fulda, S., Rajalingam, K., and Dikic, I. (2012). Ubiquitylation in immune disorders and cancer: from molecular mechanisms to therapeutic implications. *EMBO Mol. Med.* 4, 545–556. <https://doi.org/10.1002/emmm.201100707>.
- George, J.T., Jolly, M.K., Xu, S., Somarelli, J.A., and Levine, H. (2017). Survival outcomes in cancer patients predicted by a partial EMT gene expression scoring metric. *Cancer Res.* 77, 6415–6428. <https://doi.org/10.1158/0008-5472.CAN-16-3521>.
- Gupta, G.P., and Massagué, J. (2006). Cancer metastasis: building a framework. *Cell* 127, 679–695. <https://doi.org/10.1016/j.cell.2006.11.001>.
- He, W., Dorn, D.C., Erdjument-Bromage, H., Tempst, P., Moore, M.A.S., and Massagué, J. (2006). Hematopoiesis controlled by distinct TIF1gamma and Smad4 branches of the TGFbeta pathway. *Cell* 125, 929–941. <https://doi.org/10.1016/j.cell.2006.03.045>.
- He, Y., Fang, J., Taatjes, D.J., and Nogales, E. (2013). Structural visualization of key steps in human transcription initiation. *Nature* 495, 481–486. <https://doi.org/10.1038/nature11991>.
- Herquel, B., Ouararhni, K., Khetchoumian, K., Ignat, M., Teletin, M., Mark, M., Béchade, G., Van Dorsselaer, A., Sanglier-Cianféron, S., Hamiche, A., et al. (2011). Transcription cofactors TRIM24, TRIM28, and TRIM33 associate to form regulatory complexes that suppress murine hepatocellular carcinoma. *Proc. Natl. Acad. Sci. USA* 108, 8212–8217. <https://doi.org/10.1073/pnas.1101544108>.
- Hershko, A., and Ciechanover, A. (1998). The ubiquitin system. *Annu. Rev. Biochem.* 67, 425–479. <https://doi.org/10.1146/annurev.biochem.67.1.425>.
- Hu, H., Miao, Y.R., Jia, L.H., Yu, Q.Y., Zhang, Q., and Guo, A.Y. (2019). AnimalTFDB 3.0: a comprehensive resource for annotation and prediction of animal transcription factors. *Nucleic Acids Res.* 47, D33–D38. <https://doi.org/10.1093/nar/gky822>.
- Jin, W. (2020). Role of JAK/STAT3 signaling in the regulation of metastasis, the transition of cancer stem cells, and chemoresistance of cancer by epithelial-mesenchymal transition. *Cells* 9. <https://doi.org/10.3390/cells9010217>.
- Jingushi, K., Ueda, Y., Kitae, K., Hase, H., Egawa, H., Ohshio, I., Kawakami, R., Kashiwagi, Y., Tsukada, Y., Kobayashi, T., et al. (2015). miR-629 targets TRIM33 to promote TGFbeta/smad signaling and metastatic phenotypes in ccRCC. *Mol. Cancer Res.* 13, 565–574. <https://doi.org/10.1158/1541-7786.MCR-14-0300>.
- Jolly, M.K., Boareto, M., Huang, B., Jia, D., Lu, M., Ben-Jacob, E., Onuchic, J.N., and Levine, H. (2015). Implications of the hybrid epithelial/mesenchymal phenotype in metastasis. *Front. Oncol.* 5, 155. <https://doi.org/10.3389/fonc.2015.00155>.
- Kassem, L., Deygas, M., Fattet, L., Lopez, J., Goulvent, T., Lavergne, E., Chabaud, S., Carrabin, N., Chopin, N., Bachelot, T., et al. (2015). TIF1 gamma interferes with TGFbeta1/SMAD4 signaling to promote poor outcome in operable breast cancer patients. *BMC Cancer* 15, 453. <https://doi.org/10.1186/s12885-015-1471-y>.
- Kuhn, E., Morbini, P., Cancellieri, A., Damiani, S., Cavazza, A., and Comin, C.E. (2018). Adenocarcinoma classification: patterns and prognosis. *Pathologica* 110, 5–11.
- Lánczky, A., and Györfy, B. (2021). Web-based survival analysis tool tailored for medical research (KMplot): development and implementation. *J. Med. Internet Res.* 23, e27633. <https://doi.org/10.2196/27633>.
- Lei, Z., Xu, G., Wang, L., Yang, H., Liu, X., Zhao, J., and Zhang, H.T. (2014). MiR-142-3p represses TGF-beta-induced growth inhibition through repression of TGFbetaR1 in non-small cell lung cancer. *FASEB J.* 28, 2696–2704. <https://doi.org/10.1096/fj.13-247288>.
- Leichter, M., Marko, M., Ganou, V., Patrino-Georgoula, M., Tora, L., and Guialis, A. (2011). A fraction of the transcription factor TAF15 participates in interactions with a subset of the spliceosomal U1 snRNP complex. *Biochim. Biophys. Acta* 1814, 1812–1824. <https://doi.org/10.1016/j.bbapap.2011.09.008>.
- Libermann, T.A., and Baltimore, D. (1990). Activation of interleukin-6 gene expression through the NF-kappa B transcription factor. *Mol. Cell Biol.* 10, 2327–2334. <https://doi.org/10.1128/mcb.10.5.2327-2334.1990>.
- Ligr, M., Wu, X., Daniels, G., Zhang, D., Wang, H., Hajdu, C., Wang, J., Pan, R., Pei, Z., Zhang, L., et al. (2014). Imbalanced expression of Tif1gamma inhibits pancreatic ductal epithelial cell growth. *Am. J. Cancer Res.* 4, 196–210.
- Liu, R.Y., Zeng, Y., Lei, Z., Wang, L., Yang, H., Liu, Z., Zhao, J., and Zhang, H.T. (2014). JAK/STAT3 signaling is required for TGF-beta-induced epithelial-mesenchymal transition in lung cancer cells. *Int. J. Oncol.* 44, 1643–1651. <https://doi.org/10.3892/ijo.2014.2310>.
- McAvera, R.M., and Crawford, L.J. (2020). TIF1 proteins in genome stability and cancer. *Cancers* 12, E2094. <https://doi.org/10.3390/cancers12082094>.
- Mootha, V.K., Lindgren, C.M., Eriksson, K.F., Subramanian, A., Sihag, S., Lehar, J., Puigserver, P., Carlsson, E., Ridderstråle, M., Laurila, E., et al. (2003). PGC-1alpha-responsive genes involved in oxidative phosphorylation are coordinately downregulated in human diabetes. *Nat. Genet.* 34, 267–273. <https://doi.org/10.1038/ng1180>.
- Nieto, M.A., Huang, R.Y.J., Jackson, R.A., and Thiery, J.P. (2016). EMT: 2016. *Cell* 166, 21–45. <https://doi.org/10.1016/j.cell.2016.06.028>.
- O'Shea-Greenfield, A., and Smale, S.T. (1992). Roles of TATA and initiator elements in determining the start site location and direction of RNA polymerase II transcription. *J. Biol. Chem.* 267, 1391–1402.
- Oshikawa, K., Matsumoto, M., Oyama, K., and Nakayama, K.I. (2012). Proteome-wide identification of ubiquitylation sites by conjugation of engineered lysine-less ubiquitin. *J. Proteome Res.* 11, 796–807. <https://doi.org/10.1021/pr200668y>.
- Pastushenko, I., and Blanpain, C. (2019). EMT transition states during tumor progression and metastasis. *Trends Cell Biol.* 29, 212–226. <https://doi.org/10.1016/j.tcb.2018.12.001>.
- Patel, A.B., Louder, R.K., Greber, B.J., Grünberg, S., Luo, J., Fang, J., Liu, Y., Ranish, J., Hahn, S., and Nogales, E. (2018). Structure of human TFIID and

- p>mechanism of TBP loading onto promoter DNA.
- Science*
- 362, eaau8872.
- <https://doi.org/10.1126/science.aau8872>
- .
- Petit, V., Parcelier, A., Mathé, C., Barroca, V., Torres, C., Lewandowski, D., Ferri, F., Gallouët, A.S., Dalloz, M., Dinét, O., et al. (2019). TRIM33 deficiency in monocytes and macrophages impairs resolution of colonic inflammation. *EBioMedicine* 44, 60–70. <https://doi.org/10.1016/j.ebiom.2019.05.037>.
- Qi, G., Lu, G., Yu, J., Zhao, Y., Wang, C., Zhang, H., and Xia, Q. (2019). Up-regulation of TIF1gamma by valproic acid inhibits the epithelial mesenchymal transition in prostate carcinoma through TGF-beta/Smad signaling pathway. *Eur. J. Pharmacol.* 860, 172551. <https://doi.org/10.1016/j.ejphar.2019.172551>.
- Quéré, R., Saint-Paul, L., Carmignac, V., Martin, R.Z., Chrétien, M.L., Largeot, A., Hammann, A., Pais de Barros, J.P., Bastie, J.N., and Delva, L. (2014). Tif1-gamma regulates the TGF-beta1 receptor and promotes physiological aging of hematopoietic stem cells. *Proc. Natl. Acad. Sci. USA* 111, 10592–10597. <https://doi.org/10.1073/pnas.1405546111>.
- Ren, P., Xing, L., Hong, X., Chang, L., and Zhang, H. (2020). LncRNA PITPNA-AS1 boosts the proliferation and migration of lung squamous cell carcinoma cells by recruiting TAF15 to stabilize HMGB3 mRNA. *Cancer Med.* 9, 7706–7716. <https://doi.org/10.1002/cam4.3268>.
- Schliekelman, M.J., Taguchi, A., Zhu, J., Dai, X., Rodriguez, J., Celiktas, M., Zhang, Q., Chin, A., Wong, C.H., Wang, H., et al. (2015). Molecular portraits of epithelial, mesenchymal, and hybrid States in lung adenocarcinoma and their relevance to survival. *Cancer Res.* 75, 1789–1800. <https://doi.org/10.1158/0008-5472.CAN-14-2535>.
- Siegel, R.L., Miller, K.D., and Jemal, A. (2016). Cancer statistics, 2016. *CA. Cancer J. Clin.* 66, 7–30. <https://doi.org/10.3322/caac.21332>.
- Singh, A.K., Kapoor, V., Thotala, D., and Hallahan, D.E. (2020). TAF15 contributes to the radiation-inducible stress response in cancer. *Oncotarget* 11, 2647–2659. <https://doi.org/10.18632/oncotarget.27663>.
- Subramanian, A., Tamayo, P., Mootha, V.K., Mukherjee, S., Ebert, B.L., Gillette, M.A., Paulovich, A., Pomeroy, S.L., Golub, T.R., Lander, E.S., and Mesirov, J.P. (2005). Gene set enrichment analysis: a knowledge-based approach for interpreting genome-wide expression profiles. *Proc. Natl. Acad. Sci. USA* 102, 15545–15550. <https://doi.org/10.1073/pnas.0506580102>.
- Suhail, Y., Cain, M.P., Vanaja, K., Kurywchak, P.A., Levchenko, A., Kalluri, R., and Kshitiz. (2019). Systems biology of cancer metastasis. *Cell Syst.* 9, 109–127. <https://doi.org/10.1016/j.cels.2019.07.003>.
- Taniguchi, K., and Karin, M. (2014). IL-6 and related cytokines as the critical lymphins between inflammation and cancer. *Semin. Immunol.* 26, 54–74. <https://doi.org/10.1016/j.smim.2014.01.001>.
- Tong, X., Wang, S., Lei, Z., Li, C., Zhang, C., Su, Z., Liu, X., Zhao, J., and Zhang, H.T. (2020). MYOCD and SMAD3/SMAD4 form a positive feedback loop and drive TGF-beta-induced epithelial-mesenchymal transition in non-small cell lung cancer. *Oncogene* 39, 2890–2904. <https://doi.org/10.1038/s41388-020-1189-4>.
- Venturini, L., You, J., Stadler, M., Galien, R., Lallemand, V., Koken, M.H., Mattei, M.G., Ganser, A., Chambon, P., Losson, R., and de Thé, H. (1999). TIF1-gamma, a novel member of the transcriptional intermediary factor 1 family. *Oncogene* 18, 1209–1217. <https://doi.org/10.1038/sj.onc.1202655>.
- Vincent, D.F., Yan, K.P., Treilleux, I., Gay, F., Arfi, V., Kaniewski, B., Kaniewski, B., Marie, J.C., Lepinasse, F., Martel, S., et al. (2009). Inactivation of TIF1-gamma cooperates with Kras to induce cystic tumors of the pancreas. *PLoS Genet.* 5, e1000575. <https://doi.org/10.1371/journal.pgen.1000575>.
- Wang, L., Tong, X., Zhou, Z., Wang, S., Lei, Z., Zhang, T., Liu, Z., Zeng, Y., Li, C., Zhao, J., et al. (2018). Circular RNA hsa\_circ\_0008305 (circPTK2) inhibits TGF-beta-induced epithelial-mesenchymal transition and metastasis by controlling TIF1gamma in non-small cell lung cancer. *Mol. Cancer* 17, 140. <https://doi.org/10.1186/s12943-018-0889-7>.
- Wang, L., Yang, H., Lei, Z., Zhao, J., Chen, Y., Chen, P., Li, C., Zeng, Y., Liu, Z., Liu, X., and Zhang, H.T. (2016). Repression of TIF1gamma by SOX2 promotes TGF-beta-induced epithelial-mesenchymal transition in non-small-cell lung cancer. *Oncogene* 35, 867–877. <https://doi.org/10.1038/nc.2015.141>.
- Williams, E.D., Gao, D., Redfern, A., and Thompson, E.W. (2019). Controversies around epithelial-mesenchymal plasticity in cancer metastasis. *Nat. Rev. Cancer* 19, 716–732. <https://doi.org/10.1038/s41568-019-0213-x>.
- Xu, Y., Wu, G., Zhang, J., Li, J., Ruan, N., Zhang, J., Zhang, Z., Chen, Y., Zhang, Q., and Xia, Q. (2020). TRIM33 overexpression inhibits the progression of clear cell renal cell carcinoma in vivo and in vitro. *BioMed Res. Int.* 2020, 8409239. <https://doi.org/10.1155/2020/8409239>.
- Xue, J., Chen, Y., Wu, Y., Wang, Z., Zhou, A., Zhang, S., Lin, K., Aldape, K., Majumder, S., Lu, Z., and Huang, S. (2015). Tumour suppressor TRIM33 targets nuclear beta-catenin degradation. *Nat. Commun.* 6, 6156. <https://doi.org/10.1038/ncomms7156>.
- Xue, J., Lin, X., Chiu, W.T., Chen, Y.H., Yu, G., Liu, M., Feng, X.H., Sawaya, R., Medema, R.H., Hung, M.C., and Huang, S. (2014). Sustained activation of SMAD3/SMAD4 by FOXM1 promotes TGF-beta-dependent cancer metastasis. *J. Clin. Invest.* 124, 564–579. <https://doi.org/10.1172/JCI71104>.
- Yu, C., Ding, Z., Liang, H., Zhang, B., and Chen, X. (2019). The roles of TIF1-gamma in cancer. *Front. Oncol.* 9, 979. <https://doi.org/10.3389/fonc.2019.00979>.
- Zhou, Y., Zhou, B., Pache, L., Chang, M., Khodabakhshi, A.H., Tanaseichuk, O., Benner, C., and Chanda, S.K. (2019). Metascape provides a biologist-oriented resource for the analysis of systems-level datasets. *Nat. Commun.* 10, 1523. <https://doi.org/10.1038/s41467-019-09234-6>.

## STAR★METHODS

### KEY RESOURCES TABLE

REAGENT or RESOURCE	SOURCE	IDENTIFIER
<b>Antibodies</b>		
Rabbit anti-TAF15	Novus Biologicals	Cat#NB100-567; RRID: AB_10001551
Rabbit anti-TIF1 $\gamma$ (Western blot)	Cell Signaling Technology (CST)	Cat#90051; RRID: AB_2800150
Rabbit anti-HA	CST	Cat#3724s; RRID: AB_1549585
Rabbit anti-Flag	CST	Cat#14793s
Rabbit anti-IgG	CST	Cat#3900; RRID: AB_1550038
Rabbit anti-TBP	CST	Cat#44059; RRID: AB_2799258
Rabbit anti-Lamin B1	CST	Cat#13435s; RRID: AB_2737428
Mouse anti-E-cadherin	BD Biosciences	Cat#610181; RRID: AB_397580
Mouse anti-N-cadherin	BD Biosciences	Cat#610920; RRID: AB_2077527
Mouse anti-IL6	Beyotime	Cat#AF0201
Mouse anti- $\beta$ -actin	AB clonal	Cat#AC004; RRID: AB_2737399
Mouse anti-TIF1 $\gamma$ (Immunofluorescence)	Santa Cruz	Cat#sc-101179; RRID: AB_1130316
Rabbit anti-TAF15 (Immunofluorescence)	AB clonal	Cat#A8465; RRID: AB_2772511
Mouse anti-E-cadherin (Immunofluorescence)	Beyotime	Cat#AF0138
Rabbit anti-N-cadherin (Immunofluorescence)	AB clonal	Cat#A0432; RRID: AB_2757188
Anti-rabbit secondary antibody	Santa Cruz	Cat#sc-2357; RRID: AB_628497
Anti-mouse secondary antibodies	Santa Cruz	Cat#sc-2005; RRID: AB_631736
FITC-conjugated anti-mouse secondary antibody	Beyotime	Cat#A0568; RRID: AB_2893016
Cy3-conjugated anti-rabbit secondary antibody	Beyotime	Cat#A0516; RRID: AB_2893015
Cy3-conjugated anti-mouse secondary antibody	Beyotime	Cat#A5021
FITC-conjugated anti-rabbit secondary antibody	Beyotime	Cat#A0562
<b>Bacterial and virus strains</b>		
pcDNA3.1-HA	(Tong et al., 2020)	N/A
pcDNA3.1-Flag	(Tong et al., 2020)	N/A
pCDH-CMV-MCS-EF1-CopGFP	Miaolingbio	Cat#P0376
GV492	Genechem Inc.	N/A
pLKO.1-puro	GENEWIZ	N/A
pCDH-CMV-MCS-EF1-CopGFP-T2A-Puro	Miaolingbio	Cat#P0268
psPAX2	(Wang et al., 2018)	N/A
pMD2.G	(Wang et al., 2018)	N/A
pGL3-basic vector	Promega	Cat#E1751
pRL-TK	Promega	Cat#E2241
DH5 $\alpha$ Competent cell	Vazyme	Cat#C502-02
<b>Biological samples</b>		
Human LUAD and LUSC tissues	The First Affiliated Hospital of Soochow University	N/A
<b>Chemicals, peptides, and recombinant proteins</b>		
Dulbecco's modified Eagle medium (DMEM)/Ham's F12	Corning	Cat#10-092-cv
Fetal bovine serum	Invitrogen	Cat#10099141
DMEM medium	Thermo Fisher Scientific	Cat#21013024
<i>NheI</i>	New England Biolabs	Cat#R0131L
<i>AgeI</i>	New England Biolabs	Cat#R0552L

(Continued on next page)

**Continued**

REAGENT or RESOURCE	SOURCE	IDENTIFIER
BamHI	New England Biolabs	Cat#R0136L
HindIII	New England Biolabs	Cat#R0104L
EcoRI	New England Biolabs	Cat#R0101L
XbaI	New England Biolabs	Cat#R0145L
T4 DNA ligase buffer	Thermo Fisher Scientific	Cat#46300018
Lipofectamine 3000	Invitrogen	Cat#L3000015
Puromycin	Solarbio	Cat#P8230
RIPA buffer	Thermo Fisher Scientific	Cat#89900
Protease inhibitor cocktail	Sangon Biotech	Cat#C600387
Phosphatase inhibitor cocktail	Sangon Biotech	Cat#C500017
Native sample loading buffer	Sangon Biotech	Cat#C506032
DTT	Sangon Biotech	Cat#B645939
TRIzol	Thermo Fisher Scientific	Cat#15596018
M-MLV (H-) Reverse Transcriptase	Vazyme	Cat#R021-01
Act-D	Sigma-Aldrich	Cat#129935
Nonidet P-40	Yeasten	Cat#20103ES60
Protein A/G magnetic beads	Thermo Fisher Scientific	Cat#88802
Magnetic beads carrying antibodies against Flag	Bimake	Cat#B26102
Magnetic beads carrying antibodies against HA	Bimake	Cat#B26202
4',6-diamidino-2-phenylindole (DAPI)	Beyotime	Cat#P0131
Matrigel	Corning	Cat#354230
Human IL6	MESGEN	Cat#MIL1006
<b>Critical commercial assays</b>		
Enhanced Chemiluminescence (ECL) kit	Fdbio science	Cat#FB8020
Silver Staining Kit	CWBIO	Cat#CW2012
ChIP-IT® Express Kit	Active Motif	Cat#53008
Human IL6 ELISA Kit	Beyotime	Cat#PI330
Dual-Luciferase® Reporter Assay System	Promega	Cat#E1910
<b>Deposited data</b>		
RNA-seq	This paper	GSE210093
<b>Experimental models: Cell lines</b>		
Human HBE cells	Procell Life Science & Technology company	Cat#CL-0346
Human BEAS-2B cells	the Cell Bank of Chinese Academy of Sciences	Cat# <a href="#">SCSP-5067</a>
Human A549 cells	the Cell Bank of Chinese Academy of Sciences	Cat# <a href="#">SCSP-503</a>
Human H1650 cells	the Cell Bank of Chinese Academy of Sciences	Cat# <a href="#">SCSP-592</a>
Human H1299 cells	the Cell Bank of Chinese Academy of Sciences	Cat# <a href="#">SCSP-589</a>
Human embryonic kidney (HEK) 293T cells	the Cell Bank of Chinese Academy of Sciences	Cat# <a href="#">SCSP-502</a>
<b>Experimental models: Organisms/strains</b>		
Mouse: female BALB/c nude mice	the Laboratory Animal Center of Soochow University	N/A

(Continued on next page)



### Continued

REAGENT or RESOURCE	SOURCE	IDENTIFIER
<b>Oligonucleotides</b>		
Primers used for plasmid construction, qRT-PCR, and ChIP (Table S6)	GENEWIZ	N/A
shRNA sequence (Table S6)	GENEWIZ	N/A
si-RNA oligo (Table S6)	GenePharma	N/A
<b>Software and algorithms</b>		
GraphPad Prism 7.01	GraphPad	<a href="https://www.graphpad.com/">https://www.graphpad.com/</a>
ImageJ 1.46r	National institutes of health	<a href="https://imagej.nih.gov/ij/">https://imagej.nih.gov/ij/</a>
GSEA 4.0.3	(Mootha et al., 2003; Subramanian et al., 2005)	<a href="https://www.gsea-msigdb.org/gsea/index.jsp">https://www.gsea-msigdb.org/gsea/index.jsp</a>
Metascape	(Zhou et al., 2019)	<a href="https://metascape.org/gp/index.html#/main/step1">https://metascape.org/gp/index.html#/main/step1</a>
The Eukaryotic Promoter Database	(Dreos et al., 2015)	<a href="https://epd.epfl.ch/index.php">https://epd.epfl.ch/index.php</a>
AnimalTFDB database	(Hu et al., 2019)	<a href="http://bioinfo.life.hust.edu.cn/AnimalTFDB/">http://bioinfo.life.hust.edu.cn/AnimalTFDB/</a>
Kaplan–Meier Plotter	(Lanczky and Gyorffy, 2021)	<a href="http://kmplot.com/analysis/">http://kmplot.com/analysis/</a>
BioRender	BioRender	<a href="https://biorender.com/">https://biorender.com/</a>

## RESOURCE AVAILABILITY

### Lead contact

Further information and requests for resources and reagents should be directed to and will be fulfilled by the lead contact, Hong-Tao Zhang ([htzhang@suda.edu.cn](mailto:htzhang@suda.edu.cn)).

### Materials availability

All unique/stable reagents generated in this study are available from the [lead contact](#) upon request. The sources and identifiers of all materials are listed in the [key resources table](#).

### Data and code availability

- The RNA-seq data generated in [Tables S4](#) and [S5](#) have been deposited to the Gene Expression Omnibus (GEO) with accession code GSE210093. All data reported in this study will be available from the [lead contact](#) upon request.
- This paper does not report original code.
- Any additional information required to reanalyze the data reported in this paper is available from the [lead contact](#) upon request.

## EXPERIMENTAL MODEL AND SUBJECT DETAILS

### Cell culture

Human LUAD cell lines A549, H1650, and H1299, immortalized human bronchial epithelial cell line BEAS-2B, and human embryonic kidney (HEK) 293T cell line, were purchased from the Cell Bank of Chinese Academy of Sciences. HBE, another immortalized human bronchial epithelial cell line, was bought from Procell Life Science & Technology company. Cells were cultured in Dulbecco's modified Eagle medium (DMEM)/Ham's F12 (Corning, #10-092-cv) with 10% fetal bovine serum (FBS; Invitrogen, #10099141) with 10% FBS at 37°C in a 5% CO<sub>2</sub> humidified incubator, except for HEK 293T cells which were cultured in DMEM with high glucose (Thermo Fisher Scientific, #21013024).

### In vivo metastasis assays

Forty 4-week-old female BALB/c nude mice were purchased from the Laboratory Animal Center of Soochow University and housed in a specific pathogen-free condition. The mice were randomly divided into four groups, including control vector group and TIF1γ-overexpressing group, control sh-NC group and sh-TAF15-1 group (10 mice per group). TIF1γ-overexpressing, TAF15-silenced, and control A549 cells in 200-μL of PBS were i.v. injected into murine tail vein ( $2.5 \times 10^6$  cells/mice). At 8 weeks post-inoculation, the mice were euthanized and their lungs and/or livers were taken out and fixed in Bouin's solution for macroscopically metastatic nodule

analysis. Lung and/or liver tissues were histologically examined with H&E staining for micrometastatic foci analysis. Animal studies were approved and supervised by the Animal Ethics Committee of Soochow University.

### Human LUAD and LUSC tissue specimens

Sixty-two LUAD and twenty-five LUSC fresh-frozen tissues, and matched adjacent noncancerous tissues were collected after informed consent from patients in the First Affiliated Hospital of Soochow University (Suzhou, China). LUAD and LUSC patients were pathologically diagnosed and assessed according to the Revised International System for Staging Lung Cancer. Detailed clinical information of patients is listed in [Tables S1](#) and [S2](#), metastatic tissues were from LUAD ( $n = 29$ ) and LUSC ( $n = 16$ ) patients characterized with local lymph node metastasis ( $T_{1-4}N_{1-2}M_0$ ) or distant organ metastasis ( $T_{1-4}N_{any}M_1$ ), and non-metastatic tissues were from LUAD ( $n = 33$ ) and LUSC ( $n = 9$ ) patients without any metastasis ( $T_{1-4}N_0M_0$ ). None of patients received chemotherapy or radiotherapy before surgical operation. This study was authorized by the Ethics Committee of Soochow University.

## METHOD DETAILS

### Gene set enrichment analysis (GSEA)

The software GSEA 4.0.3 (Broad Institute) was utilized to analyze the correlation of EMT gene set with TIF1 $\gamma$  expression. GSE29016 dataset including 39 LUAD and 13 LUSC samples was downloaded from GEO database, and samples were divided into high and low subgroups by TIF1 $\gamma$  median expression value. For each analysis, the gene set permutations were run for 1,000 times. Gene sets with adjusted  $p$  value  $< 0.05$ , normalized enrichment score (NES)  $> 1$ , and false discovery rate (FDR)  $< 0.25$  were considered significantly enriched.

### Mass spectrometry assay

Samples were analyzed on an Orbitrap Elite hybrid mass spectrometer (Thermo Fisher) coupled with a Dionex liquid chromatography (LC) according to the instructions. Briefly, samples were purified by solvent A [0.2% trifluoroacetic acid (TFA)] and solvent B (80% acetonitrile and 0.2% TFA) using a C18 column. Then the purified samples were separated with an LC gradient from 6 to 44% of solvent B (80% acetonitrile, 0.1% formic acid) in an analytical column over 120 min. Mass spectrometry (MS) analysis were conducted in the positive-ion mode. Each selected precursor ion was analyzed twice in 60 s. The resolution of the precursor ion was set to 120,000, and MS/MS spectra were collected for the selected precursor ions within a 2 Da mass isolation window. Data of MS-based analysis are described in [Table S3](#).

### Construction of vectors

All CDS DNA of interested genes were directly synthesized (GENEWIZ). TIF1 $\gamma$  CDS (GeneBank Accession number: NM\_015906) was subcloned into pcDNA3.1-HA and pcDNA3.1-Flag vectors with endonucleases *NheI*/*Agel* (New England Biolabs, NEB; #R0131L/R0552L) to generate pcDNA3.1-TIF1 $\gamma$ -HA and pcDNA3.1-TIF1 $\gamma$ -Flag transient expression vectors; TIF1 $\gamma$  CDS was subcloned into a pCDH-CMV-MCS-EF1-CopGFP lentiviral vector (Miaolingbio., #P0376) using *NheI*/*Bam*HI (NEB, #R0136L) to yield a pCDH-TIF1 $\gamma$  stable expression vector. Truncated CDS domains of TIF1 $\gamma$  were amplified with the corresponding PCR primers ([Table S6](#)) and subcloned into pcDNA3.1-HA and pcDNA3.1-Flag vectors to create various expression vectors.

TAF15 CDS (NM\_139215) was respectively subcloned into pcDNA3.1-Flag or GV492 lentiviral expression vector (Genechem Inc.) with a C-terminal FLAG tag using endonucleases *NheI*/*Hind*III (NEB, #R0104L) or *Bam*HI/*Agel* to produce pcDNA3.1-TAF15-Flag or GV492-TAF15-Flag. Two short hairpin RNAs (shRNA) specific to TAF15 (sh-TAF15) and negative control shRNA (sh-NC) were synthesized and subcloned into a lentiviral vector pLKO.1-puro (GENEWIZ) with endonucleases *Agel*/*Eco*RI (NEB, #R0101L) to generate pLKO.1-TAF15-1/2 and pLKO.1-sh-NC. The shRNA sequences are listed in [Table S6](#).

TBP CDS (NM\_003194) was separately subcloned into pcDNA3.1-HA or pCDH-CMV-MCS-EF1-CopGFP-T2A-Puro lentiviral expression vector (Miaolingbio., #P0268) with a C-terminal HA-tag using endonucleases *NheI*/*Agel* or *Xba*I (NEB, #R0145L)/*Bam*HI to generate pcDNA3.1-TBP-HA or pCDH-TBP-HA.

### Generation of stable cell lines

The aforementioned lentiviral vectors pCDH-TIF1 $\gamma$ , GV492-TAF15-Flag, pLKO.1-TAF15-1/2, and pCDH-TBP-HA were respectively co-transfected with packaging plasmids psPAX2 and pMD2.G (RIBOBIO) into HEK 293T cells using Lipofectamine 3000 (Invitrogen, #L3000015) for 48 h. The empty vectors served as negative controls. Packaged lentiviruses were collected and used to infect LUAD cells for 72 h. GFP-positive stable cells infected with pCDH-TIF1 $\gamma$  lentivirus were sorted using a FACSCalibur flow cytometer (BD Biosciences) and stable cells infected with GV492-TAF15-Flag, pLKO.1-TAF15-1/2 and pCDH-TBP-HA lentiviruses were selected with 1  $\mu$ g/mL puromycin (Solarbio, #P8230).

### RNA interference

Short interfering RNAs (siRNAs) for human TAF15 or TBP (si-TAF15 or si-TBP) were designed and synthesized (GenePharma). A scrambled siRNA was used as a negative control (si-NC). The sequences of siRNAs are listed in [Table S6](#). Cells were transiently transfected with 100 pmol of siRNAs using Lipofectamine 3000. After transfection for 48 h, the cells were collected for further experiments.

### Western blot analysis

Western blot analysis was performed as previously described by us (Lei et al., 2014). Cells were lysed with RIPA buffer (Thermo Fisher Scientific, #89900) supplemented with protease inhibitor cocktail (Sangon Biotech, #C600387) and phosphatase inhibitor cocktail (Sangon Biotech, #C500017), then protein samples containing native sample loading buffer (Sangon Biotech, #C506032) and DTT (Sangon Biotech, #B645939) were boiled at 100°C for 10 min before SDS-PAGE gel electrophoresis. The proteins were transferred to nitrocellulose membrane (MERCK, #HATF00010) and blocked with 5% BSA in TBST for 1 h at room temperature (RT) before overnight incubation with following primary antibodies: rabbit anti-TAF15 (Novus Biologicals, #NB100-567), rabbit anti-TIF1 $\gamma$  (CST, #90051), rabbit anti-HA (CST, #3724s), rabbit anti-Flag (CST, #14793s), rabbit anti-TBP (CST, #44059), mouse anti-E-cadherin (BD Biosciences, #610181), mouse anti-N-cadherin (BD Biosciences, #610920), mouse anti-IL6 (Beyotime, #AF0201), mouse anti- $\beta$ -actin (AB clonal, #AC004), mouse anti-TIF1 $\gamma$  (Santa Cruz, #sc-101179). Membranes were then washed three times with TBST buffer and incubated with horseradish peroxidase (HRP)-conjugated secondary mouse anti-rabbit (Santa Cruz, sc-101179) or secondary goat anti-mouse (Santa Cruz, sc-2005) for 2 h at RT. Finally, proteins were detected by Enhanced Chemiluminescence (ECL) kit (Fdbio science, FB8020).

### Protein silver-staining assay

Protein silver-staining assay was performed using Silver Staining Kit (CWBIO, #CW2012). Briefly, proteins were separated on PAGE gel and fixed twice for 15 min each time. Then the gel was washed and treated with silver stain sensitizer for 1 min and stained with silver stain solution for 30 min. Finally, protein bands were clearly stained by incubating the gel with a silver staining developer for 2 min. Staining reaction was immediately terminated with acetic acid to avoid overstaining.

### Real-time quantitative reverse transcriptase PCR (qRT-PCR) and mRNA half-life assays

Total RNA from cells or tissues was isolated with TRIzol (Thermo Fisher Scientific, #15596018) according to the manufacturer's protocol. cDNA was synthesized with M-MLV (H-) Reverse Transcriptase (Vazyme, #R021-01). SYBR Green I method was used to perform qRT-PCR on Roche LightCycler 96 instrument (Roche Diagnostics). Primers used for qRT-PCR analysis are listed in Table S6. The expression levels of TIF1 $\gamma$ , TAF15, TBP and IL6 mRNAs were equilibrated to  $\beta$ -actin. Relative expression of each mRNA was calculated using the  $\Delta\Delta C_t$  method. For mRNA half-life assay, cells were treated with 10  $\mu$ g/mL Act-D (Sigma-Aldrich, #129935) for 0, 2, 4 or 6 h and RNA was extracted at different time points for qRT-PCR.

### Co-immunoprecipitation (Co-IP)

Cells were grown on 10-cm dishes and then lysed with IP buffer (50 mM Tris-HCl (pH 7.5), 150 mM NaCl, 0.5% Nonidet P-40, 10% glycerol) for 30 min. Before immunoprecipitation, 10% of the extracts were reserved as the input control. Cell lysates were incubated with antibodies against HA (CST, #3724), FLAG (CST, #14793), TIF1 $\gamma$  (CST, #90051), TAF15 (Novus Biologicals, #NB100-567), TBP (CST, #44059) or IgG (CST, #3900) on a rotator at 4°C overnight. Protein A/G magnetic beads (Thermo Fisher Scientific, #88802) were added and incubated at room temperature for 2 h to capture the immune complexes. Besides, immune complexes can also be enriched by directly incubating cell lysates with magnetic beads carrying antibodies against Flag or HA (Bimake, #B26102 or #B26202) at 4°C. Finally, after being washed with IP buffer, the immunoprecipitants containing target and interacting proteins were separated from the magnetic beads and subjected to Western blot or MS-based analysis.

### Immunofluorescence analysis

Immunofluorescent analysis was carried out as described by us (Wang et al., 2016) with some modification. Briefly, cells were cultured on coverslips, fixed with 4% paraformaldehyde for 30 min, washed with PBS buffer, and incubated with 5% BSA for 1 h. Subsequently, cells were incubated with mouse anti-TIF1 $\gamma$  (Santa Cruz, #sc-101179) and rabbit anti-TAF15 primary antibodies (AB clonal, #A8465) at 4°C overnight. After being washed with PBST buffer, cells were incubated with FITC-conjugated anti-mouse secondary antibody (Beyotime, #A0568) and Cy3-conjugated anti-rabbit secondary antibody (Beyotime, #A0516) for 2 h at room temperature. Alternatively, cells were incubated with mouse anti-E-cadherin (Beyotime, #AF0138) and rabbit anti-N-cadherin primary antibodies (AB clonal, #A0432), followed by incubation with Cy3-conjugated anti-mouse secondary antibody (Beyotime, #A5021) and anti-rabbit secondary antibody (Beyotime, #A0562). Nuclei were counterstained with 4',6-diamidino-2-phenylindole (DAPI). Eventually, protein subcellular localization was examined using a confocal laser microscope (Carl Zeiss).

### Chromatin immunoprecipitation (ChIP)

ChIP analysis was performed with ChIP-IT Express Kit (Active Motif, #53008), which has been described in our previous work (Tong et al., 2020). Briefly, A549 cells transfected with Flag-tagged TAF15 or HA-tagged TBP expression vectors were grown on 10-cm dishes and fixed with 1% formaldehyde and terminated by glycine stop-fix solution. After centrifugation, cell nuclear sediment was collected, resuspended in shearing buffer and sonicated in ice to yield cross-linked DNA fragments with 200-1,000 bp length. Subsequently, the sheared chromatin was incubated with Protein G magnetic beads and anti-Flag or HA antibody at 4°C overnight. Rabbit IgG antibody served as a negative control. Protein G magnetic beads-antibody/chromatin complexes were magnetically collected, eluted and de-crosslinked in elution buffer to garner ChIP DNA. The ChIP DNA was purified and subjected to PCR amplification. Specific ChIP primers used for PCR are provided in Table S6.



### Transwell migration and invasion assays

Transwell assays were conducted as described by us (Wang et al., 2016) with modification. Briefly,  $5 \times 10^4$  cells were resuspended in 1% FBS medium and then added to each upper chamber with 8- $\mu$ m pore permeable or Matrigel-coated membrane, and 20% FBS medium was placed as chemoattractant in each well of Transwell plates (BD Biosciences). After incubation at 37°C for 30 h, migrated or invasive cells were fixed, stained with 1% crystal violet and counted in three microscopic fields.

### Wound-healing migration assay

Cells were cultured in 6-well plates until 90% confluency. Monolayers of cells were then gently scratched with a sterilized pipette tip and the cells were continued to culture in serum-free medium for 24 h. Cells were photographed in three random microscopic fields at 0 h and 24 h. The scratched wound width was measured using ImageJ Launcher software (National Institutes of Health). Each wound-healing analysis was repeated in triplicate.

### RNA-seq analysis

The mRNA expression profile was determined in TIF1 $\gamma$ -overexpressing or TAF15-silenced (sh-TAF15-1) A549 cells, and the corresponding control A549 cells (vector and sh-NC) by transcriptome sequencing on an Illumina HiSeq platform (GENEWIZ). Briefly, total RNA of each sample was extracted, quantified and qualified by TRIzol Reagent, Agilent 2100 Bioanalyzer (Agilent Technologies), NanoDrop (Thermo Fisher Scientific Inc.), and 1% agarose gel. Total RNA (1  $\mu$ g) with RIN value above 6.5 was used for performing library preparation according to the manufacturer's protocol. Then libraries were loaded on an Illumina HiSeq instrument and sequencing was carried out using a 2x150 bp paired-end (PE) configuration. Image analysis and base calling were conducted by the HiSeq Control Software + OLB + GAPIipeline-1.6 on the HiSeq instrument. Raw data were processed with Cutadapt (V1.9.1) to generate high-quality clean data, which was aligned to the Homo\_sapiens\_GRCh37.91 using the software Hisat2 (v2.0.1). HTSeq (v0.6.1) was used to estimate gene and isoform expression levels from the pair-end clean data. Differential expression analysis was performed using the DESeq2 Bioconductor package. DEGs with q value < 0.05 and fold change (FC) > 1.3 were chosen for further investigation. Each group was analyzed in triplicate. RNA-seq data were processed by GENEWIZ Biotech Inc. and presented in Tables S4 and S5.

### Enzyme-linked immunosorbent assay (ELISA)

IL6 concentration in cell culture media was measured using a Human IL6 ELISA Kit (Beyotime, #PL330). Cell culture media were harvested and stored at -20°C before analysis. According to the manual, 100  $\mu$ L of study samples or IL6 standard samples were added into wells of the microplate and incubated for 2 h at room temperature. After 5 washes, 100  $\mu$ L of biotinylated-IL6 antibodies were added into the microplate and incubated with samples for 1 h. Following another 5 washes, 100  $\mu$ L of horseradish peroxidase-labeled streptavidin was added and incubated for 20 min in dark. Following a final wash, a color reaction was developed with 100  $\mu$ L of TMB solution for 20 min and terminated by adding 50  $\mu$ L stop solution. Finally, the optical density at 450 nm was measured on a CMax Plus microplate reader (Molecular Devices).

### Luciferase reporter assay

To investigate transcriptional regulation of TAF15 or TBP on IL6, different IL6 promoter (IP) fragments (Table S7) were synthesized and subcloned into pGL3-basic vector (Promega, #E1751) to generate pGL3-IP1~4, pGL3-IP1~3, pGL3-IP4-wild type and pGL3-IP4-mutant vectors. Then the aforementioned constructs and pRL-TK plasmids were co-transfected into A549 cells (TAF15- or TBP-overexpressing; TBP-overexpressing and TAF15-knockdown; TAF15-overexpressing and TBP-knockdown) using Lipofectamine 3000. After transfection for 48 h, cells were harvested and luciferase activities were determined with a Dual-LuciferaseReporter Assay System (Promega, #E1910). Results are shown as relative luciferase activities (firefly/Renilla) and each luciferase reporter analysis was performed in triplicate.

### Gene ontology (GO) analysis

Gene ontology (GO) analyses were performed using Metascape tool (<https://metascape.org/gp/index.html#/main/step1>). The adjusted p value was reported with the GO terms.

### QUANTIFICATION AND STATISTICAL ANALYSIS


Unpaired Student's t-test (2-tailed) was applied for comparisons between two groups *in vitro* and *in vivo* data, LUAD and LUSC samples except where otherwise stated. Data were presented as mean  $\pm$  SD. p values less than 0.05 were considered to be statistically significant. Statistical analyses were performed using GraphPad Prism 7.01 software (GraphPad).

RESEARCH

Open Access



# Circular RNA hsa\_circ\_0008305 (circPTK2) inhibits TGF- $\beta$ -induced epithelial-mesenchymal transition and metastasis by controlling TIF1 $\gamma$ in non-small cell lung cancer

Longqiang Wang<sup>1†</sup>, Xin Tong<sup>1†</sup>, Zhengyu Zhou<sup>1,5†</sup>, Shengjie Wang<sup>1,6†</sup>, Zhe Lei<sup>1</sup>, Tianze Zhang<sup>2</sup>, Zeyi Liu<sup>3</sup>, Yuanyuan Zeng<sup>3</sup>, Chang Li<sup>4</sup>, Jun Zhao<sup>4</sup>, Zhiyue Su<sup>1</sup>, Cuijuan Zhang<sup>1</sup>, Xia Liu<sup>1</sup>, Guangquan Xu<sup>2\*</sup> and Hong-Tao Zhang<sup>1,7\*</sup> 

## Abstract

**Background:** TGF- $\beta$  promotes tumor invasion and metastasis through inducing epithelial-mesenchymal transition (EMT) in non-small cell lung cancer (NSCLC). Circular RNAs (circRNAs) are recognized as functional non-coding RNAs involved in human cancers. However, whether and how circRNAs contribute to TGF- $\beta$ -induced EMT and metastasis in NSCLC remain vague. Here, we investigated the regulation and function of Circular RNA hsa\_circ\_0008305 (circPTK2) in TGF- $\beta$ -induced EMT and tumor metastasis, as well as a link between circPTK2 and transcriptional intermediary factor 1  $\gamma$  (TIF1 $\gamma$ ) in NSCLC.

**Methods:** Circular RNAs were determined by human circRNA Array analysis, real-time quantitative reverse transcriptase PCR and northern blot. Luciferase reporter, RNA-binding protein immunoprecipitation (RIP), RNA pull-down and fluorescence in situ hybridization (FISH) assays were employed to test the interaction between circPTK2 and miR-429/miR-200b-3p. Ectopic overexpression and siRNA-mediated knockdown of circPTK2, TGF- $\beta$ -induced EMT, Transwell migration and invasion in vitro, and in vivo experiment of metastasis were used to evaluate the function of circPTK2. Transcription and prognosis analyses were done in public databases.

(Continued on next page)

\* Correspondence: [xvguangquanlb@163.com](mailto:xvguangquanlb@163.com); [htzhang@suda.edu.cn](mailto:htzhang@suda.edu.cn)

<sup>†</sup>Longqiang Wang, Xin Tong, Zhengyu Zhou and Shengjie Wang contributed equally to this work.

<sup>2</sup>Department of Thoracic Surgery, The Second Affiliated Hospital of Harbin Medical University, 246 Xuefu Road, Harbin 150086, Heilongjiang, China

<sup>1</sup>Soochow University Laboratory of Cancer Molecular Genetics, Medical College of Soochow University, 199 Ren'ai Road, Suzhou 215123, Jiangsu, China

Full list of author information is available at the end of the article



© The Author(s). 2018 **Open Access** This article is distributed under the terms of the Creative Commons Attribution 4.0 International License (<http://creativecommons.org/licenses/by/4.0/>), which permits unrestricted use, distribution, and reproduction in any medium, provided you give appropriate credit to the original author(s) and the source, provide a link to the Creative Commons license, and indicate if changes were made. The Creative Commons Public Domain Dedication waiver (<http://creativecommons.org/publicdomain/zero/1.0/>) applies to the data made available in this article, unless otherwise stated.

(Continued from previous page)

**Results:** CircPTK2 and TIF1 $\gamma$  were significantly down-regulated in NSCLC cells undergoing EMT induced by TGF- $\beta$ . CircPTK2 overexpression augmented TIF1 $\gamma$  expression, inhibited TGF- $\beta$ -induced EMT and NSCLC cell invasion, whereas circPTK2 knockdown had the opposite effects. CircPTK2 functions as a sponge of miR-429/miR-200b-3p, and miR-429/miR-200b-3p promote TGF- $\beta$ -induced EMT and NSCLC cell invasion by targeting TIF1 $\gamma$ . CircPTK2 overexpression inhibited the invasion-promoting phenotype of endogenous miR-429/miR-200b-3p in NSCLC cells in response to TGF- $\beta$ . CircPTK2 overexpression significantly decreased the expression of Snail, an important downstream transcriptional activator of TGF- $\beta$ /Smad signaling. In an in vivo experiment of metastasis, circPTK2 overexpression suppressed NSCLC cell metastasis. Moreover, circPTK2 expression was dramatically down-regulated and positively correlated with TIF1 $\gamma$  expression in human NSCLC tissues. Especially, circPTK2 was significantly lower in metastatic NSCLC tissues than non-metastatic counterparts.

**Conclusion:** Our findings show that circPTK2 (hsa\_circ\_0008305) inhibits TGF- $\beta$ -induced EMT and metastasis by controlling TIF1 $\gamma$  in NSCLC, revealing a novel mechanism by which circRNA regulates TGF- $\beta$ -induced EMT and tumor metastasis, and suggesting that circPTK2 overexpression could provide a therapeutic strategy for advanced NSCLC.

**Keywords:** NSCLC, CircPTK2, TIF1 $\gamma$ , EMT, miR-429/miR-200b-3p

## Background

Lung cancer is the leading cause of cancer-related deaths worldwide, and ~ 85% of all lung cancers are non-small cell lung cancer (NSCLC) [1, 2]. Despite improvement in therapeutic strategies, NSCLC patients yet exhibits poor prognosis [3]. This is predominantly attributed to tumor metastasis [4], suggesting that elucidation of the mechanisms underlying NSCLC metastasis is becoming a big challenge.

Transforming growth factor  $\beta$  (TGF- $\beta$ ) is highly expressed in NSCLCs [5–7]. Our previous study showed that TGF- $\beta$  can promote epithelial-mesenchymal transition (EMT) and NSCLC cell invasion [8, 9]. In fact, there are compelling data that TGF- $\beta$ /Smad signaling potently contributes to EMT and tumor metastasis in various human cancers [10, 11]. Recently, we have provided evidence that repression of transcriptional intermediary factor 1  $\gamma$  (TIF1 $\gamma$ ), a regulator of TGF- $\beta$ /Smad signaling [12, 13], enhanced TGF- $\beta$ -induced EMT in NSCLC cells [14]. In support of this, TIF1 $\gamma$  exerts its repressive activity on TGF- $\beta$ /Smad signaling and plays an antagonistic role in TGF- $\beta$ -induced EMT in mammary epithelial cells [11, 15, 16]. These data strongly suggest that TIF1 $\gamma$  functions as a tumor metastasis suppressor in human cancers, including NSCLC, by inhibiting TGF- $\beta$ -induced EMT.

CircRNAs, a class of non-coding RNAs, are involved in gene regulation at both transcriptional and post-transcriptional levels [17]. Most of circRNAs are derived from a single exon or multiple exons and are detected in the cytoplasm [18, 19]. CircRNAs have been discovered to work as miRNA sponges [17, 20, 21]. The best-known ones so far include the recently identified circRNA, ciRS-7, which can efficiently tether miR-7, leading to reduced miR-7 activity and increased levels of oncogenic factors in cancer-associated signaling pathways [22]. Most recently, Hsiao et al. found that circCCDC66 may

protect *MYC* mRNA from the attack of miRNA-33b and miR-93 to promote colon cancer growth and metastasis [23]; Han et al. reported that circMTO1 inhibits hepatocellular carcinoma progression by disrupting oncogenic miR-9 and promoting p21 expression [24]. However, the regulatory mechanisms of circRNAs in cancer need to be extensively validated [21]. Of more importance, hundreds of circRNAs were regulated in human mammary cells undergoing EMT [25], suggesting that certain circRNAs play important roles in TGF- $\beta$ -induced EMT and thus influence cancer metastasis. RNA-binding protein Quaking (QKI) was identified to control biogenesis of > 30% of abundant circRNAs during EMT in response to TGF- $\beta$  [25]. Furthermore, QKI is frequently down-regulated in NSCLC tissues and significantly associated with poorer prognosis [26]. These findings suggested that down-regulated circRNAs may be implicated in NSCLC progression, invasion and metastasis.

Taken together, we hypothesized that there may be several dysregulated circRNAs affecting TIF1 $\gamma$  activity and thereby promoting TGF- $\beta$ -induced EMT and invasion in NSCLC. To test this, we first performed Human circRNA Array analysis in NSCLC cells before and after they underwent EMT in response to TGF- $\beta$ , and identified 187 differentially expressed circRNAs. From the viewpoint of prediction, we focus on a down-regulated circRNA (hsa\_circ\_0008305 in circBase: <http://www.circbase.org>) produced from the *PTK2* gene, termed as circPTK2. Intriguingly, we further investigated the regulation and function of circPTK2 in TGF- $\beta$ -induced EMT and tumor metastasis, as well as a link between circPTK2 and TIF1 $\gamma$  in NSCLC. Our findings show that circPTK2 suppresses TGF- $\beta$ -induced EMT and tumor cell invasion by controlling TIF1 $\gamma$  in NSCLC, revealing a novel mechanism by which circRNA regulates TGF- $\beta$ -induced EMT and tumor metastasis.

## Results

### TIF1 $\gamma$ and circPTK2 are down-regulated during TGF- $\beta$ -induced EMT in NSCLC cells

Public data suggest that TIF1 $\gamma$  is a tumor suppressor in NSCLC progression (Additional file 1: Figure S1A-D). Moreover, increased expression of TGF- $\beta$  has been proved in NSCLC [5–7, 27] and TIF1 $\gamma$  knockdown promotes TGF- $\beta$ -induced EMT in NSCLC cells [14]. To investigate whether TGF- $\beta$  can down-regulate TIF1 $\gamma$  expression in EMT, we first examined TIF1 $\gamma$  expression in A549 cells before and after they had undergone EMT in response to TGF- $\beta$ 1. The TGF- $\beta$ 1-treated A549 cells were steadily mesenchymal with typical morphology and marker expression (Fig. 1a). Meanwhile, TIF1 $\gamma$  expression was significantly reduced in TGF- $\beta$ -induced EMT of A549 cells (Fig. 1a). Next, RNA from epithelial and mesenchymal A549 cells was subjected to Arraystar Human circRNA Array analysis. We found that 88 circRNAs were up-regulated and 99 circRNAs were down-regulated when comparing mesenchymal A549 cells with epithelial A549 cells ( $\geq 1.5$ -fold;  $P < 0.05$ ) (Fig. 1b and Additional file 2: Table S1). Using computational algorithms based on TargetScan/miRBase and miRanda, we predicted that circPTK2 (Arraystar ID: hsa\_circRNA\_104703) and TIF1 $\gamma$  3'-UTR harbor the binding sites for miR-429/miR-200b-3p (Additional file 3: Figure S2A-C). Therefore, we focused on circPTK2 which was down-regulated 1.6-fold in TGF- $\beta$ -induced EMT (Fig. 1b and Additional file 2: Table S1), and validated the characterization of circPTK2 in A549 and H226 cells (Fig. 1c-f). To confirm the microarray result, we performed qRT-PCR analysis and found that circPTK2 expression was significantly reduced in A549 and H226 cells treated with TGF- $\beta$ 1 for 24 h (Fig. 1g). Moreover, miR-429/miR-200b-3p levels were unchanged in A549 and H226 cells treated with TGF- $\beta$ 1 (Fig. 1h and i), which is supported by the findings that miR-200 family members were not altered by TGF- $\beta$ 1 in A549 cells [28]. Taken together, we deduced that circPTK2 may be positively associated with TIF1 $\gamma$  by acting as sponges of miR-429/miR-200b-3p in TGF- $\beta$ -induced EMT of NSCLC cells.

### CircPTK2 binds directly to miR-429/miR-200b-3p in NSCLC cells

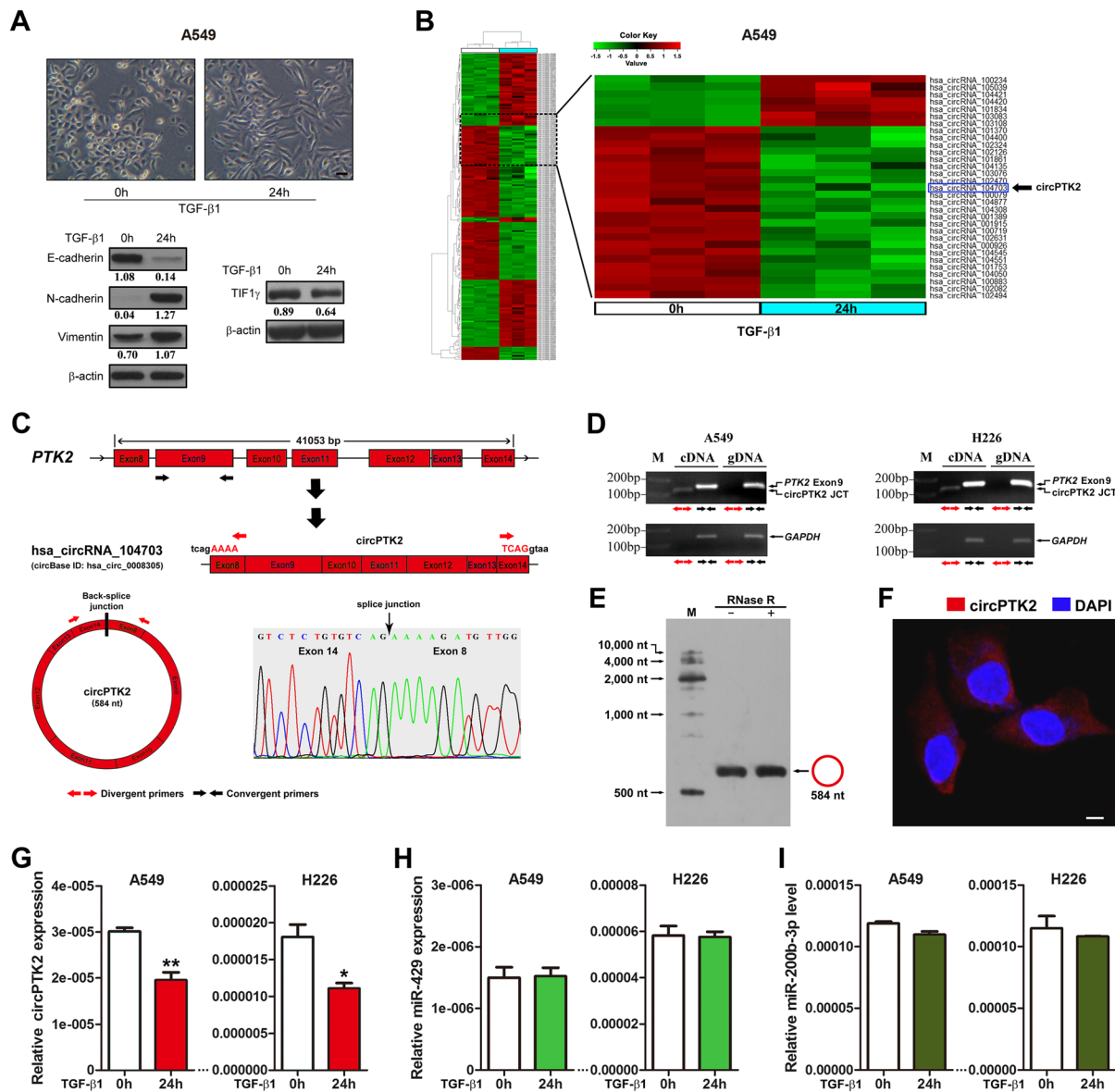
Endogenous circRNAs have been discovered to work as miRNA sponges [21, 29]. In view of the prediction that there is a shared binding site for miR-429/miR-200b-3p in each circPTK2 molecule (Additional file 3: Figure S2A), we performed the following experiments to verify whether circPTK2 binds to miR-429/miR-200b-3p in NSCLC cells. Firstly, we subcloned the circPTK2 region (Additional file 4: Table S2) containing miR-429/miR-200b-3p binding sites (wild type/mutant) into psiCHECK-2 luciferase vectors

(Fig. 2a) and transiently cotransfected the reporter construct with miR-429/miR-200b-3p mimics into A549 and H226 cells. The luciferase activity assay showed that circPTK2 was bound by miR-429/miR-200b-3p (Fig. 2b and c). Secondly, given that miRNAs exert their biological functions in an AGO2-dependent manner [30], we performed anti-AGO2 RIP in A549 cells transiently overexpressing miR-429/miR-200b-3p. Endogenous circPTK2 pull-down by AGO2 was specifically enriched in A549 cells transfected with miR-429/miR-200b-3p (Fig. 2d), validating the direct binding of circPTK2 with miR-429/miR-200b-3p. Thirdly, RNA pull-down analysis demonstrated that endogenous miR-429/miR-200b-3p were significantly pulled down by biotinylated probes against circPTK2 (Fig. 2e), confirming the existence of circPTK2-miR-429/miR-200b-3p complexes. Fourthly, fluorescence in situ hybridization (FISH) experiments showed that circPTK2 and miR-429/miR-200b-3p were preferentially co-localized in the cytoplasm (Fig. 2f), supporting the direct interaction of circPTK2 with miR-429/miR-200b-3p. Furthermore, we transiently overexpressed more than 20-fold circPTK2 in A549 and H226 cells (Fig. 2g) and observed nonsignificant difference in miR-429/miR-200b-3p levels between cells overexpressing circPTK2 and control cells (Fig. 2h and i). Taken together, these results suggested that circPTK2 can function as a sponge for miR-429/miR-200b-3p in NSCLC cells.

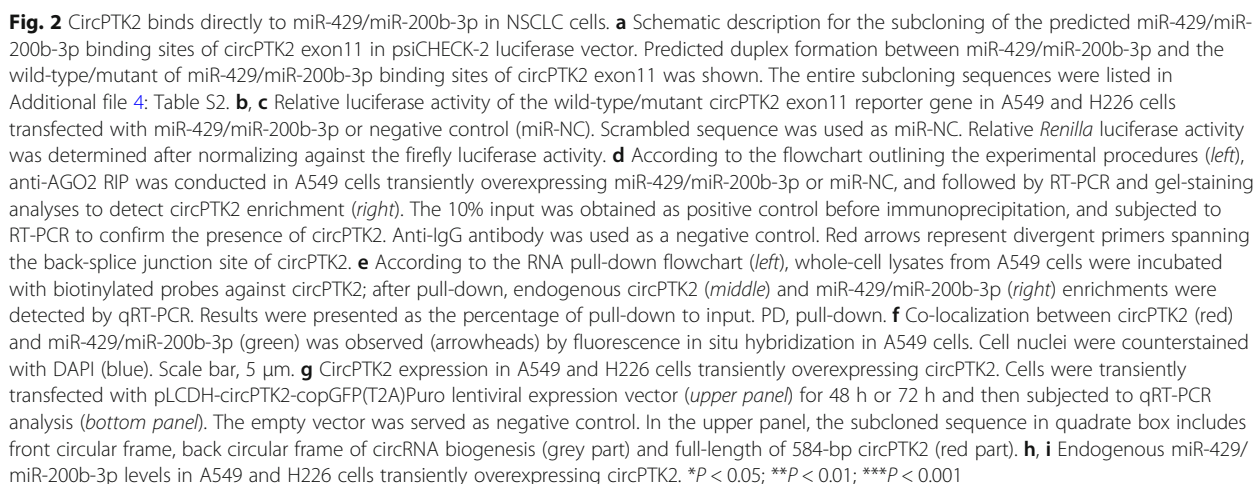
### miR-429/miR-200b-3p represses TIF1 $\gamma$ expression by targeting 3'-UTR of TIF1 $\gamma$

Next, we predicted in silico that four different regions of TIF1 $\gamma$  3'-UTR were putative targets of miR-429/miR-200b-3p (Additional file 3: Figure S2B and C). To test this, we subcloned the TIF1 $\gamma$  3'-UTR regions (Additional file 4: Table S2) containing miR-429/miR-200b-3p binding sites (wild type/mutant) into psiCHECK-2 luciferase vectors (Fig. 3a and Additional file 5: Figure S3A) and transiently cotransfected the reporter construct with miR-429/miR-200b-3p mimics into A549 and H226 cells. The results showed that TIF1 $\gamma$  3'-UTR was a target of miR-429/miR-200b-3p and the positions 145–152 and 2690–2696 of TIF1 $\gamma$  3'-UTR were bona fide target sites of miR-429 and miR-200b-3p, respectively (Fig. 3b and Additional file 5: Figure S3B). Moreover, transiently overexpressed miR-429/miR-200b-3p (Fig. 3c and Additional file 5: Figure S3C) remarkably inhibited TIF1 $\gamma$  expression in A549 and H226 cells (Fig. 3d and e; Additional file 5: Figure S3D and E). In contrast, transient overexpression of miR-429/miR-200b-3p inhibitors (Fig. 3f and Additional file 5: Figure S3F) augmented TIF1 $\gamma$  expression in A549 and H226 cells (Fig. 3g and h; Additional file 5: Figure S3G and H). Taken together, these results demonstrated that miR-429/miR-200b-3p can





**Fig. 1** TIF1 $\gamma$  and circPTK2 are down-regulated during TGF- $\beta$ -induced EMT in NSCLC cells. **a** A549 cells underwent epithelial-mesenchymal transition (EMT) after TGF- $\beta$ 1 (5 ng/ml) treatment for 24 h. Cell morphology was observed and photographed with a phase-contrast microscope (upper). Scale bar, 50  $\mu$ m. The expression of EMT-related makers including E-cadherin, N-cadherin and Vimentin (bottom left), and TIF1 $\gamma$  protein (bottom right) were examined by western blot.  $\beta$ -actin was used as internal control. Densitometry values for each protein were normalized to  $\beta$ -actin and shown below the corresponding bands. **b** RNA from epithelial and mesenchymal A549 cells were subjected to Arraystar Human circRNA Array analysis as described in Methods. Hierarchical cluster analysis (heat map) of microarray data was used to show the significant expression of circRNAs when comparing mesenchymal cells with epithelial cells (left). Red and green denoted high and low expression, respectively. Each column represents a test sample and each row represents a circRNA. Each group (treated with TGF- $\beta$ 1 for 0 h or 24 h) was analyzed in triplicate. In a zoomed-in view of partial (right), the expression of circPTK2 (hsa\_circRNA\_104703) was indicated by an arrow. **c** The sketch of genomic locus of circPTK2 in *PTK2* gene. The expression of circPTK2 (circBase ID: hsa\_circ\_0008305) was validated by RT-PCR followed by sanger sequencing. Red arrows represent divergent primers, which are used to amplify the genome region of circPTK2 containing the back-splice junction site (JCT). Red and black arrows represent divergent and convergent primers, respectively. Divergent primers spanning circPTK2 JCT yield a product of 110 bp, while the convergent primers amplifying *PTK2* exon 9 yield a product of 141 bp. **d** In A549 or H226 cells, divergent primers amplify circPTK2 JCT in cDNA but not in genomic DNA (gDNA), convergent primers amplify both circPTK2 JCT and linear *PTK2* Exon 9. *GAPDH* was used as linear control. Red and black arrows represent divergent and convergent primers, respectively. Divergent primers spanning circPTK2 JCT yield a product of 110 bp, while the convergent primers amplifying *PTK2* exon 9 yield a product of 141 bp. **e** Endogenous circPTK2 expression in A549 cells was validated by northern blots. RNase R was used to digest linear RNA. **f** Representative image of RNA fluorescence in situ hybridization for endogenous circPTK2 in A549 cells. Cell nuclei were counterstained with 4,6-diamidino-2-phenylindole (DAPI). Scale bar, 5  $\mu$ m. **g** qRT-PCR analysis of circPTK2 expression in A549 and H226 cells treated with TGF- $\beta$ 1 for 24 h. Relative circPTK2 expression was determined with normalization against  $\beta$ -actin. **h**, **i** qRT-PCR analysis of miR-429/miR-200b-3p expression levels in A549 and H226 cells treated with TGF- $\beta$ 1 for 24 h. U6 was used as internal control. \* $P$  < 0.05; \*\* $P$  < 0.01



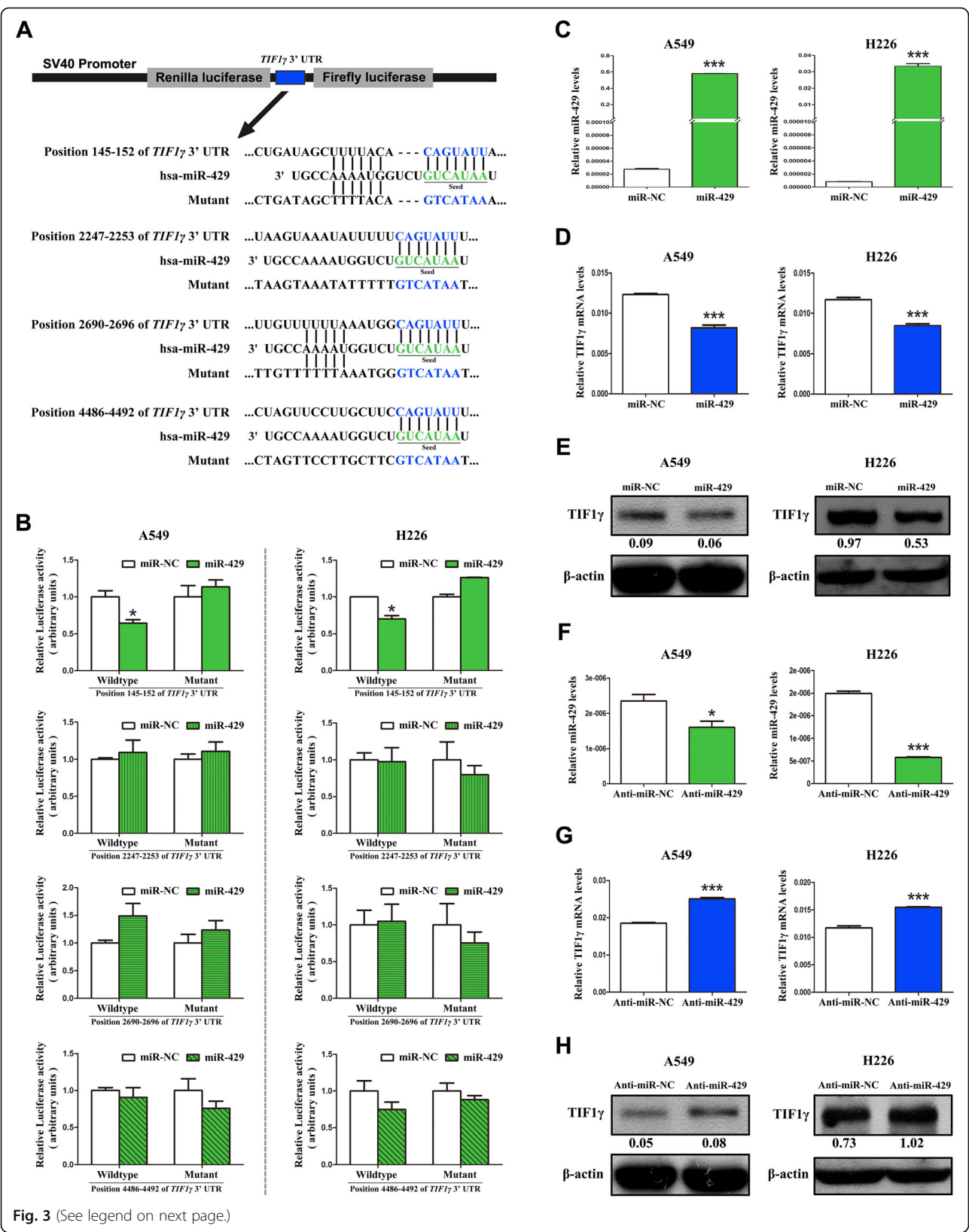


Fig. 3 (See legend on next page.)

(See figure on previous page.)

**Fig. 3** miR-429 represses TIF1 $\gamma$  expression by targeting 3'-UTR of *TIF1 $\gamma$*  transcript. **a** Schematic description for the subcloning of the predicted miR-429 binding sites of *TIF1 $\gamma$*  3'-UTR in psiCHECK-2 luciferase vector. Predicted duplex formation between miR-429 and the wild-type/mutant of miR-429 binding sites was indicated. The entire subcloning sequences were listed in Additional file 4: Table S2. **b** Relative luciferase activity of the wild-type/mutant *TIF1 $\gamma$*  3'-UTR reporter gene in A549 and H226 cells transfected with miR-429 or negative control (miR-NC). Scrambled sequence was used as miR-NC. Relative *Renilla* luciferase activity was determined after normalizing against the firefly luciferase activity. **c** qRT-PCR analysis of miR-429 expression levels in A549 and H226 cells transfected with miR-429 mimics or miR-NC. U6 was employed as internal control. **d, e** TIF1 $\gamma$  mRNA and protein expression in A549 and H226 cells transfected with miR-429 mimics or miR-NC.  $\beta$ -actin was used as internal control. **f** miR-429 expression levels in A549 and H226 cells transfected with miR-429 inhibitors (anti-miR-429) or negative control (anti-miR-NC). Scrambled sequence was used as anti-miR-NC. **g, h** TIF1 $\gamma$  mRNA and protein expression in A549 and H226 cells transfected with anti-miR-429 or anti-miR-NC.

\* $P < 0.05$ ; \*\*\* $P < 0.001$

inhibit TIF1 $\gamma$  expression by directly targeting the 3'-UTR of *TIF1 $\gamma$*  in NSCLC cells.

#### CircPTK2 functions as sponge to protect TIF1 $\gamma$ from the attack of miR-429/miR-200b-3p

To investigate whether circPTK2 abolished endogenous miR-429/miR-200b-3p-mediated repression of TIF1 $\gamma$ , we administrated miR-429/miR-200b-3p mimics into A549 cells transiently overexpressing circPTK2 and examined TIF1 $\gamma$  expression. As illustrated in Additional file 6: Figure S4A and B, circPTK2 overexpression promoted TIF1 $\gamma$  expression while exogenous miR-429/miR-200b-3p mimics abrogated circPTK2 overexpression effect. Combined with the aforementioned results obtained in Figs. 2, 3, and Additional file 5: Figure S3, these findings confirmed that circPTK2 protected TIF1 $\gamma$  by sponging out miR-429/miR-200b-3p in NSCLC cells.

#### miR-429/miR-200b-3p enhances TGF- $\beta$ -induced EMT and invasion in NSCLC cells

Our previous findings demonstrated that TIF1 $\gamma$  knockdown promotes TGF- $\beta$ -induced EMT and NSCLC cell invasion [14]. Considering the present findings that miR-429/miR-200b-3p repressed TIF1 $\gamma$  expression, we thus hypothesized that miR-429/miR-200b-3p may lead to the same phenotype caused by TIF1 $\gamma$  knockdown in A549 and H226 cells. Upon TGF- $\beta$ 1 stimulation, A549 and H226 cells overexpressing miR-429/miR-200b-3p showed higher expression of *Snail* mRNA and N-cadherin compared with the cells transfected with miR-NC (Fig. 4a and b; Additional file 7: Figure S5A and B). Furthermore, miR-429/miR-200b-3p increased TGF- $\beta$ -induced migratory and invasive abilities of A549 and H226 cells (Fig. 4c and d; Additional file 7: Figure S5C and D). In contrast, in the presence of TGF- $\beta$ 1, A549 and H226 cells transfected with miR-429/miR-200b-3p inhibitor showed lower expression of *Snail* mRNA and N-cadherin (Fig. 4e and f; Additional file 7: Figure S5E and F), and displayed a reduction in migration and invasion (Fig. 4g and h; Additional file 7: Figure S5G and H). Taken together, the results indicated that miR-429/miR-200b-3p can enhance TGF- $\beta$ -induced EMT and NSCLC cell invasion.

#### CircPTK2 overexpression enhances TIF1 $\gamma$ expression and inhibits TGF- $\beta$ -induced EMT and NSCLC cell invasion

We next examined whether circPTK2 influenced TIF1 $\gamma$  expression and TGF- $\beta$ -induced EMT and invasive phenotypes in NSCLC cells. As a result, transient overexpression of circPTK2 (Fig. 2g) significantly augmented TIF1 $\gamma$  expression in A549 and H226 cells (Fig. 5a). Moreover, upon TGF- $\beta$ 1 stimulation, A549 and H226 cells transiently overexpressing circPTK2 showed lower expression of *Snail* and N-cadherin compared with control cells (Fig. 5b and c). Comparably, circPTK2 significantly suppressed TGF- $\beta$ -induced migratory and invasive abilities of A549 and H226 cells (Fig. 5d and e). The phenotype of circPTK2 overexpression (Fig. 5d and e) copied the invasion-suppressing phenotype of miR-429/miR-200b-3p inhibitors in A549 and H226 cells (Fig. 4g and h; Additional file 7: Figure S5G and H) and circPTK2 overexpression inhibited the invasion-promoting phenotype of endogenous miR-429/miR-200b-3p in A549 cells in response to TGF- $\beta$  (Additional file 6: Figure S4C and D). Collectively, the results indicated that circPTK2 overexpression can promote TIF1 $\gamma$  expression and inhibit TGF- $\beta$ -induced EMT and NSCLC cell invasion by abrogating the effects of miR-429/miR-200b-3p.

#### CircPTK2 knockdown inhibits TIF1 $\gamma$ expression and promotes TGF- $\beta$ -induced EMT and NSCLC cell invasion

To verify the aforementioned roles of circPTK2 in vitro, we designed siRNA specifically targeting circPTK2 back-splice junction (JCT) to knockdown circPTK2 function (Additional file 8: Figure S6A, left). Transfection with this siRNA effectively silenced circPTK2 levels in A549 and H226 cells (Additional file 8: Figure S6A, right) but had no effect on linear *PTK2* mRNA levels (Additional file 8: Figure S6B). CircPTK2 knockdown remarkably attenuated TIF1 $\gamma$  expression in A549 and H226 cells (Additional file 8: Figure S6C). On TGF- $\beta$ 1 stimulation, circPTK2-silenced A549 and H226 cells showed higher expression of *Snail* and N-cadherin than those of control cells (Additional file 8: Figure S6D). Moreover, circPTK2 knockdown significantly increased TGF- $\beta$ -induced migratory and invasive abilities of A549 and H226 cells (Additional file 8: Figure S6E and F).



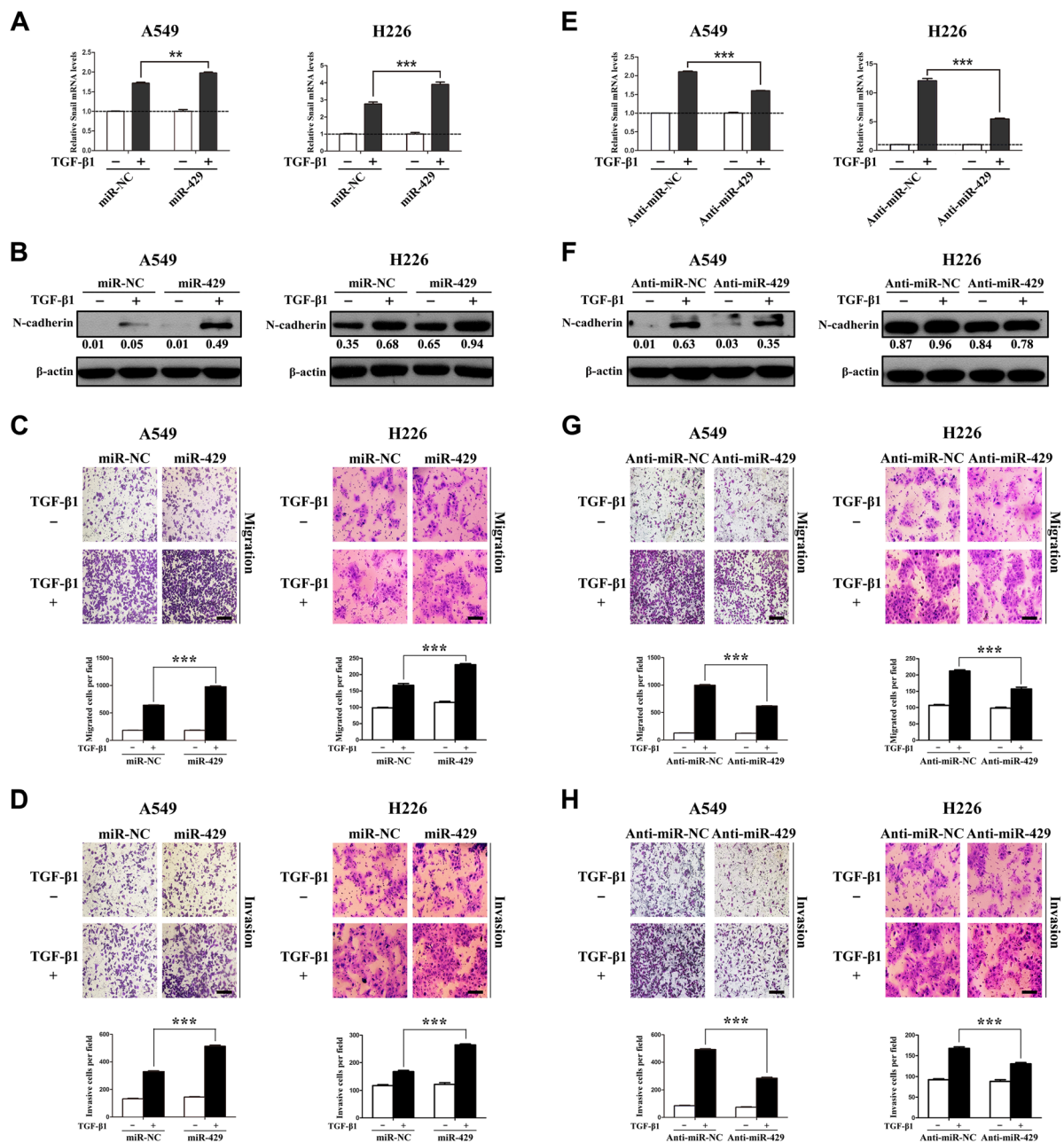
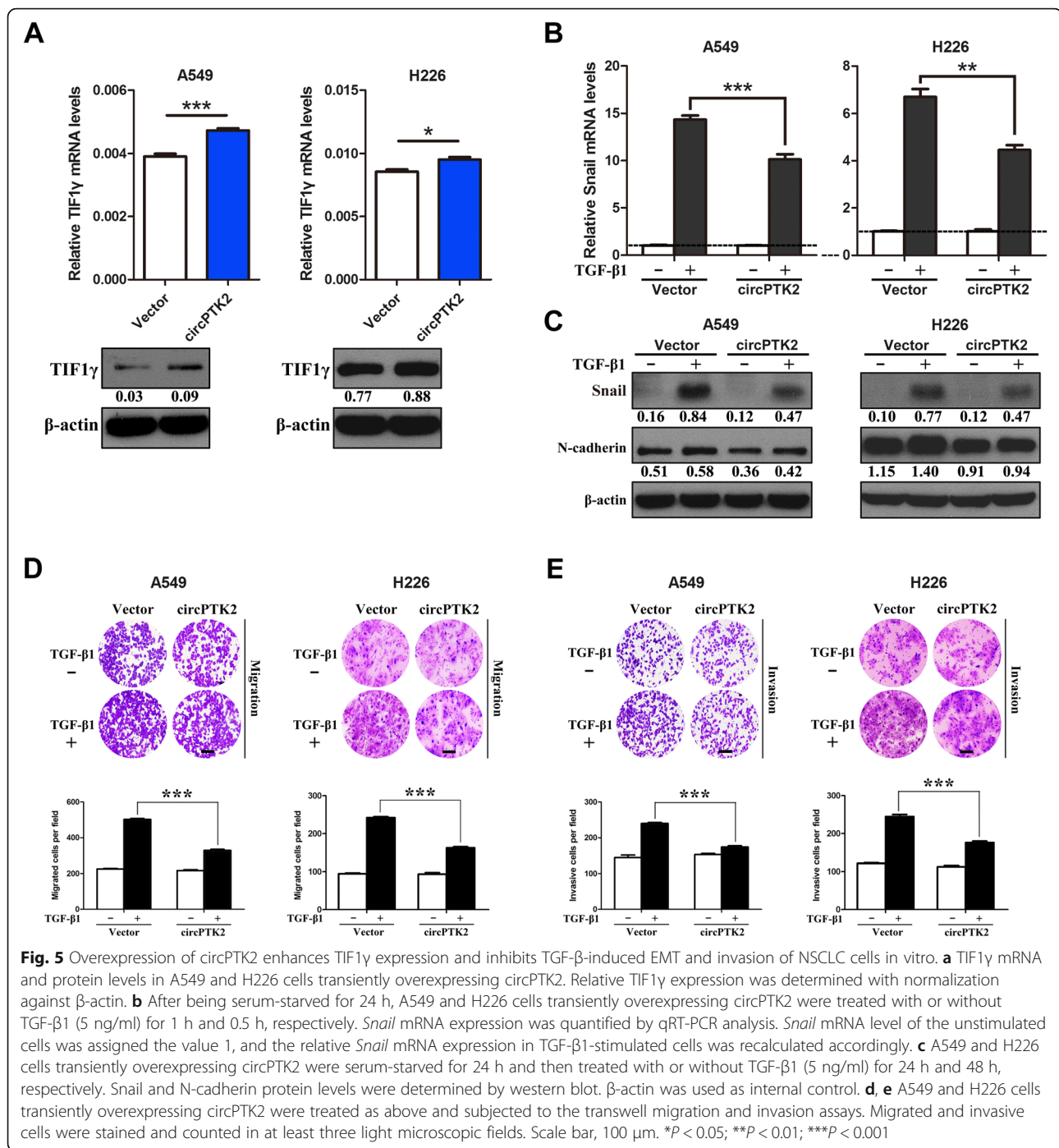


**Fig. 4** miR-429 enhances TGF- $\beta$ -induced EMT and invasion in NSCLC cells. **a** After being serum-starved for 24 h, A549 and H226 cells transiently overexpressing miR-429 were treated with or without TGF- $\beta$ 1 (5 ng/ml) for 1 h and 2 h, respectively. *Snail* mRNA expression was quantified by qRT-PCR analysis. *Snail* mRNA level of the unstimulated cells was assigned the value 1, and the relative *Snail* mRNA expression in TGF- $\beta$ 1-stimulated cells was recalculated accordingly. **b** After being serum-starved for 24 h, A549 and H226 cells transiently overexpressing miR-429 were treated with or without TGF- $\beta$ 1 (5 ng/ml) for 24 h and 48 h, respectively. Western blot analysis was performed to examine the expression of N-cadherin, which was normalized to  $\beta$ -actin. **c** A549 and H226 cells transiently overexpressing miR-429 were treated as above and allowed to migrate through an 8- $\mu$ m pore in transwells. Migrated cells were stained and counted in at least three light microscopic fields. Scale bar, 100  $\mu$ m. **d** Cells were treated as above and allowed to invade through Matrigel-coated membrane in transwells. Invasive cells were stained and counted under a light microscope. Scale bar, 100  $\mu$ m. **e** After being serum-starved for 24 h, A549 and H226 cells transiently overexpressing anti-miR-429 were treated with or without TGF- $\beta$ 1 (5 ng/ml) for 1 h and 2 h, respectively. qRT-PCR analysis was done to determine the relative *Snail* mRNA expression. **f** After being serum-starved for 24 h, A549 and H226 cells transiently overexpressing anti-miR-429 were treated with or without TGF- $\beta$ 1 (5 ng/ml) for 24 h and 48 h, respectively. N-cadherin expression was analyzed by western blot. **g** A549 and H226 cells transiently overexpressing anti-miR-429 were treated as above and allowed to migrate through an 8- $\mu$ m pore in transwells. Migrated cells were stained and counted in at least three light microscopic fields. Scale bar, 100  $\mu$ m. **h** Cells were treated as above and allowed to invade through Matrigel-coated membrane in transwells. Invasive cells were stained and counted under a light microscope. Scale bar, 100  $\mu$ m. \*\* $P$  < 0.01; \*\*\* $P$  < 0.001



Taken together, these results revealed that circPTK2 knockdown can inhibit TIF1γ expression and promote TGF-β-induced EMT and NSCLC cell invasion.

#### CircPTK2 overexpression attenuates NSCLC cell metastasis in vivo

To further investigate the role of circPTK2 overexpression in NSCLC cell metastasis in vivo, we first established

A549 cells where circPTK2 can stably overexpress. About 5-fold high expression of circPTK2 was consistently exhibited in A549 cells infected with the packaged lentivirus containing pLCDH-circPTK2-copGFP(T2A)Puro plasmids; Northern blot analysis confirmed the presence of circPTK2 overexpression in A549 cells (Fig. 6a). Then, circPTK2-overexpressed and control A549 cells were injected i.v. into BALB/c nude mice through the tail

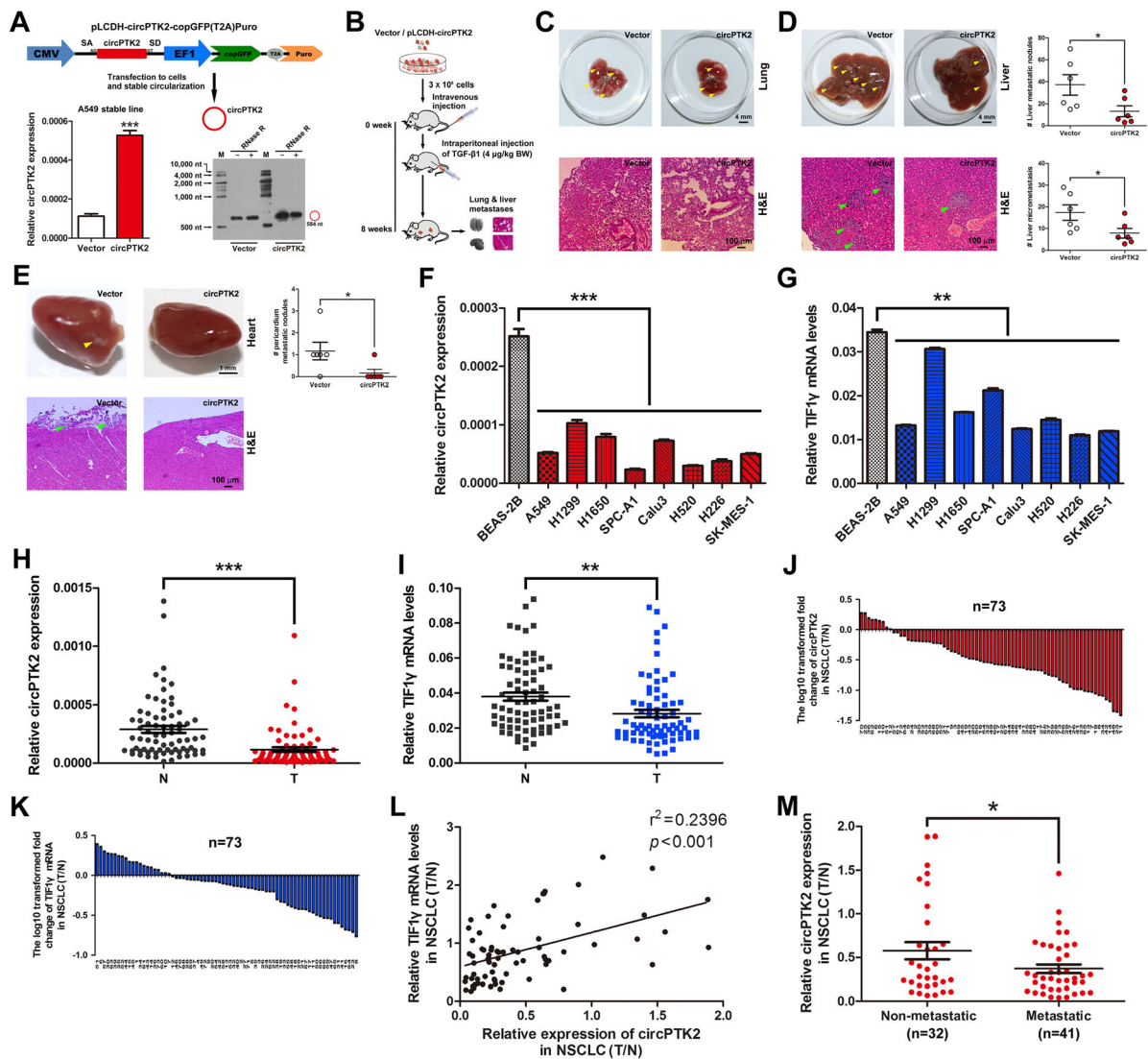


**Fig. 6** CircPTK2 overexpression attenuates NSCLC cell metastasis in vivo, and circPTK2 levels were lower in metastatic NSCLC tissues than non-metastatic counterparts. **a** CircPTK2 expression in A549 cells stably overexpressing circPTK2. A549 stable cell line overexpressing circPTK2 was generated as described in Methods. pLCDH-circPTK2-copGFP(T2A)Puro lentiviral expression vector (upper) was used to stably overexpress circPTK2. The empty vector was served as negative control. CircPTK2 expression was determined by qRT-PCR (bottom left). CircPTK2 expression in circPTK2-overexpressed A549 cells was determined using northern blots. RNase R was used to digest linear RNA (bottom right). **b** Schematic flowchart of the in vivo metastasis experiments with A549 cells stably transfected with pLCDH-circPTK2 or vector (i.v.) and TGF- $\beta$ 1 (i.p.) injected into BALB/c nude mice ( $n = 6$  mice per group in circPTK2 + TGF- $\beta$ 1 and vector + TGF- $\beta$ 1). **c** Representative images showing metastatic nodules established in lung taken from the mice injected with circPTK2-overexpressed A549 cells or vector control cells (upper). Scale bar, 4 mm. Haematoxylin and eosin (H&E) staining was performed for histological confirmation of metastasizing tumor cells in lung (bottom). Scale bar, 100  $\mu$ m. **d** Gross view of metastatic nodules developed in liver (upper left) and dot plots showing the number of metastatic nodules in liver (upper right,  $n = 6$  mice per group). Scale bar, 4 mm. Microscopic images of H&E staining for liver metastases (bottom left) and the distribution of the number of metastases in per section of liver (bottom right,  $n = 6$  mice per group). Scale bar, 100  $\mu$ m. Yellow and green arrowheads indicate metastatic nodules and micrometastases. **e** Representative images indicating metastatic nodules developed in pericardium (upper,  $n = 6$  mice per group) and H&E staining of heart (bottom). Scale bar, 1 mm or 100  $\mu$ m. **f, g** CircPTK2 and *TIF1 $\gamma$*  mRNA expression levels in human lung epithelial and NSCLC cells.  $\beta$ -actin was used as internal control. Each qRT-PCR analysis was performed in triplicate. **h, i** qRT-PCR analysis of circPTK2 and *TIF1 $\gamma$*  mRNA levels in 73 human NSCLC tissues and paired noncancerous lung tissues. Mean values are indicated by solid bars, and values are expressed as mean  $\pm$  SEM. T, NSCLC tissues; N, paired noncancerous lung tissues. **j, k** Relative expression of circPTK2 and *TIF1 $\gamma$*  mRNA in 73 paired NSCLC tissues. Y-axis represents the log<sub>10</sub> transformed fold change of T/N expression ratios of circPTK2 and *TIF1 $\gamma$*  mRNA. The number of each specimen is shown below x-axis. **l** Correlation between circPTK2 level and *TIF1 $\gamma$*  mRNA expression in 73 paired NSCLC tissues. X and y axes represent the T/N expression ratios of circPTK2 and *TIF1 $\gamma$*  mRNA, respectively. **m** Relative expression (T/N) of circPTK2 in metastatic ( $n = 41$ ) and non-metastatic ( $n = 32$ ) NSCLC tissues. Metastatic tissues were from NSCLC patients with lymph node metastasis or distant metastasis and non-metastatic tissues were from NSCLC patients without any metastasis, respectively. \* $P < 0.05$ ; \*\* $P < 0.01$ ; \*\*\* $P < 0.001$ .



vein, and TGF- $\beta$ 1 was injected i.p. post cell inoculation (Fig. 6b). Eight weeks post-inoculation, we euthanized the mice and surgically resected lungs, livers and hearts for evaluation of metastases and histology. As expected, the mice injected with circPTK2-overexpressed A549 cells or vector control cells effectively exhibited lung metastasis (Fig. 6c). Importantly, the mice injected with circPTK2-overexpressed A549 cells developed less metastatic nodules in livers and pericardia compared with those injected with control cells (Fig. 6d and e). Moreover, we monitored lung metastasis of luciferase-tagged A549 cells in vivo by the bioluminescent imaging at day 42 post-inoculation, and confirmed the metastasis-suppressing function of circPTK2 (Additional file 9: Figure S7A-G). Collectively, the in vivo experiment of metastasis shows that circPTK2 overexpression inhibits NSCLC cell metastasis in vivo.

#### CircPTK2 expression was lower in metastatic NSCLC tissues than non-metastatic counterparts

We determined that circPTK2 and *TIF1 $\gamma$*  mRNA levels were significantly lower in 8 NSCLC cell lines than human lung normal epithelial cells (Fig. 6f and g). To further evaluate whether these data are reflected in patients, we detected circPTK2 and *TIF1 $\gamma$*  mRNA levels in 73 NSCLC and paired noncancerous lung tissues. NSCLC tissues showed a significant reduction in their expression (87.7% for circPTK2 and 69.9% for *TIF1 $\gamma$*  mRNA, respectively) when compared with noncancerous lung tissues (Fig. 6h-k). Among 64 NSCLC tissues with low circPTK2 expression, 49 tumors (76.6%) showed low *TIF1 $\gamma$*  expression (Fig. 6j and k; Additional file 10: Table S3); In contrast, of 7 NSCLC tissues with high circPTK2 expression, 4 tumors (57.1%) presented high *TIF1 $\gamma$*  expression (Fig. 6j and k; Additional file 10: Table S3). Moreover, the ratio of circPTK2 expression (T/N) was positively correlated with that of *TIF1 $\gamma$*  mRNA level (T/N) in NSCLC tissues ( $P < 0.001$ ; Fig. 6l). Importantly, circPTK2 was significantly lower in metastatic NSCLC tissues as compared to their non-metastatic counterparts (Fig. 6m). Therefore, a close link between circPTK2 and *TIF1 $\gamma$*  was established in NSCLC, supporting the notion that circPTK2 functions as a tumor suppressor through regulating *TIF1 $\gamma$* .

#### Discussion

To date, whether and how circRNAs contribute to TGF- $\beta$ -induced EMT in NSCLC remains elusive. In the present study, we reveal that circPTK2 inhibits TGF- $\beta$ -induced EMT by up-regulating *TIF1 $\gamma$*  in NSCLC, and establish a novel mechanistic role of circPTK2-*TIF1 $\gamma$*  axis in regulating TGF- $\beta$ -induced EMT (Additional file 11: Figure S8).

*TIF1 $\gamma$*  (alias, TRIM33/RFG7/PTC7/Ectodermin), a regulator of TGF- $\beta$ /Smad signaling, acts as an “antagonist” by ubiquitinating Smad4 or a “complementary agonist” by competing with Smad4 to regulate TGF- $\beta$ /Smad signaling [12, 13]. *TIF1 $\gamma$*  has been proved to contribute to multiple malignancies [16, 31–33], and *TIF1 $\gamma$*  is essential for regulating TGF- $\beta$  signaling [34, 35] and EMT [11]. Our previous studies show that *TIF1 $\gamma$*  expression is frequently reduced in NSCLC and *TIF1 $\gamma$*  repression enhances TGF- $\beta$ -induced EMT and NSCLC cell invasion [14, 36]. Knockdown of *TIF1 $\gamma$*  increases the expression of Snail [14], an important downstream transcriptional activator of TGF- $\beta$ /Smad signaling [9]. Here, we show that reduced *TIF1 $\gamma$*  is not just associated with poor survival of NSCLC patients but also positively correlated with circPTK2 expression in NSCLC tissues. Moreover, circPTK2 expression were significantly reduced in NSCLC cells and circPTK2 overexpression augmented *TIF1 $\gamma$*  expression in NSCLC cells. Thus, for the first time, we established a link between *TIF1 $\gamma$*  and circPTK2 in NSCLC. Actually, circPTK2 is produced from the *PTK2* gene, which spans seven of its exons. We validated the characterization of circPTK2 in NSCLC cells (Fig. 1c-f). It has been well documented that exon-intron or intron-derived circRNAs promote their parent gene transcription in cell nucleus, but exon-derived circRNAs do not affect the expression of their parent genes [29]. In the present study, circPTK2 derived from multiple exons of *PTK2* was detected in the cytoplasm (Fig. 1f) and circPTK2 did not influence its parent gene *PTK2* expression (Additional file 8: Figure S6B). To the best of our knowledge, circPTK2 is a circular RNA which function has not yet been defined in human cancers. In this study, we identified that circPTK2 can function as a sponge for miR-429/miR-200b-3p to counter degradation of *TIF1 $\gamma$* . Moreover, miR-429/miR-200b-3p promoted TGF- $\beta$ -induced EMT and cell invasion by inhibiting *TIF1 $\gamma$*  in NSCLC cells. These data suggests that circPTK2 has potential functional role in TGF- $\beta$ -induced EMT and NSCLC metastasis.

Although circRNAs' expression is often low, circRNAs are emerging as oncogenic stimuli or tumor suppressors in cancer [37]. To date, the mechanistic roles of circRNAs in TGF- $\beta$ -induced EMT are poorly understood in NSCLC. Therefore, we primarily performed circRNA microarray analysis and identified that circPTK2 was significantly reduced during TGF- $\beta$ -induced EMT of NSCLC cells. Moreover, circPTK2 overexpression inhibited TGF- $\beta$ -induced EMT and NSCLC cell invasion, whereas its knockdown had the opposite effect. Especially, circPTK2 was significantly lower in metastatic NSCLC tissues than non-metastatic counterparts, supporting the roles of circPTK2 in NSCLC cell invasion in vitro. Furthermore, the in vivo experiment of metastasis



showed that circPTK2 overexpression suppressed NSCLC cell metastasis. Collectively, these results suggested that circPTK2 may function as a tumor metastasis suppressor by controlling TGF- $\beta$  signaling activity.

There are multiple and diverse molecular mechanisms of TGF- $\beta$ -induced EMT in human cancers [38, 39]. In fact, it is not surprising because various molecules participate in TGF- $\beta$  signaling, which is a potent inducer of EMT. Unexceptionally, long non-coding RNAs (lncRNAs) and microRNAs (miRNAs) are also implicated in TGF- $\beta$  signaling and EMT [40–42]. As exemplified, miR-145 and miR-203 repressed SMAD3, a downstream effector in canonical TGF- $\beta$ /Smad signaling, then inhibited TGF- $\beta$ -induced EMT in NSCLC cells [43]. In the present study, miR-429/miR-200b-3p acted as invasion-promoting miRNAs to promote TGF- $\beta$ -induced EMT in NSCLC cells. Our results are different from the previous findings where miR-429/miR-200b-3p was recognized as anti-metastatic miRNAs in glioma and renal cell carcinoma [44, 45]. However, Lang et al. reported that miR-429 promoted the metastasis of NSCLC cells [46], supporting our results obtained in NSCLC cells. This can be explained by the idea that miRNAs may exert distinct roles depending on the cellular context, which is probably attributed to the availability of specific targets or downstream effectors [47]. Moreover, the invasion-promoting phenotype of miR-429/miR-200b-3p overexpression was copied by knockdown of TIF1 $\gamma$ , which promoted TGF- $\beta$ -induced EMT in NSCLC cells [14]. In fact, our data and a public data set (GSE36681) suggests that miR-429/miR-200b exerts a tumor-promoting role in NSCLCs (Additional file 12: Table S4 and Additional file 13: Figure S9A–F). It has been proposed that TGF- $\beta$  induces EMT by driving the expression of ZEB transcription factors, which in turn inhibit miR-200 family members via a double-negative feedback loop [48]. However, on TGF- $\beta$ 1 stimulation, miR-429/miR-200b-3p levels were still unchanged in time-independent manner, albeit a dynamic alteration of ZEB1/ZEB2 expression in A549 cells (Additional file 14: Figure S10A–D). In support of this, Zhang et al. reported that miR-200 family members were not altered by TGF- $\beta$ 1 in A549 cells [28]. More importantly, we here provided the first evidence that TGF- $\beta$  promotes EMT via circRNAs in NSCLC, albeit circPTK2 may be one of several circRNAs affecting TGF- $\beta$ -induced EMT. Interestingly, TGF- $\beta$  was able to down-regulate circPTK2 expression but failed to alter miR-429/miR-200b-3p levels in NSCLC cells. This result is consistent with that circPTK2 is frequently reduced in NSCLC tissues (Fig. 6h and j), where increased expression of TGF- $\beta$  has been detected [6, 7, 27]. More recently, Conn et al. identified that formation of >30% of abundant circRNAs was regulated by QKI during TGF- $\beta$ -mediated EMT in human mammary cells [25]. Zong et al. reported

that QKI is frequently reduced in NSCLC [26]. The two investigations on QKI might provide an explanation for why TGF- $\beta$  diminished circPTK2 expression in NSCLC cells. Interestingly, QKI plays an important role in TGF- $\beta$ -mediated downregulation of circPTK2 (Additional file 15: Figure S11A–D).

More interestingly, another circRNA hsa\_circ\_0003221 (also named after circPTK2), with a spliced sequence length of 625 nt in circBase (<http://www.circbase.org>), has been reported to promote the proliferation and migration of bladder cancer cells [49]. Although hsa\_circ\_0003221 and hsa\_circ\_0008305 are derived from the same parent gene *PTK*, they exert different functions. In fact, this is not surprising because they could have distinct mechanisms depending on the cellular context or downstream target molecules.

In summary, our findings show that circPTK2 (hsa\_circ\_0008305) inhibits TGF- $\beta$ -induced EMT through regulating TIF1 $\gamma$  and NSCLC cell metastasis, as well as establish a positive relationship between TIF1 $\gamma$  and circPTK2 in NSCLC, revealing a novel mechanism by which circRNA regulates TGF- $\beta$ -mediated EMT and tumor metastasis, and suggesting that overexpression of circPTK2 could provide a therapeutic strategy for advanced NSCLC.

## Methods

### Cell lines and cell culture

Human lung normal epithelial cell BEAS-2B, and NSCLC cells A549, H1299, H1650, SPC-A1, and Calu3 (lung adenocarcinoma cells) and H226, H520, and SK-MES-1 (lung squamous carcinoma cells) from Cell Bank of Chinese Academy of Sciences were cultured in RPMI 1640 medium (HyClone, South Logan, UT, USA) supplemented with penicillin/streptomycin, L-glutamine and 10% fetal bovine serum (FBS, Invitrogen, Carlsbad, CA, USA) at 37 °C in a humidified atmosphere with 5% CO<sub>2</sub>. A549 and H226 cells were induced by TGF- $\beta$ 1 to undergo EMT as per our description [9, 14].

### Tissue samples

Seventy-three fresh NSCLC tissues and paired adjacent noncancerous lung tissues (Additional file 10: Table S3) were collected after informed consent from patients in the First Affiliated Hospital of Soochow University. Histological and pathological diagnostics for NSCLC patients were evaluated based on the Revised International System for Staging Lung Cancer. Patients received neither chemotherapy nor radiotherapy before tissue sampling. As listed in Additional file 10: Table S3, metastatic tissues ( $n = 41$ ) were from NSCLC patients with local lymph node metastasis (T<sub>1-4</sub> N<sub>1-2</sub> M<sub>0</sub>) or distant organ metastasis (T<sub>1-4</sub> N<sub>any</sub> M<sub>1</sub>), and non-metastatic tissues ( $n = 32$ ) were from NSCLC patients without any

metastasis (T<sub>1-4</sub>N<sub>0</sub>M<sub>0</sub>). The samples were snap-frozen in liquid nitrogen and stored at -80 °C before RNA extraction. This study was approved by the Ethics Committee of Soochow University.

#### Real-time quantitative reverse transcriptase PCR (qRT-PCR)

RNA was isolated using TRIzol (Thermo Fisher Scientific, Carlsbad, CA, USA). cDNA synthesis and qRT-PCR analysis were performed as described by us [50] with some modification. Primers are listed in Additional file 16: Table S5. U6 levels were used to normalize miR-429/miR-200b-3p expression.  $\beta$ -actin was endogenous control for *TIF1 $\gamma$*  mRNA, *Snail* mRNA, *PTK2* mRNA and circPTK2. Relative expression of each RNA was determined using the  $\Delta\Delta C_t$  method. Each qRT-PCR analysis was done in triplicate.

#### Western blot analysis

Cells were lysed and subjected to western blot analysis as described by us [51]. Antibodies were as follows: mouse anti-TIF1 $\gamma$  (Santa Cruz Biotechnology, Santa Cruz, CA, USA), mouse anti-E-cadherin, anti-N-cadherin and anti-Vimentin (BD Biosciences, San Jose, CA, USA), mouse anti-Snail (Cell Signaling Technology, Danvers, MA, USA), mouse anti- $\beta$ -actin and anti-mouse secondary antibodies (Santa Cruz Biotechnology). Molecular sizes of TIF1 $\gamma$ , E-cadherin, N-cadherin, Vimentin, Snail and  $\beta$ -actin proteins shown on the immunoblots are 150kD, 120kD, 130kD, 57kD, 29kD and 43kD, respectively. Each experiment was carried out in triplicate.

#### CircRNA microarray analysis

Total RNA from A549 cells treated without and with TGF- $\beta$ 1 was used for Arraystar Human circRNA Array (Arraystar Inc., Rockville, MD, USA). CircRNA microarray analysis was performed as described [52]. CircRNAs (fold change  $\geq 1.5$  and *P*-value < 0.05) were considered to be differentially expressed between two groups. Each group (cells treated with TGF- $\beta$ 1 for 0 h or 24 h, respectively) was analyzed in triplicate.

#### Northern blot with denaturing agarose gels

Digoxin-labeled DNA probes (351 nt), spanning the back-splice junction of circPTK2, were prepared from cDNA using PCR DIG Probe Synthesis Kit (Roche, Mannheim, Germany). PCR primers were as follows: 5'-GAATATGGCTGACCTAATAGA-3' (forward); 5'-ACACTTGAAGCATTCCTTATC-3' (reverse).

Total RNA (15  $\mu$ g) denatured in formaldehyde was resolved on 1% agarose-formaldehyde gel and transferred onto a Hybond-N<sup>+</sup> nylon membrane (GE Healthcare, Buckinghamshire, UK). Membranes were crosslinked, pre-hybridized in DIG Easy Hyb (Roche), and hybridized with DIG-labeled DNA probes overnight. After stringent

washing, the membranes was incubated with alkaline phosphatase (AP)-conjugated anti-DIG antibodies (Roche). Immunoreactive bands were visualized using chemiluminescent substrate CSPD (Roche) followed by exposure to X-ray film.

#### Prediction of miRNA targets

CircRNA/miRNA interaction was predicted with miRNA target prediction software (Arraystar's home-made) based on TargetScan and miRanda. TargetScan (Release 7.1, <http://www.targetscan.org>) or miRBase (Release 21, <http://www.mirbase.org>) were employed to identify the miRNA targeting sites in *TIF1 $\gamma$*  3'-UTR.

#### Luciferase reporter assay

A series of constructs containing *TIF1 $\gamma$*  3'-UTR and circPTK2 exon11 were generated using psiCHECK2 dual luciferase vector (Promega, Madison, WI, USA). Different fragments (Additional file 4: Table S2) were directly synthesized (GENEWIZ Inc., Suzhou, China), subcloned into the psiCHECK-2 vector to create various constructs. Each construct was subsequently cotransfected with miR-429 mimic (5'-UAAUACUGUCUGGUAAAACCGU-3') or miR-200b-3p mimic (5'-UAAUACUGCCUGGUAAUGAUGA-3') and a negative control (miR-NC, 5'-UUCUCCGAACGUGUCACGUTT-3') into A549 and H226 cells. All the transient transfections, including miR-429 inhibitor (5'-ACGGUUUUACCAGACAGUAUUA-3') or miR-200b-3p inhibitor (5'-UCAUCAUACCAGGCAGUAUUA-3') and anti-miR-NC (5'-CAGUACUUUGUGUAGUACAA-3'), were performed using Lipofectamine 2000 (Invitrogen). After 48 h, cells were harvested, and luciferase activities were determined by the Dual-Luciferase Reporter Assay Kit (Promega). Results are presented as relative *Renilla* luciferase activities, which are normalized to firefly luciferase activities. Each experiment was performed in triplicate.

#### RNA-binding protein immunoprecipitation (RIP) assay

RIP assay was performed using EZ-Magna RIP Kit (Millipore, Billerica, MA, USA). The AGO2-RIP experiments were performed in A549 cells transiently overexpressing miR-429/miR-200b-3p or miR-NC. Briefly, cells were lysed using RIP lysis buffer with proteinase and RNase inhibitors (Millipore), and the RIP lysates were incubated with RIP buffer containing magnetic beads conjugated with human anti-Ago2 antibody or nonspecific mouse IgG antibody (Millipore). Each immunoprecipitate was digested with proteinase K, and the immunoprecipitated RNAs were subjected to RT-PCR and gel-staining analyses to detect circPTK2 enrichment. Each RIP assay was repeated three times.

### RNA pull-down analysis

RNA pull-down analysis was performed as previously described [53] with some modification. Briefly, the RIP lysates from A549 cells were incubated with biotin (Bio)-labeled oligonucleotide probes against circPTK2 (**Bio**-5'-TTAAACCAACATCTTTTCTGACACAGAGACGGCG-3', RiboBio, Guangzhou, China) for 2 h at 25 °C. CircPTK2/miRNA complexes were captured with Streptavidin-coupled Dynabeads (Invitrogen). CircPTK2/miRNA/beads complexes were incubated with RIP wash buffer (Millipore) containing proteinase K for 1 h at 25 °C. CircPTK2 and miR-429/miR-200b-3p in the pull-down were determined using qRT-PCR analysis. The retrieved circPTK2 or miR-429/miR-200b-3p were evaluated as the percentage of pull-down to input. Each experiment was performed in triplicate.

### Fish

Cells were cultured on coverslips, fixed and permeabilized as previously described by us [14]. Subsequently, the coverslips were hybridized in hybridization buffer (Genesee Biotech, Guangzhou, China) with digoxin (Dig) and biotin (Bio)-labeled single-stranded DNA probes at 37 °C overnight. Digoxin-labeled probes (**Dig**-5'-CATCTTTTC TGACACAGAGACGGCG-3'-**Dig**) specific to circPTK2 back-splice region and biotin-labeled probes against miR-429/miR-200b-3p (for miR-429, **Bio**-5'-ACGG TTTTACCAGACAGTATTA-3'-**Bio**; for miR-200b-3p, **Bio**-5'-TCATCATTACCAGGCAGTATTA-3'-**Bio**) were prepared (Genesee Biotech). The signals were detected by Cy3-conjugated anti-digoxin and FITC-conjugated anti-biotin antibodies (Jackson ImmunoResearch Inc., West Grove, PA, USA). Cell nuclei were counterstained with 4,6-diamidino-2-phenylindole (DAPI). Finally, the images were obtained on a Zeiss LSM 700 confocal microscope (Carl Zeiss, Oberkochen, Germany). Each experiment was performed three times.

### Establishment of NSCLC cells transiently and stably overexpressing circPTK2

To establish A549 and H226 cell lines transiently overexpressing circPTK2, we subcloned full-length of 584-bp circPTK2 into a pLCDH-ciR lentiviral expression vector (Genesee Biotech) to generate pLCDH-circPTK2-copGFP(T2A)Puro construct. The subcloned sequence containing front circular frame (SA), back circular frame (SD) of circRNA biogenesis and full-length of circPTK2, 5'-TGAAATATGCTATCTTACAG-circPTK2-GTGA ATATATTTTTTCTTGA-3', was directly synthesized (GENEWIZ Inc.). Cells were transiently transfected with the construct using Lipofectamine 2000. The empty vector was used as negative control. After transfection for 48 or 72 h, cells were harvested for additional more experiments.

To generate A549 cells stably overexpressing circPTK2, we cotransfected the above-mentioned construct or empty vector with packaging plasmids psPAX2 and pMD2.G (Genesee Biotech) into HEK 293 T cells using Lipofectamine 2000 (Invitrogen). After HEK 293 T cells were cultured for 48 h, the packaged lentiviruses were harvested. A549 cells were infected with the virus and cultured for 3 days. Finally, A549 cells were selected with 0.5 µg/ml of puromycin (Sigma-Aldrich, St. Louis, MO, USA) for in vivo experiments of metastasis.

### RNA interference for circPTK2 knockdown

CircPTK2 was specifically knockdown using siRNA (si-circPTK2, 5'-GUGUCAGAAAAGAUGUUGGUU-3'), which was designed by CircInteractome (<http://circinteractome.nia.nih.gov>) and synthesized (GenePharma, Shanghai, China) to target circPTK2 back-splice junction. Scramble siRNA (5'-CACAGUCAAAGAUGUUGGUU-3') was used as a negative control. A549 and H226 cells were transfected with 100 pmol of siRNA using Lipofectamine 2000 (Invitrogen). After 48 or 72 h, cells were harvested for qRT-PCR analysis of circPTK2 and linear *PTK2* mRNA expression or for other experiments.

### Transwell migration and invasion assays

Transwell assays were conducted to evaluate cell migration and invasion abilities as described by us [14]. Briefly, A549 and H226 cells transiently overexpressing miR-429/miR-200b-3p or circPTK2 were incubated with TGF-β1 (5 ng/ml) in Transwell plates (BD Biosciences) for 24 h and 48 h. Then cells were allowed to migrate through an 8-µm pored membrane or invade through Matrigel-coated membrane. Migrated and invasive cells were stained and counted under a light microscope. Transwell assays were done in triplicate.

### In vivo experiments of metastasis

Female BALB/c nude mice (4–6 weeks, 18–20 g) were purchased from the Laboratory Animal Center of Soochow University, and were bred and maintained in specific pathogen-free conditions. Mice were divided into two groups, including circPTK2 overexpression group and control group (6 mice per group). CircPTK2-overexpressed and control A549 cells ( $3 \times 10^6$  cells/mouse) in PBS were intravenously (i.v.) injected into the tail vein of mice. TGF-β1 (4 µg/kg bodyweight) was injected intraperitoneally (i.p.) every 5th day post cell inoculation as previously described [27] to facilitate TGF-β-induced cancer cell invasion. Fifty-six days post-inoculation, the mice were sacrificed and their lung, liver and heart tissues were histologically analyzed with H&E staining for the presence of metastasizing tumor cells. Before H&E staining, the number of metastatic



nodules established in lung, liver and pericardium was counted. To monitor tumor cells metastasized to lung, bioluminescent imaging was performed using an IVIS® Spectrum in vivo imaging system (Caliper Life Sciences, Hopkinton, MA, USA). Approximately 15 min before imaging, the mice were injected i.p. with D-luciferin sodium salt (Yeasen Biotech, Shanghai, China) in PBS (15 mg/ml) at a dose of 150 mg/kg bodyweight. Following air anaesthesia with isoflurane, live images were acquired using photography and photons emitted from active luciferase within a region of interest (ROI) were quantified using Living Image® 4.0 software (measured in photons/sec/cm<sup>2</sup>/steradian). Animal studies were approved by the Ethics Committee of Soochow University.

### Statistical analysis

Difference between two groups was assessed using paired or unpaired *t* test (two-tailed). Pearson's correlation test was used to determine the association between two groups. Results were presented as mean ± SEM. *P* values of < 0.05 were considered significant. Statistical analyses were performed using GraphPad Prism 5.02 software (GraphPad, San Diego, CA, USA).

### Conclusions

In conclusion, our findings show that circPTK2 (hsa\_circ\_0008305) inhibits TGF-β-induced EMT and metastasis by controlling TIF1γ in NSCLC, revealing that circPTK2 has an important role in regulating TGF-β-induced EMT and tumor metastasis, and suggesting a rationale for therapeutically upregulating circular RNAs in patients with advanced NSCLC.

### Additional files

**Additional file 1: Figure S1.** Reduced TIF1γ is expressed in NSCLC tissues and associated with poor survival of NSCLC patients. (A, B) Data regarding *TIF1γ* mRNA expression in lung adenocarcinoma, squamous cell carcinoma tissues and normal lung tissues from several study groups in Oncomine database (<http://www.oncomine.org>). (C, D) Kaplan-Meier survival curves for 85 patients with lung adenocarcinoma (AdC) and 71 patients with lung squamous cell carcinoma (SqC). Primary data were taken from GSE30219 and TCGA in Kaplan-Meier Plotter (<http://www.kmplot.com>). (TIF 2402 kb)

**Additional file 2: Table S1.** Arraystar Human circRNA Array analysis of A549 cells treated with TGF-β1. Among 187 differentially expressed circRNAs (fold change ≥ 1.5, *P*-value < 0.05 and FDR < 0.05), 88 circRNAs were up-regulated and 99 circRNAs were down-regulated in A549 cells after TGF-β1 treatment for 24 h. CircRNA ID: encoded in circBase (<http://www.circbase.org>). *P*-value: estimated by paired *t*-test. FDR: false discovery rate, calculated from Benjamini Hochberg FDR. Fold change: the absolute ratio (no log scale) of normalized intensities between two conditions (treated with TGF-β1 vs. treated without TGF-β1). (DOC 195 kb)

**Additional file 3: Figure S2.** The in silico prediction of the interaction between miR-429/miR-200b-3p and circPTK2 or *TIF1γ* 3'-UTR. (A) The interaction of circPTK2 and miR-429/miR-200b-3p was predicted with miRNA target prediction software (Arraystar's home-made) based on TargetScan and miRanda. (B, C) The target interaction between miR-429/

miR-200b-3p and *TIF1γ* 3'-UTR was in silico predicted by TargetScan (Release 7.1 <http://www.targetscan.org>)/miRBase (Release 21, <http://www.mirbase.org>). Four different sites (positions 145–152, 2247–2253, 2690–2696 and 4486–4492) of *TIF1γ* 3'-UTR were predicted to be targets of miR-429/miR-200b-3p. (TIF 6394 kb)

**Additional file 4: Table S2.** Sequences for construction of luciferase reporter plasmids containing predicted miR-429 and miR-200b-3p target sites in *TIF1γ* 3'-UTR and circPTK2. (DOC 38 kb)

**Additional file 5: Figure S3.** miR-200b-3p inhibits TIF1γ expression by targeting 3'-UTR of *TIF1γ* transcript. (A) Schematic description for the subcloning of the predicted miR-200b-3p binding sites of *TIF1γ* 3'-UTR in psiCHECK-2 luciferase vector. Predicted duplex formation between miR-200b-3p and the wild-type/mutant of miR-200b-3p binding sites was indicated. The entire subcloning sequences were listed in Additional file 4: Table S2. (B) Relative luciferase activity of the wild-type/mutant *TIF1γ* 3'-UTR reporter gene in A549 and H226 cells transfected with miR-200b-3p or negative control (miR-NC). Scrambled sequence was used as miR-NC. Relative *Renilla* luciferase activity was determined after normalizing against the firefly luciferase activity. (C) qRT-PCR analysis of miR-200b-3p expression levels in A549 and H226 cells transfected with miR-200b-3p mimics or miR-NC. U6 was employed as internal control. (D, E) *TIF1γ* mRNA and protein expression in A549 and H226 cells transfected with miR-200b-3p mimics or miR-NC. β-actin was used as internal control. Densitometry values for TIF1γ protein were normalized to β-actin and shown below the corresponding bands. (F) miR-200b-3p expression levels in A549 and H226 cells transfected with miR-200b-3p inhibitors (anti-miR-200b-3p) or negative control (anti-miR-NC). Scrambled sequence was used as anti-miR-NC. (G, H) *TIF1γ* mRNA and protein expression in A549 and H226 cells transfected with anti-miR-200b-3p or anti-miR-NC. \**P* < 0.05; \*\**P* < 0.01; \*\*\**P* < 0.001. (TIF 5059 kb)

**Additional file 6: Figure S4.** CircPTK2 abolishes endogenous miR-429/miR-200b-3p-mediated repression of TIF1γ and inhibits TGF-β-induced invasion of NSCLC cells. (A) *TIF1γ* mRNA expression in A549 cells transiently overexpressing circPTK2 or empty vector in the presence or absence of miR-429/miR-200b-3p mimics. OE, overexpression. (B) TIF1γ protein levels in A549 cells transiently overexpressing circPTK2 in the above-mentioned condition. Densitometry values for TIF1γ protein were normalized to β-actin and indicated below the corresponding bands. (C, D) A549 cells overexpressing circPTK2 and miR-429/miR-200b-3p mimics were serum-starved for 24 h, and then were subjected to Transwell migration and invasion assays in the presence or absence of TGF-β1 described as Methods. Migrated and invasive cells were stained and counted in at least three light microscopic fields. Scale bar, 100 μm. \**P* < 0.05; \*\**P* < 0.01; \*\*\**P* < 0.001. (TIF 14297 kb)

**Additional file 7: Figure S5.** miR-200b-3p promotes TGF-β-induced EMT and invasion in NSCLC cells. (A) After being serum-starved for 24 h, A549 and H226 cells transiently overexpressing miR-200b-3p were treated with or without TGF-β1 (5 ng/ml) for 1 h and 2 h, respectively. *Snail* mRNA expression was quantified by qRT-PCR analysis. *Snail* mRNA level of the unstimulated cells was assigned the value 1, and the relative *Snail* mRNA expression in TGF-β1-stimulated cells was recalculated accordingly. (B) After being serum-starved for 24 h, A549 and H226 cells transiently overexpressing miR-200b-3p were treated with or without TGF-β1 (5 ng/ml) for 24 h and 48 h, respectively. Western blot analysis was performed to examine the expression of N-cadherin, which was normalized to β-actin. (C) A549 and H226 cells transiently overexpressing miR-200b-3p were treated as above and allowed to migrate through an 8-μm pore in transwells. Migrated cells were stained and counted in at least three light microscopic fields. Scale bar, 100 μm. (D) Cells were treated as above and allowed to invade through Matrigel-coated membrane in transwells. Invasive cells were stained and counted under a light microscope. Scale bar, 100 μm. (E) After being serum-starved for 24 h, A549 and H226 cells transiently overexpressing anti-miR-200b-3p were treated with or without TGF-β1 (5 ng/ml) for 1 h and 2 h, respectively. qRT-PCR analysis was done to determine the relative *Snail*



mRNA expression. (F) After being serum-starved for 24 h, A549 and H226 cells transiently overexpressing anti-miR-200b-3p were treated with or without TGF- $\beta$ 1 (5 ng/ml) for 24 h and 48 h, respectively. N-cadherin expression was analyzed by western blot. (G) A549 and H226 cells transiently overexpressing anti-miR-200b-3p were treated as above and allowed to migrate through an 8- $\mu$ m pore in transwells. Migrated cells were stained and counted in at least three light microscopic fields. Scale bar, 100  $\mu$ m. (H) Cells were treated as above and allowed to invade through Matrigel-coated membrane in transwells. Invasive cells were stained and counted under a light microscope. Scale bar, 100  $\mu$ m. \* $P$  < 0.05; \*\*\* $P$  < 0.001. (TIF 5920 kb)

**Additional file 8: Figure S6.** CircPTK2 knockdown inhibits TIF1 $\gamma$  expression and promotes TGF- $\beta$ -induced EMT and invasion of NSCLC cells in vitro. (A) *Left panel*, a siRNA targeting circPTK2 JCT (si-circPTK2) was designed to specifically knockdown circPTK2. *Right panel*, A549 and H226 cells were transfected with si-circPTK2 and siRNA negative control (si-NC). qRT-PCR was performed to detect circPTK2 expression in the siRNA-transfected cells. (B) Linear PTK2 mRNA expression in circPTK2-silenced A549 and H226 cells. (C) TIF1 $\gamma$  mRNA and protein levels in A549 and H226 cells transfected with si-circPTK2 or si-NC. (D) siRNA-transfected A549 and H226 cells were serum-starved for 24 h and then treated with or without TGF- $\beta$ 1 (5 ng/ml) for 24 h and 48 h, respectively. Snail and N-cadherin protein levels were determined by western blot. (E, F) A549 and H226 cells were treated as above and subjected to the transwell migration and invasion assays. Migrated and invasive cells were stained and counted in at least three light microscopic fields. Scale bar, 100  $\mu$ m. \* $P$  < 0.05; \*\* $P$  < 0.01; \*\*\* $P$  < 0.001. (TIF 4550 kb)

**Additional file 9: Figure S7.** CircPTK2 overexpression attenuates NSCLC cell metastasis in vivo by the bioluminescent imaging. (A) CircPTK2 expression in A549 cells stably overexpressing circPTK2. pLV-Luci(2A)Puro lentiviral expression vector (*upper panel*) was used to stably overexpress circPTK2. The empty vector was served as negative control. CircPTK2 expression was determined by qRT-PCR (*bottom panel*). (B) Schematic flowchart of the in vivo metastasis experiments with A549 cells stably transfected with pLV-circPTK2 or vector (i.v.) and TGF- $\beta$ 1 (i.p.) injected into BALB/c nude mice ( $n$  = 10 mice per group in circPTK2 + TGF- $\beta$ 1 and vector + TGF- $\beta$ 1). (C) Representative images of in vivo bioluminescence of mice injected with circPTK2-overexpressed A549 cells or vector-control cells at day 42 post-inoculation. Color bar represents extent of luciferase bioluminescence intensity (blue, green and red indicate low, medium and high intensity, respectively). (D) Quantification of radiance emitted from active luciferase in lung of mice ( $n$  = 10 mice for each group) at day 42. (E) Representative images showing metastatic nodules established in lung taken from the mice injected with circPTK2-overexpressed A549 cells or vector control cells at day 49 (*upper*). Scale bar, 4 mm. H&E staining was performed for histological confirmation of metastasizing tumor cells in lung (*bottom*). Scale bar, 100  $\mu$ m. Green arrowhead indicate micrometastasis. (F) Gross view of liver of mice at day 49 post-inoculation (*upper*) and microscopic images of H&E staining for liver metastases (*bottom*). Scale bar, 4 mm or 100  $\mu$ m. Green arrowhead indicate micrometastasis. (G) Dot plots showing the distribution of the number of micrometastases in per section of liver ( $n$  = 10 mice for each group). \* $P$  < 0.05; \*\* $P$  < 0.01; \*\*\* $P$  < 0.001. (TIF 5869 kb)

**Additional file 10: Table S3.** Demographic and clinical characteristics of 73 NSCLC patients and relative expression of circPTK2 and TIF1 $\gamma$  mRNA in 73 paired NSCLC tissues. (DOC 134 kb)

**Additional file 11: Figure S8.** A work model of the mechanistic interaction between circPTK2, miR-429/miR-200b-3p and TIF1 $\gamma$  for controlling TGF- $\beta$ -induced EMT in NSCLC cells: Circular RNA circPTK2 upregulates the expression of TIF1 $\gamma$ , a well-known negative regulator of TGF- $\beta$  signaling, by sponging miR-429/miR-200b-3p in NSCLC cells, and in turn inhibits TGF- $\beta$ -induced EMT. (TIF 449 kb)

**Additional file 12: Table S4.** Demographic and clinical characteristics of 73 NSCLC patients and relative expression of miR-429 and miR-200b-3p in 73 paired NSCLC tissues. (DOC 151 kb)

**Additional file 13: Figure S9.** miR-429/miR-200b-3p are upregulated in NSCLC tissues. (A, B) qRT-PCR analysis of miR-429/miR-200b-3p levels in 73 human NSCLC tumors and paired noncancerous lung tissues. (C, D) Relative expression of miR-429/miR-200b-3p in 73 paired NSCLC tissues. Y-axis represents the log<sub>10</sub> transformed fold change of T/N expression ratios of miR-429 or miR-200b-3p. The number of each specimen is shown below x-axis. (E, F) Relative miR-429/miR-200b expression levels of 56 human NSCLC tumors and paired adjacent normal lung tissues in a public data set (GSE36681). Mean values are indicated by solid bars, and values are expressed as mean  $\pm$  SEM. \*\* $P$  < 0.01; \*\*\* $P$  < 0.001. (TIF 2543 kb)

**Additional file 14: Figure S10.** Expression of ZEB1/ZEB2 and miR-429/miR-200b-3p in A549 cells treated with TGF- $\beta$ 1 in time-dependent manner. After being serum-starved for 24 h, A549 cells were exposed to 5 ng/ml TGF- $\beta$ 1 for the indicated times, and the expression of ZEB1/ZEB2 (A, B) and miR-429/miR-200b-3p (C, D) were determined by qRT-PCR analysis. (TIF 2073 kb)

**Additional file 15: Figure S11.** TGF- $\beta$  inhibits QKI expression and QKI knockdown reduces circPTK2 expression in A549 cells. (A, B) After being serum-starved for 24 h, A549 cells were exposed to 5 ng/ml TGF- $\beta$ 1 for the indicated times, and the expression of QKI and circPTK2 was determined by qRT-PCR analysis. (C, D) qRT-PCR analysis of QKI and circPTK2 levels in A549 cells transfected with two siRNAs specific for QKI (si-QKI-1 and si-QKI-2). Scramble siRNA was used as negative control (si-NC). \*\* $P$  < 0.01; \*\*\* $P$  < 0.001. (TIF 557 kb)

**Additional file 16: Table S5.** Primers for qRT-PCR analysis. (DOC 31 kb)

## Abbreviations

CircRNA: Circular RNA; EMT: Epithelial-mesenchymal transition; FISH: Fluorescence in situ hybridization; miRNA: microRNA; NSCLC: Non-small cell lung cancer; PTK2: Protein tyrosine kinase 2; QKI: Quaking; RIP: RNA-binding protein immunoprecipitation; TGF- $\beta$ : Transforming growth factor  $\beta$ ; TIF1 $\gamma$ : Transcriptional intermediary factor 1 $\gamma$ ; ZEB: Zinc finger E-box binding homeobox

## Acknowledgements

We are grateful for participation and cooperation from the patients with NSCLC. We also acknowledge Prof. Lijuan Pang of Department of Pathology, Shihezi University School of Medicine for performing histopathological assessment. We would like to thank the online software TargetScan, miRanda, miRBase, circBase and CircInteractome for providing in silico prediction, and the online databases Oncomine and Kaplan-Meier plotter for sharing NSCLC data.

## Funding

This study was supported by National Natural Science Foundation of China (81872343, 81672277, 81502498 and 81372277), and Suzhou Key Laboratory for Molecular Cancer Genetics (SZS201209), and Soochow Scholar Project of Soochow University (SSPSU2010-51), and A Project Funded by the Priority Academic Program Development of Jiangsu Higher Education Institutions (PAPD-XL2014014).

## Availability of data and materials

Please contact the corresponding author for all data requests.

## Authors' contributions

LW and HTZ designed the research. LW, XT, ZZ, SW, ZS, CZ, and XL performed experiments. LW, XT, ZL, GX, and HTZ analyzed data. TZ, ZL, YZ, CL and JZ conducted the histological/pathological analysis. HT Z wrote the paper. GX and HTZ edited the paper. All authors read and approved the final version of the manuscript.

## Ethics approval and consent to participate

This study was approved by the Ethics Committee of Soochow University.

## Consent for publication

Not applicable.

**Competing interests**

The authors declare that they have no competing interests.

**Publisher's Note**

Springer Nature remains neutral with regard to jurisdictional claims in published maps and institutional affiliations.

**Author details**

<sup>1</sup>Soochow University Laboratory of Cancer Molecular Genetics, Medical College of Soochow University, 199 Ren'ai Road, Suzhou 215123, Jiangsu, China. <sup>2</sup>Department of Thoracic Surgery, The Second Affiliated Hospital of Harbin Medical University, 246 Xuefu Road, Harbin 150086, Heilongjiang, China. <sup>3</sup>Department of Respiratory Medicine, The First Affiliated Hospital of Soochow University, Medical College of Soochow University, Suzhou 215006, Jiangsu, China. <sup>4</sup>Department of Thoracic Surgery, The First Affiliated Hospital of Soochow University, Medical College of Soochow University, Suzhou 215006, Jiangsu, China. <sup>5</sup>Laboratory Animal Center, Medical College of Soochow University, Suzhou 215123, Jiangsu, China. <sup>6</sup>Department of Basic Medicine, Kangda College of Nanjing Medical University, Lianyungang 222000, China. <sup>7</sup>Suzhou Key Laboratory for Molecular Cancer Genetics, Suzhou 215123, Jiangsu, China.

Received: 22 March 2018 Accepted: 13 September 2018

Published online: 27 September 2018

**References**

- Siegel RL, Miller KD, Jemal A. Cancer statistics, 2016. *CA Cancer J Clin*. 2016;66:7–30.
- Chen W, Zheng R, Baade PD, Zhang S, Zeng H, Bray F, Jemal A, Yu XQ, He J. Cancer statistics in China, 2015. *CA Cancer J Clin*. 2016;66:115–32.
- Feng J, Zhang X, Zhu H, Wang X, Ni S, Huang J. High expression of FoxP1 is associated with improved survival in patients with non-small cell lung cancer. *Am J Clin Pathol*. 2012;138:230–5.
- Gupta GP, Massague J. Cancer metastasis: building a framework. *Cell*. 2006;127:679–95.
- Asselin-Paturel C, Echchakir H, Carayol G, Gay F, Opolon P, Grunenwald D, Chouaib S, Mami-Chouaib F. Quantitative analysis of Th1, Th2 and TGF-beta1 cytokine expression in tumor, TIL and PBL of non-small cell lung cancer patients. *Int J Cancer*. 1998;77:7–12.
- Saji H, Nakamura H, Awut I, Kawasaki N, Hagiwara M, Ogata A, Hosaka M, Saijo T, Kato Y, Kato H. Significance of expression of TGF-beta in pulmonary metastasis in non-small cell lung cancer tissues. *Ann Thorac Cardiovasc Surg*. 2003;9:295–300.
- Donatelli SS, Zhou JM, Gilvary DL, Eksioglu EA, Chen X, Cress WD, Haura EB, Schabath MB, Coppola D, Wei S, Djieu JY. TGF-beta-inducible microRNA-183 silences tumor-associated natural killer cells. *Proc Natl Acad Sci U S A*. 2014;111:4203–8.
- Zhang HJ, Wang HY, Zhang HT, Su JM, Zhu J, Wang HB, Zhou WY, Zhang H, Zhao MC, Zhang L, Chen XF. Transforming growth factor-beta1 promotes lung adenocarcinoma invasion and metastasis by epithelial-to-mesenchymal transition. *Mol Cell Biochem*. 2011;355:309–14.
- Liu RY, Zeng Y, Lei Z, Wang L, Yang H, Liu Z, Zhao J, Zhang HT. JAK/STAT3 signaling is required for TGF-beta-induced epithelial-mesenchymal transition in lung cancer cells. *Int J Oncol*. 2014;44:1643–51.
- Massague J. TGFbeta in Cancer. *Cell*. 2008;134:215–30.
- Xue J, Lin X, Chiu WT, Chen YH, Yu G, Liu M, Feng XH, Sawaya R, Medema RH, Hung MC, Huang S. Sustained activation of SMAD3/SMAD4 by FOXM1 promotes TGF-beta-dependent cancer metastasis. *J Clin Invest*. 2014;124:564–79.
- Dupont S, Zacchigna L, Cordenonsi M, Soligo S, Adorno M, Rugge M, Piccolo S. Germ-layer specification and control of cell growth by Ectoderm, a Smad4 ubiquitin ligase. *Cell*. 2005;121:87–99.
- He W, Dorn DC, Erdjument-Bromage H, Tempst P, Moore MA, Massague J. Hematopoiesis controlled by distinct TIF1gamma and Smad4 branches of the TGFbeta pathway. *Cell*. 2006;125:929–41.
- Wang L, Yang H, Lei Z, Zhao J, Chen Y, Chen P, Li C, Zeng Y, Liu Z, Liu X, Zhang HT. Repression of TIF1gamma by SOX2 promotes TGF-beta-induced epithelial-mesenchymal transition in non-small-cell lung cancer. *Oncogene*. 2016;35:867–77.
- Fattet L, Ay AS, Bonneau B, Jallades L, Mikaelian I, Treilleux I, Gillet G, Hesling C, Rimokh R. TIF1gamma requires sumoylation to exert its repressive activity on TGFbeta signaling. *J Cell Sci*. 2013;126:3713–23.
- Hesling C, Fattet L, Teyre G, Jury D, Gonzalo P, Lopez J, Vanbelle C, Morel AP, Gillet G, Mikaelian I, Rimokh R. Antagonistic regulation of EMT by TIF1gamma and Smad4 in mammary epithelial cells. *EMBO Rep*. 2011;12:665–72.
- Hansen TB, Jensen TI, Clausen BH, Bramsen JB, Finsen B, Damgaard CK, Kjems J. Natural RNA circles function as efficient microRNA sponges. *Nature*. 2013;495:384–8.
- Salzman J, Gawad C, Wang PL, Lacayo N, Brown PO. Circular RNAs are the predominant transcript isoform from hundreds of human genes in diverse cell types. *PLoS One*. 2012;7:e30733.
- Du WW, Yang W, Liu E, Yang Z, Dhaliwal P, Yang BB. Foxo3 circular RNA retards cell cycle progression via forming ternary complexes with p21 and CDK2. *Nucleic Acids Res*. 2016;44:2846–58.
- Memczak S, Jens M, Elefsinioti A, Torti F, Krueger J, Rybak A, Maier L, Mackowiak SD, Gregersen LH, Munschauer M, et al. Circular RNAs are a large class of animal RNAs with regulatory potency. *Nature*. 2013;495:333–8.
- Kulcheski FR, Christoff AP, Margis R. Circular RNAs are miRNA sponges and can be used as a new class of biomarker. *J Biotechnol*. 2016;238:42–51.
- Hansen TB, Kjems J, Damgaard CK. Circular RNA and miR-7 in cancer. *Cancer Res*. 2013;73:5609–12.
- Hsiao KY, Lin YC, Gupta SK, Chang N, Yen L, Sun HS, Tsai SJ. Non-coding effects of circular RNA CCDC66 promote colon cancer growth and metastasis. *Cancer Res*. 2017;77:2339–50.
- Han D, Li J, Wang H, Su X, Hou J, Gu Y, Qian C, Lin Y, Liu X, Huang M, et al. Circular RNA circMTO1 acts as the sponge of microRNA-9 to suppress hepatocellular carcinoma progression. *Hepatology*. 2017;66:1151–64.
- Conn SJ, Pillman KA, Toubia J, Conn VM, Salmandis M, Phillips CA, Roslan S, Schreiber AW, Gregory PA, Goodall GJ. The RNA binding protein quaking regulates formation of circRNAs. *Cell*. 2015;160:1125–34.
- Zong FY, Fu X, Wei WJ, Luo YG, Heiner M, Cao LJ, Fang Z, Fang R, Lu D, Ji H, Hui J. The RNA-binding protein QKI suppresses cancer-associated aberrant splicing. *PLoS Genet*. 2014;10:e1004289.
- Marwitz S, Depner S, Dvornikov D, Merkle R, Szczygiel M, Muller-Decker K, Lucarelli P, Wasch M, Mairbaurl H, Rabe KF, et al. Downregulation of the TGFbeta Pseudoreceptor BAMBI in non-small cell lung Cancer enhances TGFbeta signaling and invasion. *Cancer Res*. 2016;76:3785–801.
- Zhang N, Liu Y, Wang Y, Zhao M, Tu L, Luo F. Decitabine reverses TGF-beta1-induced epithelial-mesenchymal transition in non-small-cell lung cancer by regulating miR-200/ZEB axis. *Drug Des Devel Ther*. 2017;11:969–83.
- Cortes-Lopez M, Miura P. Emerging functions of circular RNAs. *Yale J Biol Med*. 2016;89:527–37.
- Gregory RI, Chendrimada TP, Cooch N, Shiekhattar R. Human RISC couples microRNA biogenesis and posttranscriptional gene silencing. *Cell*. 2005;123:631–40.
- Vincent DF, Yan KP, Treilleux I, Gay F, Arfi V, Kaniewski B, Marie JC, Lepinasse F, Martel S, Goddard-Leon S, et al. Inactivation of TIF1gamma cooperates with Kras to induce cystic tumors of the pancreas. *PLoS Genet*. 2009;5:e1000575.
- Aucagne R, Droin N, Paggetti J, Lagrange B, Largeot A, Hammann A, Bataille A, Martin L, Yan KP, Fenaux P, et al. Transcription intermediary factor 1gamma is a tumor suppressor in mouse and human chronic myelomonocytic leukemia. *J Clin Invest*. 2011;121:2361–70.
- Xue J, Chen Y, Wu Y, Wang Z, Zhou A, Zhang S, Lin K, Aldape K, Majumder S, Lu Z, Huang S. Tumour suppressor TRIM33 targets nuclear beta-catenin degradation. *Nat Commun*. 2015;6:6156.
- Dupont S, Mamidi A, Cordenonsi M, Montagner M, Zacchigna L, Adorno M, Martello G, Stinchfield MJ, Soligo S, Morsut L, et al. FAM/USP9x, a deubiquitinating enzyme essential for TGFbeta signaling, controls Smad4 monoubiquitination. *Cell*. 2009;136:123–35.
- Agricola E, Randall RA, Gaarenstroom T, Dupont S, Hill CS. Recruitment of TIF1gamma to chromatin via its PHD finger-bromodomain activates its ubiquitin ligase and transcriptional repressor activities. *Mol Cell*. 2011;43:85–96.
- Wang L, Lei Z, Liu X, Liu R, Zhang H. Association of mutation and methylation in the promoter region of TIF1gamma with non-small cell lung cancer. *Zhongguo Fei Ai Za Zhi*. 2013;16:227–32.
- Lyu D, Huang S. The emerging role and clinical implication of human exonic circular RNA. *RNA Biol*. 2016:1–7.
- Derynck R, Muthusamy BP, Saetern KY. Signaling pathway cooperation in TGF-beta-induced epithelial-mesenchymal transition. *Curr Opin Cell Biol*. 2014;31:56–66.

39. Saitoh M. Epithelial-mesenchymal transition is regulated at post-transcriptional levels by transforming growth factor-beta signaling during tumor progression. *Cancer Sci.* 2015;106:481–8.
40. Yuan JH, Yang F, Wang F, Ma JZ, Guo YJ, Tao QF, Liu F, Pan W, Wang TT, Zhou CC, et al. A long noncoding RNA activated by TGF-beta promotes the invasion-metastasis cascade in hepatocellular carcinoma. *Cancer Cell.* 2014;25:666–81.
41. Zeng Y, Zhu J, Shen D, Qin H, Lei Z, Li W, Huang JA, Liu Z. Repression of Smad4 by miR205 moderates TGF-beta-induced epithelial-mesenchymal transition in A549 cell lines. *Int J Oncol.* 2016;49:700–8.
42. Jingushi K, Ueda Y, Kitae K, Hase H, Egawa H, Ohshio I, Kawakami R, Kashiwagi Y, Tsukada Y, Kobayashi T, et al. miR-629 targets TRIM33 to promote TGFbeta/Smad signaling and metastatic phenotypes in ccRCC. *Mol Cancer Res.* 2015;13:565–74.
43. Hu H, Xu Z, Li C, Xu C, Lei Z, Zhang HT, Zhao J. MiR-145 and miR-203 represses TGF-beta-induced epithelial-mesenchymal transition and invasion by inhibiting SMAD3 in non-small cell lung cancer cells. *Lung Cancer.* 2016;97:87–94.
44. Wu J, Cui H, Zhu Z, Wang L. MicroRNA-200b-3p suppresses epithelial-mesenchymal transition and inhibits tumor growth of glioma through down-regulation of ERK5. *Biochem Biophys Res Commun.* 2016;478:1158–64.
45. Machackova T, Mlcochova H, Stanik M, Dolezel J, Fedorko M, Pacik D, Poprach A, Svoboda M, Slaby O. MiR-429 is linked to metastasis and poor prognosis in renal cell carcinoma by affecting epithelial-mesenchymal transition. *Tumour Biol.* 2016;37:14653–8.
46. Lang Y, Xu S, Ma J, Wu J, Jin S, Cao S, Yu Y. MicroRNA-429 induces tumorigenesis of human non-small cell lung cancer cells and targets multiple tumor suppressor genes. *Biochem Biophys Res Commun.* 2014;450:154–9.
47. Ling N, Gu J, Lei Z, Li M, Zhao J, Zhang HT, Li X. microRNA-155 regulates cell proliferation and invasion by targeting FOXO3a in glioma. *Oncol Rep.* 2013;30:2111–8.
48. Brabletz S, Brabletz T. The ZEB/miR-200 feedback loop—a motor of cellular plasticity in development and cancer? *EMBO Rep.* 2010;11:670–7.
49. Xu ZQ, Yang MG, Liu HJ, Su CQ. Circular RNA hsa\_circ\_0003221 (circPTK2) promotes the proliferation and migration of bladder cancer cells. *J Cell Biochem.* 2018;119:3317–25.
50. Lei Z, Xu G, Wang L, Yang H, Liu X, Zhao J, Zhang HT. MiR-142-3p represses TGF-beta-induced growth inhibition through repression of TGFbetaR1 in non-small cell lung cancer. *FASEB J.* 2014;28:2696–704.
51. Yang H, Wang L, Zhao J, Chen Y, Lei Z, Liu X, Xia W, Guo L, Zhang HT. TGF-beta-activated SMAD3/4 complex transcriptionally upregulates N-cadherin expression in non-small cell lung cancer. *Lung Cancer.* 2015;87:249–57.
52. Zhong Z, Lv M, Chen J. Screening differential circular RNA expression profiles reveals the regulatory role of circTCF25-miR-103a-3p/miR-107-CDK6 pathway in bladder carcinoma. *Sci Rep.* 2016;6:30919.
53. Panda AC, Grammatikakis I, Kim KM, De S, Martindale JL, Munk R, Yang X, Abdelmohsen K, Gorospe M. Identification of senescence-associated circular RNAs (SAC-RNAs) reveals senescence suppressor CircPVT1. *Nucleic Acids Res.* 2017;45:4021–35.

**Ready to submit your research? Choose BMC and benefit from:**

- fast, convenient online submission
- thorough peer review by experienced researchers in your field
- rapid publication on acceptance
- support for research data, including large and complex data types
- gold Open Access which fosters wider collaboration and increased citations
- maximum visibility for your research: over 100M website views per year

**At BMC, research is always in progress.**

Learn more [biomedcentral.com/submissions](https://biomedcentral.com/submissions)



## ORIGINAL ARTICLE

Repression of TIF1 $\gamma$  by SOX2 promotes TGF- $\beta$ -induced epithelial–mesenchymal transition in non-small-cell lung cancerL Wang<sup>1,2,6</sup>, H Yang<sup>1,2,6</sup>, Z Lei<sup>1,2,6</sup>, J Zhao<sup>2,3,6</sup>, Y Chen<sup>4,6</sup>, P Chen<sup>5</sup>, C Li<sup>2,3</sup>, Y Zeng<sup>2,3</sup>, Z Liu<sup>2,3</sup>, X Liu<sup>1,2</sup> and H-T Zhang<sup>1,2</sup>

TIF1 $\gamma$  is a novel regulator of transforming growth factor (TGF)- $\beta$ /Smad signaling. Our previous studies show that dysregulated expression of transcriptional intermediary factor 1  $\gamma$  (TIF1 $\gamma$ ) and abnormal TGF- $\beta$ /Smad signaling are implicated in non-small-cell lung cancer (NSCLC) separately. However, how TIF1 $\gamma$  contributes to NSCLC by controlling TGF- $\beta$ /Smad signaling is poorly understood. Here, we investigated the mechanistic role of TIF1 $\gamma$  in TGF- $\beta$ -induced epithelial–mesenchymal transition (EMT), as well as a link between TIF1 $\gamma$  and SOX2 in NSCLC. We show that TIF1 $\gamma$  is a downstream target of SOX2 in NSCLC cells. SOX2 overexpression negatively regulated *TIF1 $\gamma$*  promoter activity and thereby attenuated *TIF1 $\gamma$*  mRNA and protein expression levels; SOX2 knockdown significantly enhanced *TIF1 $\gamma$*  promoter activity and augmented *TIF1 $\gamma$*  expression. Moreover, *TIF1 $\gamma$*  mRNA expression was downregulated in human NSCLC tissues and negatively correlated with SOX2 protein, which was upregulated in NSCLC tissues. Importantly, knockdown of TIF1 $\gamma$  or SOX2 overexpression augmented SMAD4 (human Mad (mothers against decapentaplegic)-related homologous protein 4)-dependent transcriptional responses, and enhanced TGF- $\beta$ -induced EMT and human NSCLC cell invasion; knockdown of SOX2 impaired TGF- $\beta$ -induced EMT and NSCLC cell invasion. In an *in vivo* model of metastasis, knockdown of TIF1 $\gamma$  promotes NSCLC cell metastasis. In addition, our data suggested that TIF1 $\gamma$  inhibited TGF- $\beta$ -induced EMT through competing with SMAD4 in NSCLC cells. Taken together, our findings reveal a new mechanism by which SOX2-mediated transcription repression of TIF1 $\gamma$  promotes TGF- $\beta$ -induced EMT in NSCLC.

*Oncogene* (2016) 35, 867–877; doi:10.1038/onc.2015.141; published online 11 May 2015

## INTRODUCTION

Lung cancer is the leading cause of cancer deaths worldwide and non-small-cell lung cancer (NSCLC) accounts for ~85% of all lung cancers.<sup>1</sup> Despite improvement in therapeutic strategies, the prognosis for NSCLC patients is still poor, with 5-year survival rate of ~10%.<sup>2</sup> In fact, more than 90% of deaths from solid tumors, including NSCLC, are mainly attributed to metastasis.<sup>3</sup> Therefore, good understanding of the mechanisms underlying NSCLC metastasis is very important.

The TGF- $\beta$  signaling pathway plays versatile roles in cell growth, differentiation, apoptosis, development and tumorigenesis in cancer, including NSCLC.<sup>4–6</sup> Strikingly, the canonical TGF- $\beta$ /Smad signaling has comprehensively been understood. In the canonical signaling, TGF- $\beta$  binds directly to TGF- $\beta$  receptor type II (TGF $\beta$ R2), and the active TGF $\beta$ R2 recruits and phosphorylates TGF $\beta$ R1. The activated TGF $\beta$ R1 causes phosphorylation of receptor-activated SMAD2 (human Mad (mothers against decapentaplegic)-related homologous protein 2)/SMAD3 (R-SMADs), which then form a hetero-oligomeric complex with the common-mediator SMAD4 (Co-SMAD). The complex translocates into the nucleus to regulate gene expression.<sup>7</sup> TGF- $\beta$  signaling alterations were reported to significantly affect NSCLC carcinogenesis.<sup>8</sup> Our previous studies

revealed that the expression of TGF $\beta$ R1 and TGF $\beta$ R2 was frequently dysregulated in NSCLC.<sup>9–11</sup> Notably, there is accumulating evidence that TGF- $\beta$  signaling is a potent inducer of epithelial–mesenchymal transition (EMT) in various cancers, including NSCLC.<sup>12–14</sup> EMT is vital for morphogenesis during embryonic development and the conversion of early-stage tumors into invasive malignancies,<sup>15,16</sup> which is marked by repression of E-cadherin and induction of N-cadherin, Vimentin and Snail.<sup>14,17</sup>

Transcriptional intermediary factor 1  $\gamma$  (TIF1 $\gamma$ ; alias, TRIM33/RFG7/PTC7/Ectoderm) is a nuclear protein, which may repress transcription by interacting with unknown molecular partners.<sup>18</sup> Recently, TIF1 $\gamma$  has been identified to participate in TGF- $\beta$ /Smad signaling through two distinct mechanisms: on one hand, TIF1 $\gamma$  ubiquitinates SMAD4 to inhibit TGF- $\beta$ -induced cytotaxis in colorectal and breast cancer cells;<sup>19</sup> on the other hand, TIF1 $\gamma$  selectively binds receptor-phosphorylated R-SMADs in competition with SMAD4.<sup>20</sup> Moreover, TIF1 $\gamma$  plays a tumor suppression role in human chronic myelomonocytic leukemia and pancreatic cancer.<sup>21,22</sup> Our recent data show that reduced expression of TIF1 $\gamma$  is also common in NSCLC.<sup>23</sup> Of note, inactivation of TIF1 $\gamma$  enhances the positive role of SMAD4 in TGF- $\beta$ -induced EMT in mammary epithelial cells.<sup>24,25</sup> However, to date, little is known

<sup>1</sup>Soochow University Laboratory of Cancer Molecular Genetics, Medical College of Soochow University, Suzhou, China; <sup>2</sup>Suzhou Key Laboratory for Molecular Cancer Genetics, Suzhou, China; <sup>3</sup>Department of Thoracic and Cardiovascular Surgery, First Affiliated Hospital of Soochow University, Medical College of Soochow University, Suzhou, China; <sup>4</sup>Department of Thoracic and Cardiovascular Surgery, Second Affiliated Hospital of Soochow University, Medical College of Soochow University, Suzhou, China and <sup>5</sup>Systems Biology Laboratory, Research Programs Unit, Genome-Scale Biology, and Institute of Biomedicine, Biochemistry and Developmental Biology, Faculty of Medicine, University of Helsinki, Haartmaninkatu 8, Helsinki, Finland. Correspondence: Professor H-T Zhang, Soochow University Laboratory of Cancer Molecular Genetics, Medical College of Soochow University, 199 Ren'ai Road, Sino-Singapore Industrial Park, Suzhou 215123, China.

E-mail: htzhang@suda.edu.cn

<sup>6</sup>These authors contributed equally to this work.

Received 22 September 2014; revised 14 March 2015; accepted 20 March 2015; published online 11 May 2015



about the role that transcription-mediated events play in TIF1 $\gamma$  inhibition and whether inactivation of TIF1 $\gamma$  can promote TGF- $\beta$ -induced EMT in NSCLC.

SOX2 is part of a highly conserved family of transcription factors with a SRY-related HMG-box (SOX) that have been identified as important players in embryonic development,<sup>26–28</sup> and SOX2 plays a vital role in maintaining stem cell characteristics, and repression of SOX2 can lead to loss of cell pluripotency and self-renewal.<sup>29–31</sup> Intriguingly, SOX2 is overexpressed in NSCLC<sup>32,33</sup> and SOX2 cooperates with PKC $\delta$  to drive NSCLC tumorigenesis.<sup>34</sup> SOX2 overexpression promotes metastasis of breast and prostate cancer cells through mediating EMT.<sup>35</sup> Comparably, silencing SOX2 is able to reverse EMT features in colorectal cancer cells.<sup>36</sup> Although TGF- $\beta$ -induced EMT is associated with increased level of SOX2 expression in primary NSCLC cells,<sup>37</sup> the question of whether SOX2 can enhance TGF- $\beta$ -induced EMT in NSCLC is still not addressed.

Taken together, we deduced an interaction between TIF1 $\gamma$  and SOX2 for controlling TGF- $\beta$ -induced EMT. Given our *in silico* prediction that TIF1 $\gamma$  promoter harbors four putative SRY-binding sites, we hypothesized that SOX2 can regulate transcription of TIF1 $\gamma$  to influence TGF- $\beta$ -induced EMT. In the present study, we explored the mechanistic role of TIF1 $\gamma$  in TGF- $\beta$ -induced EMT, as well as a link between TIF1 $\gamma$  and SOX2 in NSCLC. Our findings

demonstrate that repression of TIF1 $\gamma$  by SOX2 promotes TGF- $\beta$ -induced EMT in NSCLC.

## RESULTS

SRY-related protein is involved in transcriptional inhibition of TIF1 $\gamma$  expression

TIF1 $\gamma$  has been suggested to function as a suppressor in various types of cancer.<sup>21,22</sup> Our previous study showed that expression of TIF1 $\gamma$  was frequently reduced in NSCLC.<sup>23</sup> Here, we first explored the transcriptional regulatory mechanisms underlying down-regulation of TIF1 $\gamma$  expression in NSCLC. According to the published sequence of TIF1 $\gamma$  promoter (GenBank Accession number NG\_023287), we selected a ~2.1-kb 5'-region of TIF1 $\gamma$  promoter to generate a series of luciferase reporter constructs containing various lengths of TIF1 $\gamma$  5'-promoter (Figure 1a), and assessed basal luciferase activities in A549 cells transfected with these constructs. As shown in Figures 1b and a transcriptional inhibitory element was putatively found at position –548 to –480 in the TIF1 $\gamma$  promoter. Computational algorithms (<http://archive.is/http://mbs.cbrc.jp/research/db/TFSEARCH.html>) predicted that four putative SRY-related protein-binding sites were identified in this region (Figure 1c), which are the consensus DNA sequences A/TAACAAT/A. Accordingly, we constructed six luciferase reporter plasmids containing wild-type and mutant of the SRY-related

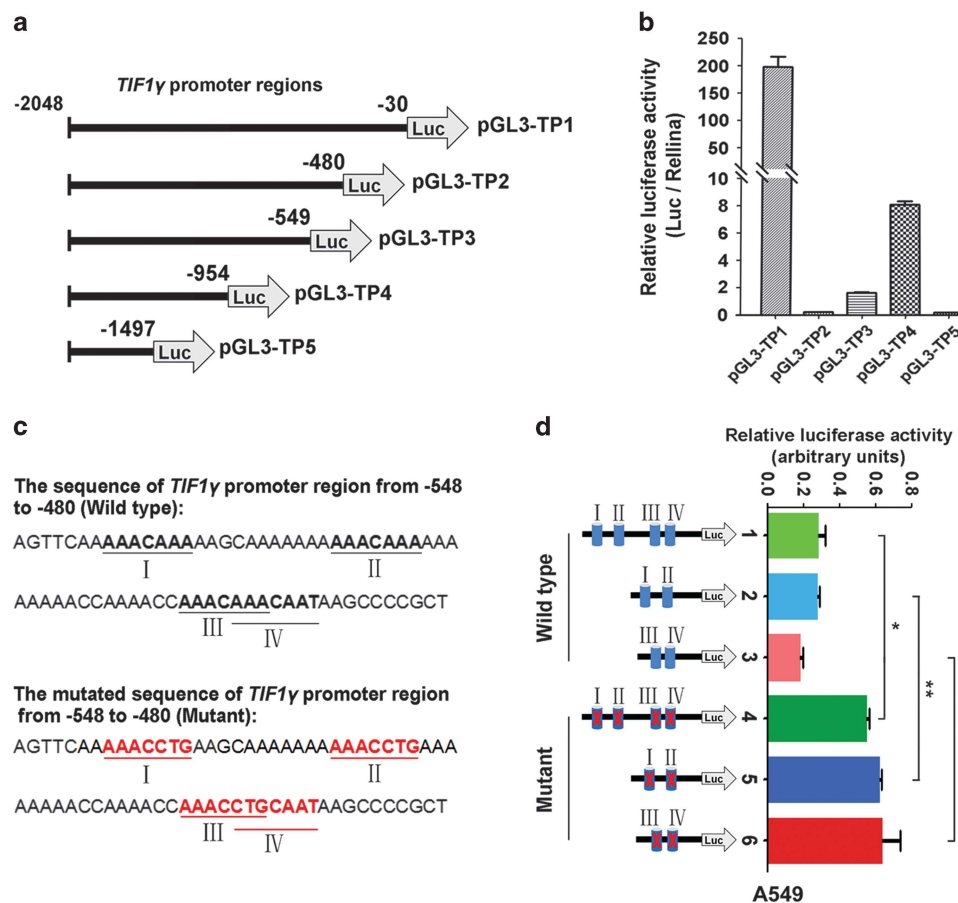


**Figure 1.** SRY-related protein is involved in transcriptional inhibition of TIF1 $\gamma$  expression. (a) A series of truncated TIF1 $\gamma$  5'-promoter luciferase constructs were prepared as described in Materials and Methods and verified by sequencing. (b) Results of luciferase reporter assays using A549 cells. The indicated constructs were transiently transfected into A549 cells and their luciferase activities were determined after 24 h as described in Materials and Methods. (c) Computational algorithms predicted that the TIF1 $\gamma$  promoter region (position –548 to –480) harbors four putative SRY-related protein-binding sites (indicated as I, II, III, IV). The mutants of the SRY-related protein-binding sites are shown in red bold letters. (d) The constructs encompassing the wild-type or mutant of SRY-related protein-binding sites (Left) were transiently transfected into A549 cell. Relative luciferase activities of the constructs are shown as fold increase over empty vectors (Right). \*P < 0.05; \*\*P < 0.01.

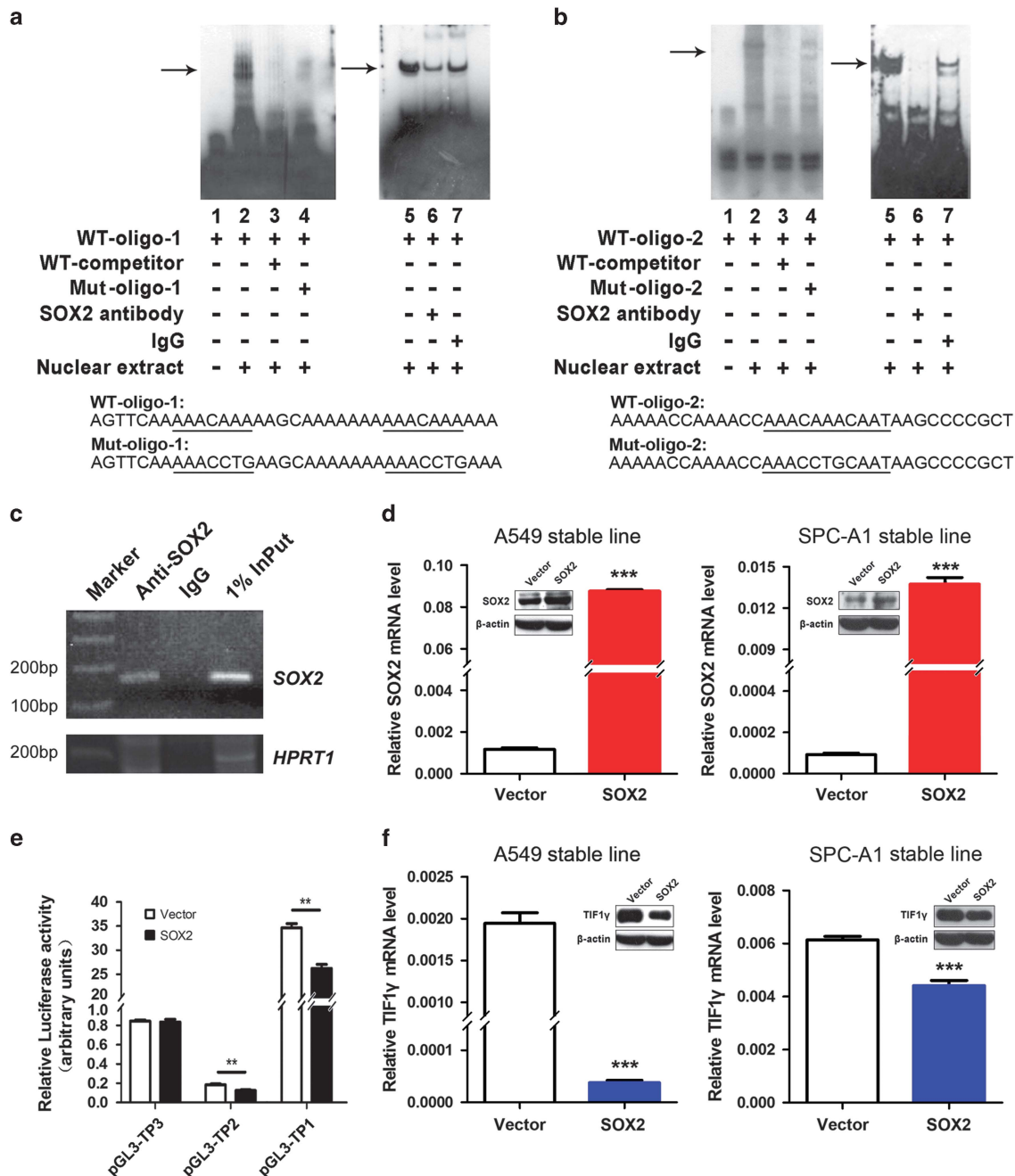


**Figure 2.** SOX2 is recruited to *TIF1 $\gamma$*  promoter and regulates negatively *TIF1 $\gamma$*  promoter activity, and overexpression of SOX2 represses *TIF1 $\gamma$*  expression. (**a** and **b**) EMSA analysis was conducted using double-stranded, biotin-labeled oligonucleotides containing four putative SRY-related protein-binding sites of *TIF1 $\gamma$*  promoter. The oligo-1 (–548 to –514) and oligo-2 (–513 to –480) contains two frontal SRY-related protein-binding sites (**a**) and two latter binding sites (**b**) of *TIF1 $\gamma$*  promoter (–548 to –480), respectively. Lane 1 represents the mobility of the labeled wild-type probes (WT-oligo-1 or -2) alone; lanes 2 and 5 represent the mobility of the labeled wild-type probes with nuclear extracts from A549 cells. Specific DNA–nuclear protein binding was completely abolished by 200-fold unlabeled wild-type probes (WT-competitor; lane 3), and partially abolished by the unlabeled mutant probes (Mut-oligo-1 or -2; lane 4). EMSA assay was also performed by adding anti-SOX2 or IgG antibodies to verify the specificity of SOX2 binding the *TIF1 $\gamma$*  promoter (lanes 6 and 7). An arrow indicates the band corresponding to specific DNA–nuclear protein complex. (**c**) A549 cells were subjected to ChIP analysis in which anti-SOX2 antibodies were used. As described in Materials and Methods, 1% input was obtained as positive control before immunoprecipitation, and allowed to PCR to confirm the presence of *TIF1 $\gamma$*  promoter sequence encompassing putative SOX-binding sites (position –595 to –426). Anti-IgG antibody was used as a negative control. PCR products were separated on 2.0% agarose gels with ethidium bromide staining. ChIP-PCR assays showing an enrichment of *TIF1 $\gamma$*  promoter or *HPRT1* DNA, which was obtained in the immunoprecipitation using anti-SOX2 antibody. (**d**) SOX2 mRNA and protein levels in stable A549 and SPC-A1 cell lines overexpressing SOX2. (**e**) Results of luciferase reporter assays using A549 cells overexpressing SOX2. Cells were transfected with the reporter plasmids (indicated in Figure 1a) and subjected to luciferase assay as described in Materials and Methods. Relative reporter activities of the constructs are normalized to that of pGL3-basic reporter. (**f**) Overexpression of SOX2 causes downregulation of *TIF1 $\gamma$*  mRNA and protein in A549 and SPC-A1 cells. *TIF1 $\gamma$*  expression was quantified by quantitative reverse transcription–PCR and western blot in stable cells overexpressing SOX2. *TIF1 $\gamma$*  protein expression was normalized to  $\beta$ -actin in western blot analysis. Values represent mean  $\pm$  s.d. of triplicate measurements. \*\* $P$  < 0.01; \*\*\* $P$  < 0.001.

protein-binding sites, respectively (Figures 1c and d). Luciferase assays showed that the mutant constructs exhibited significantly increased luciferase activities compared with the wild-type constructs (Figure 1d and Supplementary Figure 1). The results of transfection studies indicated that the region (position –548 to –480) is important for basal expression of *TIF1 $\gamma$*  and suggested that SRY-related protein may be involved in the transcriptional inhibition of *TIF1 $\gamma$*  expression.

SOX2 is recruited to TIF1 $\gamma$  promoter and regulates negatively TIF1 $\gamma$  promoter activity and overexpression of SOX2 inhibits TIF1 $\gamma$  expression

According to our observation obtained above, and considering the facts that SOX2 is a key member of SRY-related family genes<sup>26–28</sup> and upregulation of SOX2 is frequently observed in NSCLC,<sup>32,33</sup> we hypothesized that SOX2 can be recruited to the *TIF1 $\gamma$*  promoter to influence *TIF1 $\gamma$*  expression in NSCLC. As illustrated in Figures 2a–c, electrophoretic mobility shift assay (EMSA) and chromatin immunoprecipitation (ChIP) assays using anti-SOX2 antibody showed that SOX2 can bind or interact with the SRY-related protein-binding sites in the *TIF1 $\gamma$*  promoter region (position –548 to –480). The results were consistently observed in the repeated experiments, demonstrating that SOX2 can be recruited to the *TIF1 $\gamma$*  promoter. Furthermore, luciferase reporter assays showed that overexpression of SOX2 (Figure 2d) in A549 cells repressed *TIF1 $\gamma$*  promoter activity by binding to the putative SOX-binding sites (position –548 to –480; Figure 2e). SOX2 knockdown in A549 cells significantly enhanced *TIF1 $\gamma$*  promoter (–548 to –480) activity (Supplementary Figure 2).

Subsequently, we investigated the effect of SOX2 overexpression on the expression of TIF1 $\gamma$  mRNA and protein in A549 and SPC-A1 cells. As a result, stable overexpression of SOX2 (Figure 2d) significantly attenuated TIF1 $\gamma$  mRNA and protein expression (Figure 2f). Moreover, SOX2 knockdown significantly augmented *TIF1 $\gamma$*  mRNA expression in A549 and H226 cells (Supplementary Figures 3A–D). The results suggested that SOX2 can negatively regulate the expression of *TIF1 $\gamma$*  in NSCLC cells.

TIF1 $\gamma$  mRNA expression is reduced and inversely correlated with SOX2 protein expression in NSCLC tissues

To verify the relationship between TIF1 $\gamma$  and SOX2 in NSCLC carcinogenesis, we first examined the expression of *TIF1 $\gamma$*  mRNA in 70 paired NSCLC tissues and adjacent noncancerous lung tissues. As illustrated in Figure 3a and Supplementary Table 1, *TIF1 $\gamma$*  mRNA expression was significantly downregulated in 68.6% (48/70) of NSCLC tissues. Among 43 randomly selected NSCLC and paired noncancerous lung tissues in which *TIF1 $\gamma$*  mRNA expression had been evaluated (Figure 3a), 28 tumors (65.1%) and 13 tumors (30.2%) showed a significant increase and reduction in the expression of SOX2 protein, respectively (Figure 3b). Of 28 NSCLC tissues with high SOX2 protein level, 25 tumors (89.3%) presented low expression of *TIF1 $\gamma$*  mRNA. Of 13 NSCLC tissues with low SOX2 protein level, 8 tumors (61.5%) presented high expression of *TIF1 $\gamma$*  mRNA (Figure 3c). Interestingly, the ratio of SOX2 protein level

(T/N) was reversely correlated with that of *TIF1 $\gamma$*  mRNA level (T/N) in 43 paired NSCLC tissues ( $P < 0.01$ ; Figure 3d). Furthermore, the similar correlation was observed between NSCLC tissues when classified by lung cancer subtypes (Supplementary Figures 4A and B). Moreover, a public data set (GSE19188) containing 91 NSCLC tissues and 65 normal lung tissues showed that *TIF1 $\gamma$*  mRNA expression was downregulated in human NSCLC tissues (Figure 3e) and negatively correlated with SOX2 mRNA expression (Figure 3f), which was upregulated in NSCLC tissues (Figure 3e). Taken together, the results suggested that SOX2 can negatively regulate *TIF1 $\gamma$*  mRNA expression and revealed a link between TIF1 $\gamma$  and SOX2 in NSCLCs.

Knockdown of TIF1 $\gamma$  enhances TGF- $\beta$ -induced EMT and invasion of NSCLC cells *in vitro* and promotes NSCLC cell metastasis *in vivo*

Increased production of TGF- $\beta$  has been found in NSCLC cells and tissues.<sup>38,39</sup> Given the facts that TGF- $\beta$  is a primary inducer of EMT in NSCLC,<sup>12,13</sup> and TIF1 $\gamma$  is a regulator of the canonical TGF- $\beta$ /Smad signaling,<sup>19,20</sup> we hypothesized that TIF1 $\gamma$  may influence TGF- $\beta$ -induced EMT in NSCLC cells and NSCLC metastasis. To test this, we first established A549, SPC-A1 and H226 cell lines with stable knockdown of TIF1 $\gamma$ . As expected, the expression level of TIF1 $\gamma$  mRNA and protein was significantly reduced after the stable transfection of A549, SPC-A1 and H226 cells with two *TIF1 $\gamma$*  short hairpin RNAs (shRNAs; Figure 4a and Supplementary Figure 5A). Then, upon TGF- $\beta$ 1 stimulation, A549, SPC-A1 and H226 cells transfected with *TIF1 $\gamma$*  shRNA showed significantly decreased expression of E-cadherin or increased expression of N-cadherin, Snail and Vimentin compared with A549, SPC-A1 and H226 cells transfected with scrambled shRNA (Figure 4b and Supplementary Figure 5B). On TGF- $\beta$ 1 stimulation at 1 h, TIF1 $\gamma$ -silenced A549 and SPC-A1 cells showed higher expression of *Snail* mRNA compared with control cells (Supplementary Figure 6A). Furthermore, Transwell assays showed that knockdown of TIF1 $\gamma$  enhanced TGF- $\beta$ -induced migratory and invasive abilities of A549, SPC-A1 cells (Figures 4c and d) and H226 cells (Supplementary Figures 5C and D). Taken together, our findings demonstrated that knockdown of TIF1 $\gamma$  can enhance TGF- $\beta$ -induced EMT and migration and invasion of NSCLC cells *in vitro*.

To further examine the effect of TIF1 $\gamma$  knockdown on NSCLC cell metastasis *in vivo*, TIF1 $\gamma$ -silenced and control A549 cells were injected into the tail vein of nude mice. As shown in Table 1 and Supplementary Figure 7, the mice injected with TIF1 $\gamma$ -silenced A549 cells developed more pulmonary metastasis nodules than those injected with control cells.

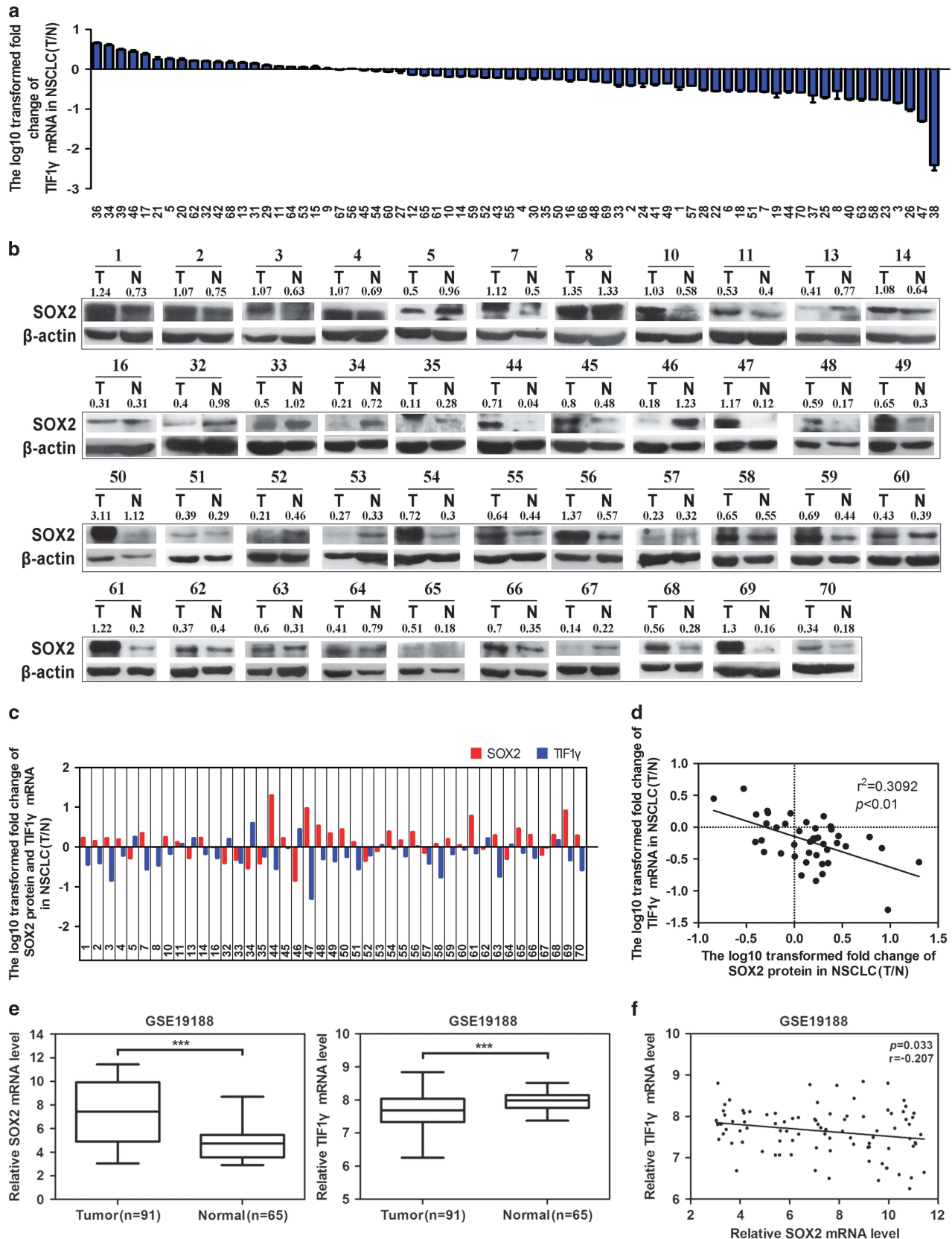
Overexpression of SOX2 enhances TGF- $\beta$ -induced EMT and invasion of NSCLC cells

On the basis of the above analyses, it is not hard to deduce that SOX2 plays an important role in TGF- $\beta$ -induced EMT and invasion of NSCLC. To test this deduction, we first established A549 and SPC-A1 cell lines with stable overexpression of SOX2. As expected, a high level of SOX2 protein was consistently observed in cells overexpressing SOX2 (Figure 5a). Then, upon TGF- $\beta$ 1 stimulation,

**Figure 3.** Expression of *TIF1 $\gamma$*  mRNA is reduced and inversely correlated with SOX2 protein expression in human NSCLC tissues. **(a)** Quantitative reverse transcription–PCR analysis of relative *TIF1 $\gamma$*  mRNA expression in 70 NSCLC tissues (T) and paired noncancerous lung tissues (N). Y axis represents the log<sub>10</sub> transformed fold change of T/N mRNA expression ratio of *TIF1 $\gamma$* . The number of each specimen is indicated below x axis. **(b)** Western blot analysis of SOX2 protein levels in 43 randomly selected NSCLC tissues and paired noncancerous lung tissues.  $\beta$ -Actin was used as an internal control. The ratio of band density (SOX2/ $\beta$ -actin) represents the relative expression of SOX2. **(c)** Relative expression of SOX2 protein and *TIF1 $\gamma$*  mRNA in 43 paired NSCLC tissues. Y axis represents the log<sub>10</sub> transformed fold change of T/N expression ratios of SOX2 protein and *TIF1 $\gamma$*  mRNA. The number of each specimen is indicated below x axis. **(d)** Correlation between SOX2 protein level and *TIF1 $\gamma$*  mRNA expression in 43 paired NSCLC tissues. X and y axes represent the log<sub>10</sub> transformed fold change of T/N expression ratios of SOX2 protein and *TIF1 $\gamma$*  mRNA, respectively. **(e)** Box plots showing relative SOX2 and *TIF1 $\gamma$*  mRNA expression levels of NSCLC tumors and adjacent normal lung tissues in a public data set (GSE19188). **(f)** Linear regression analysis on GSE19188 data set showing a negative correlation between SOX2 and *TIF1 $\gamma$*  mRNA levels in NSCLC tissues. \*\*\* $P < 0.001$ .

A549 and SPC-A1 cells overexpressing SOX2 displayed remarkably decreased expression of E-cadherin or increased expression of N-cadherin and Snail compared with A549 and SPC-A1 cells

transfected with empty vector (Figure 5b). On TGF- $\beta$ 1 stimulation at 1 h, SOX2-overexpressed A549 and SPC-A1 cells showed higher expression of *Snail* mRNA compared with control cells





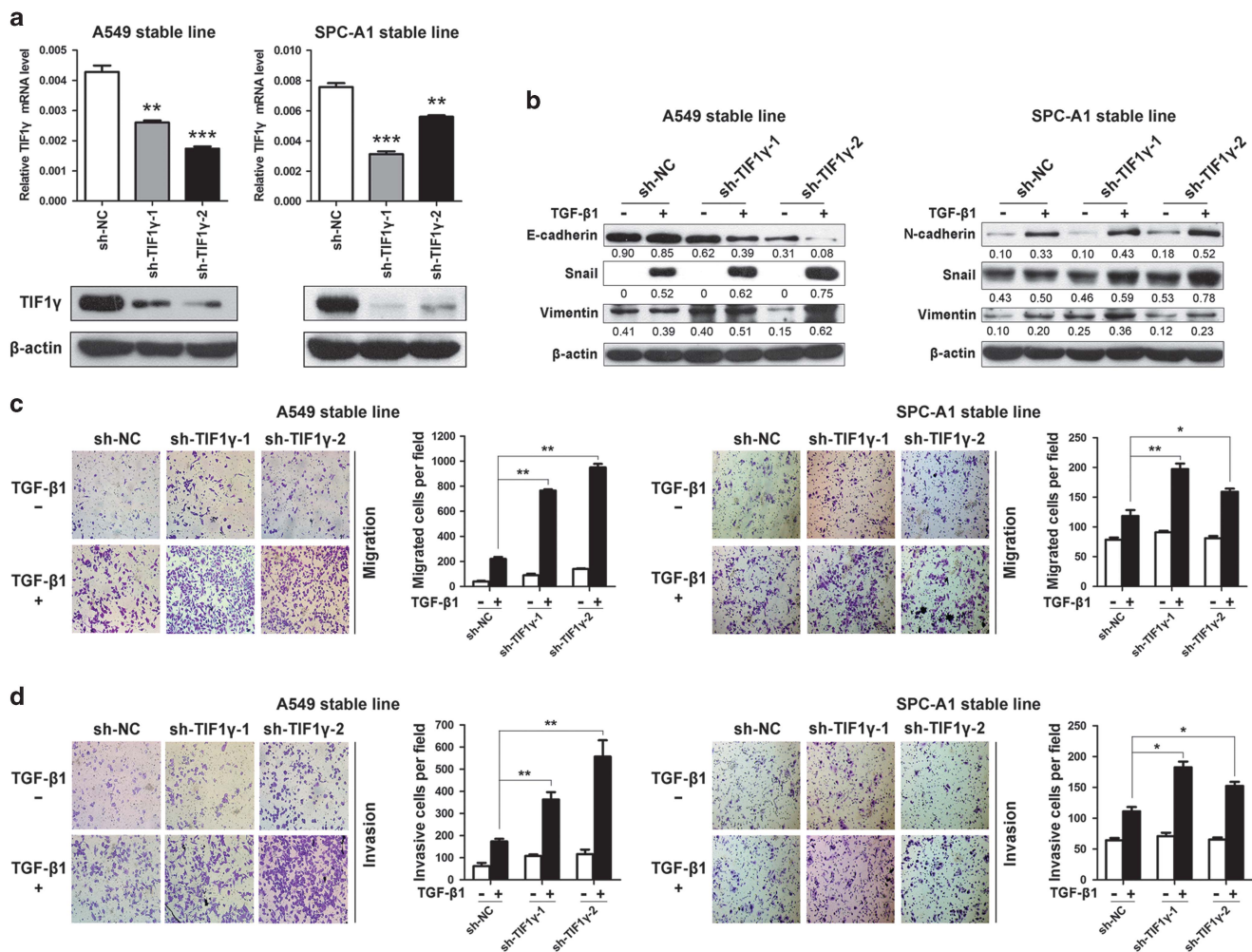


**Figure 4.** Silencing TIF1 $\gamma$  enhances TGF- $\beta$ -induced EMT and invasion of NSCLC cells. **(a)** TIF1 $\gamma$  mRNA and protein levels in stable A549 and SPC-A1 cell lines transfected with two TIF1 $\gamma$  shRNAs (sh-TIF1 $\gamma$ -1 and sh-TIF1 $\gamma$ -2) or negative control (sh-NC). Scrambled sequence was used as sh-NC. **(b)** After being serum starved for 24 h, TIF1 $\gamma$ -silenced A549 and SPC-A1 cells were treated with or without TGF- $\beta$ 1 (5 ng/ml) for 12 h and TGF- $\beta$ 1 (10 ng/ml) for 12 h, respectively. The expression levels of E-cadherin, N-cadherin, Snail and Vimentin were analyzed by western blot. Densitometry values for each protein were normalized to  $\beta$ -actin and shown below the corresponding bands. **(c)** TIF1 $\gamma$ -silenced A549 and SPC-A1 cells were treated with TGF- $\beta$ 1 (5 ng/ml) for 24 h and TGF- $\beta$ 1 (10 ng/ml) for 24 h, respectively, and allowed to migrate through an 8- $\mu$ m pore in Transwells. Migrated cells were stained and counted in at least three microscopic fields (magnification  $\times 100$ ). **(d)** Cells were treated as above and allowed to invade through Matrigel-coated membrane in Transwells. Invasive cells were stained and counted under a light microscope. \* $P < 0.05$ ; \*\* $P < 0.01$ ; \*\*\* $P < 0.001$ .

(Supplementary Figure 6B). Comparably, Transwell assays showed that overexpression of SOX2 enhanced TGF- $\beta$ -induced migratory and invasive abilities of A549 and SPC-A1 cells (Figures 5c and d). The results demonstrated that overexpression of SOX2 can enhance TGF- $\beta$ -induced EMT and migration and invasion of NSCLC cells.

#### SOX2 knockdown inhibits TGF- $\beta$ -induced EMT and invasion of NSCLC cells

As shown in Supplementary Figure 8A, on TGF- $\beta$ 1 stimulation, SOX2-silenced H226 cells (Supplementary Figure 3C) showed a reduction in the expression of N-cadherin, Snail and Vimentin compared with H226 cells transfected with scrambled small interfering RNA (siRNA; NC). Moreover, Transwell assays showed that knockdown of SOX2 impaired TGF- $\beta$ -induced migratory and invasive abilities of H226 cells (Supplementary Figures 8B and C). The results indicated that silencing SOX2 can inhibit TGF- $\beta$ -induced EMT and invasion of NSCLC cells.

#### TIF1 $\gamma$ knockdown and SOX2 overexpression enhances SMAD4-dependent PAI-1 promoter activity

In mammary epithelial cells, TGF- $\beta$ -mediated PAI-1 transcriptional activation is enhanced upon TIF1 $\gamma$  depletion and inhibited upon SMAD4 depletion.<sup>25</sup> Our results showed that PAI-1 promoter activities were significantly increased in stable NSCLC cell lines underexpressing TIF1 $\gamma$  or overexpressing SOX2 after TGF- $\beta$ 1 stimulation (Figures 6a and b). Of more interest, NSCLC cell lines underexpressing TIF1 $\gamma$  or overexpressing SOX2 had sustained expression of SMAD3 and SMAD4 compared with control cells (Figures 6c and d). In support of this, we performed an immunofluorescence analysis. As visualized in Figures 6e and f, TIF1 $\gamma$  knockdown did not influence SMAD3 and SMAD4 expression. Our results are similar to the observation from Vincent *et al.*, who reported that loss of TIF1 $\gamma$  did not significantly affect SMAD4 expression in human pancreatic tumor.<sup>22</sup> Taken together, our findings suggested that loss of TIF1 $\gamma$  led to SMAD4 enrichment onto PAI-1 promoter through competition mechanism and

thereby enhanced SMAD4-dependent transcriptional activation in NSCLC cells.

## DISCUSSION

Our previous study has implicated TIF1 $\gamma$ , a novel regulator of TGF- $\beta$ /Smad signaling,<sup>19,20</sup> in NSCLC.<sup>23</sup> However, the mechanistic role of TIF1 $\gamma$  in NSCLC remains to be defined. In this study, we reveal that TIF1 $\gamma$  repression by SOX2 promotes TGF- $\beta$ -induced EMT in

NSCLC, and establish a mechanistic interaction of TIF1 $\gamma$  and SOX2 for controlling TGF- $\beta$ -induced EMT (Figure 7).

TIF1 $\gamma$  has been proved to be a regulator of TGF- $\beta$ /Smad signaling, which acts as an 'antagonist' by ubiquitinating SMAD4 or a 'complementary agonist' by competing with SMAD4.<sup>19,20</sup> Rimokh and colleagues found that TGF- $\beta$  potently induced the EMT in TIF1 $\gamma$ -silenced mammary epithelial cells, whereas inactivation of SMAD4 impaired this process<sup>25</sup> and TIF1 $\gamma$  sumoylation repressed SMAD4-mediated TGF- $\beta$  response.<sup>24</sup> These findings supported the notion that SMAD4 is required for TGF- $\beta$ -induced EMT.<sup>40</sup> Increased production of TGF- $\beta$  has been found in NSCLC cells and tissues,<sup>38,39</sup> which promotes invasion and metastasis through the induction of EMT.<sup>41,42</sup> In this study, we found that TIF1 $\gamma$ -silenced NSCLC cells showed a sustained level of SMAD4 expression and a strong EMT phenotype upon TGF- $\beta$  stimulation, suggesting that TIF1 $\gamma$  inhibited TGF- $\beta$ -induced EMT through competing with SMAD4 in NSCLC cells. In support of this, Vincent *et al.* observed that loss of TIF1 $\gamma$  did not significantly impair SMAD4 expression level in human pancreatic tumor<sup>22</sup> and Fattet *et al.* reported that ectopic expression of TIF1 $\gamma$  inhibited

Cell line	Incidence	Mean (range) <sup>a</sup>
A549-sh-NC	8/9	19.9 (0–46)
A549-sh-TIF1 $\gamma$ -1	9/9	36.9 (7–57) <sup>b</sup>

The lung metastases were assessed. <sup>a</sup>The number of metastatic nodules on the surface of each lung. <sup>b</sup> $P < 0.05$  vs sh-NC groups.

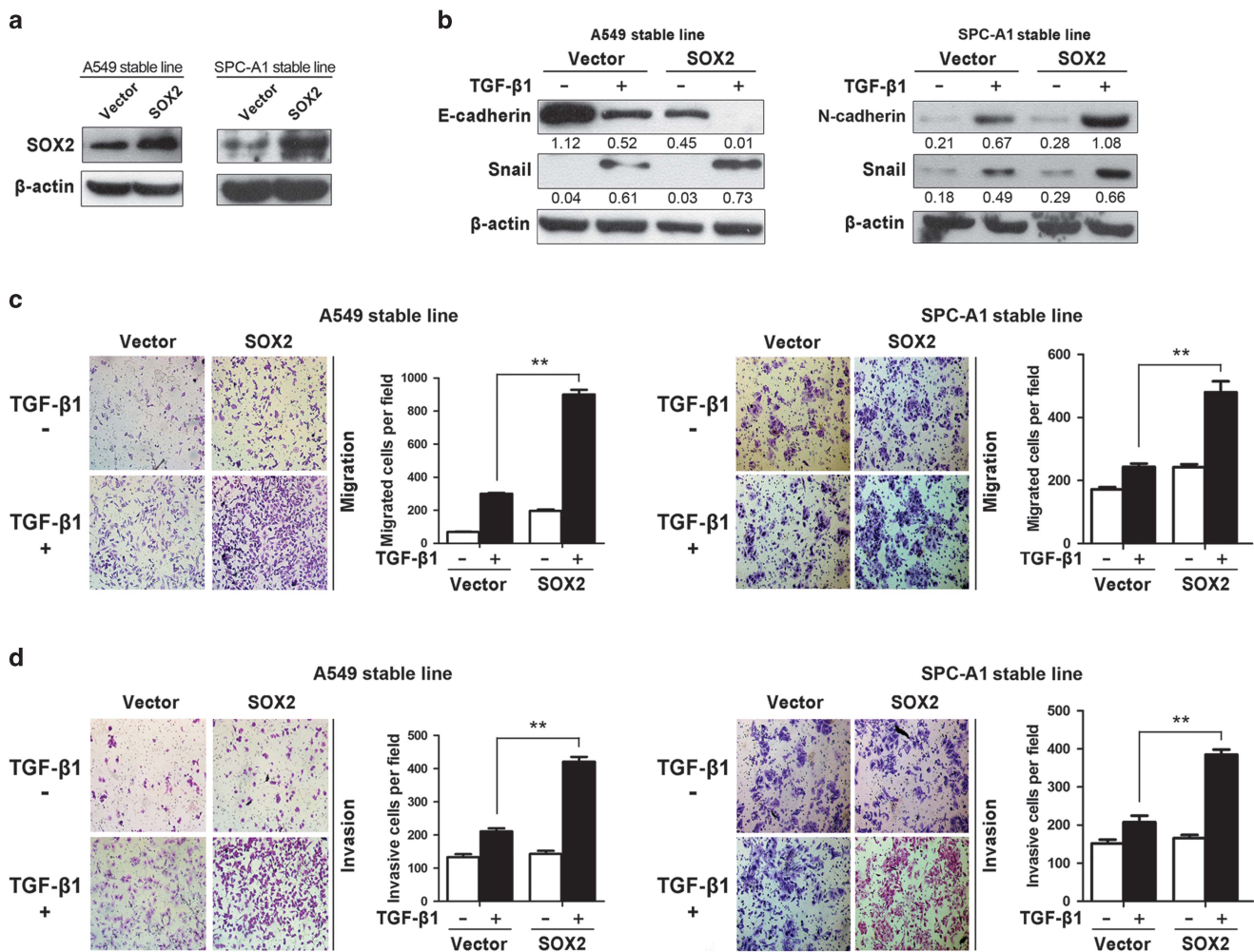


**Figure 5.** Overexpression of SOX2 enhances TGF- $\beta$ -induced EMT and invasion of NSCLC cells. **(a)** SOX2 protein levels in stable A549 and SPC-A1 cell lines overexpressing SOX2. **(b)** After being serum starved for 24 h, A549 and SPC-A1 cells overexpressing SOX2 were treated with or without TGF- $\beta$ 1 (5 ng/ml) for 12 h and TGF- $\beta$ 1 (10 ng/ml) for 12 h, respectively. Western blot was performed to examine the expression levels of E-cadherin, N-cadherin and Snail. Densitometry values for each protein were normalized to  $\beta$ -actin and shown below the corresponding bands. **(c)** A549 and SPC-A1 cells overexpressing SOX2 were treated with TGF- $\beta$ 1 (5 ng/ml) for 24 h and TGF- $\beta$ 1 (10 ng/ml) for 24 h, respectively, and allowed to migrate through an 8- $\mu$ M pore in Transwells. Migrated cells were stained and counted in at least three microscopic fields (magnification  $\times 100$ ). **(d)** Cells were treated as above and allowed to invade through Matrigel-coated membrane in Transwells. Invasive cells were stained and counted under a light microscope. \*\* $P < 0.01$ .

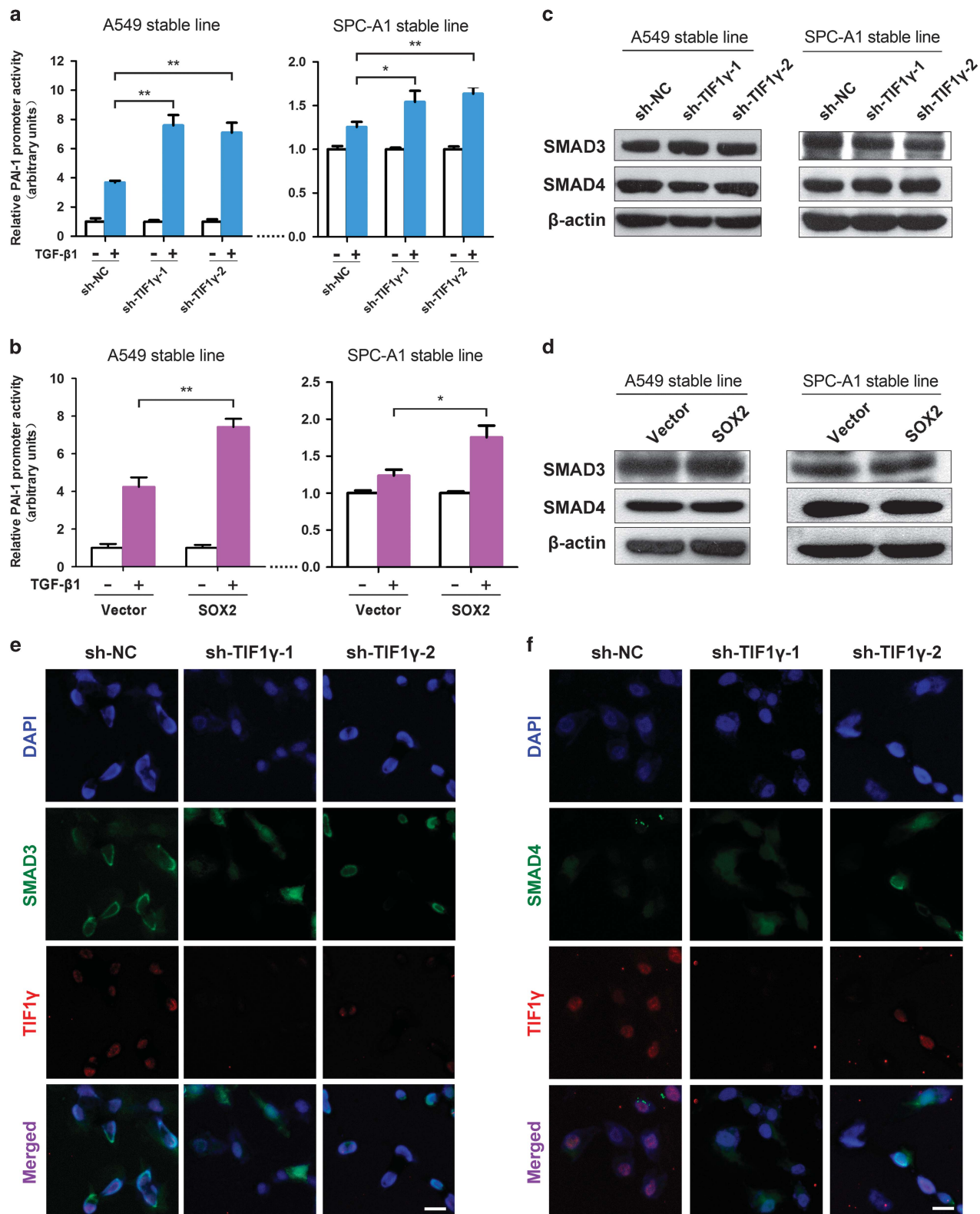


**Figure 6.** Knockdown of TIF1 $\gamma$  or SOX2 overexpression enhances SMAD4-dependent transcriptional activation and causes sustained expression of SMAD4 protein. (**a** and **b**) Relative PAI-1 promoter activities of stable A549 and SPC-A1 cell lines underexpressing TIF1 $\gamma$  in **a** or overexpressing SOX2 in **b**, respectively. Cells transfected with PAI-1 promoter luciferase constructs were incubated for 24 h in the absence or presence of 5 ng/ml TGF- $\beta$ 1, and then subjected to luciferase assay as described in Materials and Methods. (**c** and **d**) Western blot analysis of SMAD3 and SMAD4 protein levels in stable A549 and SPC-A1 cell lines underexpressing TIF1 $\gamma$  in **c** or overexpressing SOX2 in **d**.  $\beta$ -Actin was used as a loading control. (**e** and **f**) A549 sh-NC or sh-TIF1 $\gamma$  cells were stained with anti-SMAD3, anti-SMAD4 and anti-TIF1 $\gamma$  antibodies and then by a FITC-conjugated anti-rabbit IgG (green, for SMAD3 and SMAD4) or a Cy3-conjugated anti-mouse IgG (red, for TIF1 $\gamma$ ), and the nuclei were visualized with 4'-6-diamidino-2-phenylindole (DAPI; blue). Scale bar: 20  $\mu$ m. \* $P$  < 0.05; \*\* $P$  < 0.01.



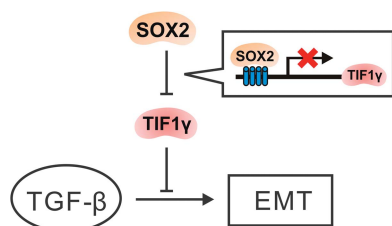


**Figure 7.** A work model of the mechanistic interaction of TIF1 $\gamma$  and SOX2 for controlling TGF- $\beta$ -induced EMT: TIF1 $\gamma$  repression by SOX2 promotes TGF- $\beta$ -induced EMT.

TGF- $\beta$ -induced EMT in mammary epithelial cells.<sup>24</sup> Here we provided the first evidence that silencing TIF1 $\gamma$  in NSCLC cells improved TGF- $\beta$ -induced EMT. Furthermore, our results obtained in an *in vivo* model of metastasis showed that knockdown of TIF1 $\gamma$  promoted NSCLC cell metastasis.

In spite of distinct models whereby TIF1 $\gamma$  could function as either an 'antagonist'<sup>19,43</sup> or an 'agonist' of TGF- $\beta$  signaling,<sup>20</sup> it is a definite fact that TIF1 $\gamma$  expression was decreased in human chronic myelomonocytic leukemia and pancreatic cancer.<sup>21,22</sup> Our previous and current studies showed that expression of TIF1 $\gamma$  was also frequently downregulated in NSCLC<sup>23</sup> (Figure 3a), suggesting that TIF1 $\gamma$  may serve as a tumor suppressor in NSCLC. In chronic myelomonocytic leukemia, TIF1 $\gamma$  expression can be epigenetically silenced due to hypermethylation of CpG sequences in the *TIF1 $\gamma$*  promoter.<sup>21</sup> However, we did not identify any epigenetic changes associated with reduced *TIF1 $\gamma$*  expression in NSCLC,<sup>23</sup> suggesting that there would be alternative mechanisms underlying the reduction of TIF1 $\gamma$  expression in NSCLC. To figure out whether there are transcription-mediated events affecting TIF1 $\gamma$  expression, we focus on the transcription factor SOX2, with a highly conserved SRY-related HMG-box, which was *in silico* predicted as a DNA-binding protein of *TIF1 $\gamma$*  promoter (Figure 1c). Cell-based and biochemical assays confirmed that SOX2 can be recruited to the *TIF1 $\gamma$*  promoter and negatively regulate *TIF1 $\gamma$*  promoter activity. Moreover, SOX2 overexpression inhibited *TIF1 $\gamma$*  expression in NSCLC cells; SOX2 knockdown enhanced *TIF1 $\gamma$*  promoter activity and augmented *TIF1 $\gamma$*  expression. Thus, our study provided the first evidence for transcriptional repression of *TIF1 $\gamma$*  expression by SOX2. Of more importance, SOX2 overexpression enhanced NSCLC cell EMT induced by TGF- $\beta$  and promoted invasion of NSCLC; knockdown of SOX2 impaired TGF- $\beta$ -induced EMT and NSCLC cell invasion. Another important result revealed that SOX2 protein levels were inversely correlated with *TIF1 $\gamma$*  mRNA levels in NSCLC tissues. In fact, this is not surprising because upregulation of SOX2 has been found common in NSCLC.<sup>32,33</sup> However, for the first time, we established a link between TIF1 $\gamma$  and SOX2 in NSCLCs.

Although our findings shed light on SOX2-mediated transcription inhibition of *TIF1 $\gamma$* , we cannot exclude the possibility that other members of SOX protein family were involved in the transcriptional repression of *TIF1 $\gamma$* . For example, SOX9 expression level was also elevated in NSCLC.<sup>44,45</sup> In this study, there are three reasons why we focused on SOX2: first, SOX2 is crucial for branching morphogenesis and epithelial cell differentiation in lung development.<sup>26</sup> Second, SOX2 is frequently upregulated in NSCLC.<sup>32,33</sup> Third, SOX2 is involved in EMT in several human epithelial-derived cancers such as breast, prostate and colorectal cancer.<sup>35,36</sup> Consequently, our results indicated that SOX2 can promote TGF- $\beta$ -induced EMT by repressing TIF1 $\gamma$  in NSCLC. More recently, Justilien *et al.* found that SOX2 cooperated with PKC $\delta$  to drive NSCLC tumorigenesis through activating Hedgehog signaling.<sup>34</sup> Li *et al.* showed that SOX2 promoted breast and prostate cancer metastasis by stimulating EMT via regulation of WNT/ $\beta$ -catenin signaling.<sup>35</sup> These findings demonstrate that SOX2

is crucial for metastatic phenotype of various cancers. In fact, SOX2 can also enhance cell growth of NSCLC via repression of BMP4.<sup>46</sup>

In summary, our findings demonstrate that SOX2 mediates transcriptional repression of *TIF1 $\gamma$*  and impaired its functions, and therefore is important for TGF- $\beta$ -induced EMT and cell invasion in NSCLC. Our findings reveal an EMT regulation by SOX2-TIF1 $\gamma$  axis in NSCLC.

## MATERIALS AND METHODS

### Cell culture

Human NSCLC cells A549, SPC-A1 (lung adenocarcinoma cell lines) and H226 (lung squamous carcinoma cell line) from Cell Bank of Chinese Academy of Sciences were cultured in RPMI 1640 medium (HyClone, South Logan, UT, USA) with 50 U/ml each of penicillin and streptomycin and 10% heat-inactivated fetal bovine serum (Invitrogen, Carlsbad, CA, USA) at 37 °C in a humidified atmosphere containing 5% CO<sub>2</sub>.

### NSCLC tissue samples

Seventy paired NSCLC tissues and adjacent noncancerous lung tissues were obtained after informed consent from patients in the First Affiliated Hospital of Soochow University between 2007 and 2013. Pathological diagnostics for patients with NSCLC were evaluated according to the Revised International System for Staging Lung Cancer. The demographic and clinical characteristics of NSCLC patients were summarized in Supplementary Table 1. NSCLC patients had not received either chemotherapy or radiotherapy before tissue sampling. The tissues were frozen rapidly in liquid nitrogen and stored at -80 °C in an ultra-deep freezer. This study was approved by the Academic Advisory Board of Soochow University.

### RNA extraction, cDNA synthesis and quantitative real-time PCR

RNA isolation, cDNA synthesis and quantitative reverse transcription-PCR analysis were performed as previously described by us.<sup>11</sup> Primers used for quantitative reverse transcription-PCR were described below: 5'-AGCAACGGCGACATCCA-3' (forward) and 5'-TGCATTCTGGCGGCATA-3' (reverse) for *TIF1 $\gamma$* ; 5'-GCCCCAGCAGACTTCACAT-3' (forward) and 5'-AGG GGCAGTGTGCGTTAAT-3' (reverse) for *SOX2*; and 5'-CACAGAGCCTC GCCTTGGCC-3' (forward) and 5'-ACCATGCCACCATCACG-3' (reverse) for  $\beta$ -actin. *C<sub>t</sub>* values of *TIF1 $\gamma$*  and *SOX2* mRNA were equilibrated to  $\beta$ -actin, which was used as an internal control. Relative expression was calculated using the  $\Delta\Delta C_t$  method.

### Western blot assay

Cells and tissues were lysed and subjected to western blot analysis as previously described by us.<sup>11</sup> Antibodies used for western blotting were as follows: mouse anti-TIF1 $\gamma$  and goat anti-SOX2 (Santa Cruz Biotechnology, Santa Cruz, CA, USA), mouse anti-E-cadherin, anti-N-cadherin and anti-Vimentin (BD Biosciences, San Jose, CA, USA), mouse anti-Snail, rabbit anti-SMAD3 and rabbit anti-SMAD4 (Cell Signaling Technology, Danvers, MA, USA), mouse anti- $\beta$ -actin and anti-mouse, -goat or -rabbit secondary antibodies (Santa Cruz Biotechnology).

### Construction of luciferase reporter plasmid, transient transfection and luciferase assay

The pGL3-basic dual luciferase vector (Promega, Madison, WI, USA) was used to produce a series of constructs containing various truncated regions of *TIF1 $\gamma$*  promoter and PAI-1 promoter. Briefly, various lengths of *TIF1 $\gamma$*  promoter were amplified using the primers (Supplementary Table 2) and PAI-1 promoter was amplified as described previously by us,<sup>14</sup> and then subcloned into pGL3-basic vectors with endonucleases *Xho*I and *Kpn*I to create several different constructs. The sequence of the constructs was confirmed by direct sequencing before transfection. Subsequently, the constructs were transiently transfected into A549, SPC-A1 or H226 cells using Lipofectamine 2000 (Invitrogen) and *Renilla* pRL-TK plasmid (Promega) was co-transfected as a normalizing control. Twenty-four hours later, cells were harvested, and luciferase activities were measured by the Dual-Luciferase Reporter Assay Kit (Promega) on a TD20/20 Luminometer (Turner Designs, Sunnyvale, CA, USA). Results were expressed as relative



firefly luciferase activities, which were obtained following normalization to *Renilla* luciferase activities.

### Electrophoretic mobility shift assay

Nuclear proteins were extracted from A549 cells with Nuclear Protein Extraction kit (Sangon Biotech, Shanghai, China). EMSA analysis was performed using LightShift Chemiluminescent EMSA kit (Pierce, Rockford, IL, USA) according to the manufacturer's protocol. The 5'-biotin-labeled and double-stranded oligonucleotides corresponding to the TIF1 $\gamma$  promoter, which contained putative SRY-related protein-binding sites (under-scored), 5'-AGTTCAAAAACAAAAGCAAAAAAACAACAAA-3' and 5'-AA AAACAAAACCAACAAACAATAAGCCCCGCT-3', were synthesized (Invitrogen) and incubated with nuclear extracts in the reaction solution. Unlabeled wild-type and mutant (5'-AGTTCAAAAACCTGAAGCAAAAAAACAACGAAA-3' and 5'-AAAAACAAAACCAACCTGCAATAAGCCCCGCT-3') double-stranded competitor oligonucleotides were added to the respective reactions. The EMSA effect was assessed by the addition of anti-SOX2 and IgG antibodies (Abcam Inc., Cambridge, MA, USA).

### ChIP assay

EZ-ChIP Chromatin Immunoprecipitation kit (Millipore, Bedford, MA, USA) was employed for ChIP assay, which was described by us<sup>47</sup> with some modification. Briefly, A549 cells were fixed with 1% formaldehyde for 10 min at 25 °C and then washed with ice-cold phosphate-buffered saline buffer containing protease inhibitors. The cells nuclei were collected and resuspended in SDS lysis buffer with protease inhibitor, and sonicated to generate crosslinked DNA fragments with 200–1000 bp length. The soluble supernatant was obtained after brief centrifugation and incubated with Protein G Agarose. An aliquot of the supernatant was saved as DNA input control, and the remaining was incubated with anti-SOX2 antibody (Abcam). Rabbit IgG was used as a negative control. Immunoprecipitation was carried out overnight at 4 °C, and immune complexes were collected using Protein G Agarose beads. The immune complexes and the input were eluted and protein–DNA complexes were de-crosslinked overnight at 65 °C. ChIP DNA was purified and subjected to PCR, which amplified TIF1 $\gamma$  promoter sequence containing putative SRY-related protein-binding sites (position –595 to –426). Specific ChIP primers used for PCR were 5'-AGTTTCTTCTACTCGGTCTTTTC-3' (forward) and 5'-GTCTCTGCTGTG CGTAGACCA-3' (reverse).

### Generation of stable cell lines overexpressing SOX2 and establishment of TIF1 $\gamma$ -silenced stable cell lines

To generate A549 and SPC-A1 cells in which SOX2 can stably overexpress, we subcloned a ~1-kb coding sequence (GenBank Accession number NP\_003097.1) of SOX2 into a pLVX-IRES-Neo vector using endonucleases *EcoRI* and *BamHI* for expression via Lenti-X lentiviral expression system (Clontech, Mountain View, CA, USA). Then the SOX2 expression construct was co-transfected with packaging plasmids into human embryonic kidney 293 T cells using Lipofectamine 2000 (Invitrogen). The empty vector was served as a negative control. Human embryonic kidney 293 T cells were cultured in Dulbecco's modified Eagle's medium with 10% fetal bovine serum at 37 °C in a humidified 5% CO<sub>2</sub> incubator for 48 h. After the incubation, the packaged lentiviruses were collected and used to infect A549 and SPC-A1 cells. After 2 days, stable cells were selected with 400  $\mu$ g/ml of G418 (Amresco, Solon, OH, USA). The coding sequence region of SOX2 was amplified using the following primers: forward, 5'-CCG GAATTCCTGATTCCAGTTTGCCTCT-3' (*EcoRI*); reverse: 5'-CGCGGATCCGCTGT CATTTCGTGTGGG-3' (*BamHI*).

To establish stable A549, SPC-A1 and H226 cell lines in which TIF1 $\gamma$  is silenced, two DNA fragments (TIF1 $\gamma$  shRNA-1, 5'-CCGGGAGCAGCA GCACTACTATACACTCGAGTGTATAGTAGTGTGCTGCTGTTTTG-3'; and TIF1 $\gamma$  shRNA-2, 5'-CCGGGAGCAGCTTGTAAATGGAAAGTCTCGAGACTTCCATTAA CAAGGCTGCTTTTTG-3') were subcloned a lentiviral vector pGLV2-U6-Puro (GenePharma, Shanghai, China) with endonucleases *AgeI* and *EcoRI*. A scrambled sequence (underscored) of TIF1 $\gamma$  shRNA, which was served as negative control, was as follows: 5'-CCGGACTACGTTGTTATAGGTG CTCGAGCACCTATAACAACGGTAGTTTTTTG-3'. Then, the TIF1 $\gamma$ -silenced construct or negative control was co-transfected with packaging plasmids into human embryonic kidney 293 T cells using Lipofectamine 2000 (Invitrogen). Forty-eight hours later, A549, SPC-A1 and H226 cells were infected with the packaged lentiviruses and cultured for 2 days, and stable cell lines were selected with 1  $\mu$ g/ml of puromycin (Sigma-Aldrich, St Louis, MO, USA).

### RNA interference

Two pre-designed short interfering RNA (siRNA) sequences, which target different coding sequence regions of SOX2, were directly synthesized (GenePharma). The target sequences of siRNA are as follows: siRNA-SOX2-1, 5'-ACCTCCGGGACATGATCAGCA-3'; siRNA-SOX2-2, 5'-CCATGGGTTCGGTG GTCAA-3'. Scrambled siRNA was used as a negative control. Cells were transiently transfected with 100 pmol of siRNA sequences using Lipofectamine 2000 (Invitrogen). After 72 h transfection, the cells were harvested for further experiments.

### Transwell migration and invasion assays

Transwell assays were performed by using Transwell plates (BD Biosciences). According to the instructions from the manufacturer, 5  $\times$  10<sup>4</sup> cells with 1% fetal bovine serum medium were added in each upper chamber and 10% fetal bovine serum medium was placed as chemoattractant in each lower chamber. Six hours later, TGF- $\beta$ 1 (5 or 10 ng/ml) was added to the lower chambers. After 24 h or 48 h incubation at 37 °C, the inserts were taken out and cells on the upper surface were removed by cotton swabs. Cells that invaded to the lower side were stained with 1% crystal violet. The cells from three microscopic fields were photographed and counted. The results were determined from three repeated experiments.

### Immunofluorescent analysis

Cells were cultured on coverslips in a 24-well plate, fixed with 4% paraformaldehyde for 15 min and permeabilized with 0.5% Triton X-100 solution for 5 min at room temperature. Then the coverslips were blocked with 5% bovine serum albumin in Tris buffered saline with Triton X-100 for 1 h and incubated with rabbit anti-SMAD3, rabbit anti-SMAD4 (Cell Signaling Technology) and mouse anti-TIF1 $\gamma$  (Santa Cruz Biotechnology) primary antibodies overnight at 4 °C. After being washed with phosphate-buffered saline three times, the coverslips were incubated with FITC-conjugated anti-rabbit IgG and Cy3-conjugated anti-mouse IgG secondary antibodies (Beyotime, Shanghai, China) for 1 h at room temperature. Finally, cells were labeled with 4'-6-diamidino-2-phenylindole (Beyotime) and examined using a confocal laser scanning microscopy (LSM700, Zeiss, Oberkochen, Germany).

### In vivo model of metastasis

Pathogen-free female nude mice were purchased from the Experimental Animal Center of Soochow University. Control A549 cells and the corresponding stable cells with knockdown of TIF1 $\gamma$  (1  $\times$  10<sup>6</sup> cells per mouse) were injected into the tail vein of mice (9 mice per group). After 60 days, the mice were killed and their lung tissues were obtained. Following fixation in Bouin's fluid, the number of metastatic nodules on the surface of each lung was counted using a dissecting microscope.

### Statistical analysis

Differences in TIF1 $\gamma$  and SOX2 expression between NSCLC tissues (T) and paired noncancerous lung tissues (N) were analyzed using unpaired t-test (two-tailed). Correlation between expression level ratios (T/N) of SOX2 protein and TIF1 $\gamma$  mRNA was assessed using the Pearson correlation test. Data were presented as mean  $\pm$  standard deviation (s.d.). Statistical differences were considered to be significant at  $P < 0.05$ . All statistical analyses were performed using GraphPad Prism 5.02 (GraphPad, San Diego, CA, USA) and SPSS 16.0 software (SPSS, Chicago, IL, USA).

### CONFLICT OF INTEREST

The authors declare no conflict of interest.

### ACKNOWLEDGEMENTS

We are grateful for participation and cooperation from the patients with NSCLC. This work was supported in part by the grants from National Natural Science Foundation of China (81372277, 81171894 and 81201575), Jiangsu Province's Key Provincial Talents Program (RC2011106), '333' Project of Jiangsu Province Government, Graduate Innovation Project of Jiangsu Province (CXZZ13\_0830), Soochow Scholar Project of Soochow University, Suzhou Key Laboratory for Molecular Cancer Genetics (SZS201209) and A Project Funded by the Priority Academic Program Development of Jiangsu Higher Education Institutions (PAPD).

## REFERENCES

- Lei Z, Liu RY, Zhao J, Liu Z, Jiang X, You W *et al*. TGFBR1 haplotypes and risk of non-small-cell lung cancer. *Cancer Res* 2009; **69**: 7046–7052.
- Feng J, Zhang X, Zhu H, Wang X, Ni S, Huang J. High expression of FoxP1 is associated with improved survival in patients with non-small cell lung cancer. *Am J Clin Pathol* 2012; **138**: 230–235.
- Gupta GP, Massague J. Cancer metastasis: building a framework. *Cell* 2006; **127**: 679–695.
- Meulmeester E, Ten Dijke P. The dynamic roles of TGF-beta in cancer. *J Pathol* 2011; **223**: 205–218.
- Massague J, Blain SW, Lo RS. TGFbeta signaling in growth control, cancer, and heritable disorders. *Cell* 2000; **103**: 295–309.
- Jeon HS, Jen J. TGF-beta signaling and the role of inhibitory Smads in non-small cell lung cancer. *J Thorac Oncol* 2010; **5**: 417–419.
- Massague J, Seoane J, Wotton D. Smad transcription factors. *Genes Dev* 2005; **19**: 2783–2810.
- Park C, Kim WS, Choi Y, Kim H, Park K. Effects of transforming growth factor beta (TGF-beta) receptor on lung carcinogenesis. *Lung Cancer* 2002; **38**: 143–147.
- Zhao J, Liu Z, Li W, Liu X, Chen XF, Zhang HT. Infrequently methylated event at sites -362 to -142 in the promoter of TGF beta R1 gene in non-small cell lung cancer. *J Cancer Res Clin Oncol* 2008; **134**: 919–925.
- Zhang HT, Chen XF, Wang MH, Wang JC, Qi QY, Zhang RM *et al*. Defective expression of transforming growth factor beta receptor type II is associated with CpG methylated promoter in primary non-small cell lung cancer. *Clin Cancer Res* 2004; **10**: 2359–2367.
- Lei Z, Xu G, Wang L, Yang H, Liu X, Zhao J *et al*. MiR-142-3p represses TGF-beta-induced growth inhibition through repression of TGFbetaR1 in non-small cell lung cancer. *FASEB J* 2014; **28**: 2696–2704.
- Massague J. TGFbeta in Cancer. *Cell* 2008; **134**: 215–230.
- Gregory PA, Bracken CP, Smith E, Bert AG, Wright JA, Roslan S *et al*. An autocrine TGF-beta/ZEB/miR-200 signaling network regulates establishment and maintenance of epithelial-mesenchymal transition. *Mol Biol Cell* 2011; **22**: 1686–1698.
- Liu RY, Zeng Y, Lei Z, Wang L, Yang H, Liu Z *et al*. JAK/STAT3 signaling is required for TGF-beta-induced epithelial-mesenchymal transition in lung cancer cells. *Int J Oncol* 2014; **44**: 1643–1651.
- Kang Y, Massague J. Epithelial-mesenchymal transitions: twist in development and metastasis. *Cell* 2004; **118**: 277–279.
- Thiery JP. Epithelial-mesenchymal transitions in tumour progression. *Nat Rev Cancer* 2002; **2**: 442–454.
- Principe DR, Doll JA, Bauer J, Jung B, Munshi HG, Bartholin L *et al*. TGF-beta: duality of function between tumor prevention and carcinogenesis. *J Natl Cancer Inst* 2014; **106**: djt369.
- Venturini L, You J, Stadler M, Galien R, Lallemand V, Koken MH *et al*. TIF1 gamma, a novel member of the transcriptional intermediary factor 1 family. *Oncogene* 1999; **18**: 1209–1217.
- Dupont S, Zacchigna L, Cordenonsi M, Soligo S, Adorno M, Rugge M *et al*. Germ-layer specification and control of cell growth by Ectoderm, a Smad4 ubiquitin ligase. *Cell* 2005; **121**: 87–99.
- He W, Dorn DC, Erdjument-Bromage H, Tempst P, Moore MA, Massague J. Hematopoiesis controlled by distinct TIF1gamma and Smad4 branches of the TGFbeta pathway. *Cell* 2006; **125**: 929–941.
- Aucagne R, Droin N, Paggetti J, Lagrange B, Largeot A, Hammann A *et al*. Transcription intermediary factor 1gamma is a tumor suppressor in mouse and human chronic myelomonocytic leukemia. *J Clin Invest* 2011; **121**: 2361–2370.
- Vincent DF, Yan KP, Treilleux I, Gay F, Arfi V, Kaniewski B *et al*. Inactivation of TIF1gamma cooperates with Kras to induce cystic tumors of the pancreas. *PLoS Genet* 2009; **5**: e1000575.
- Wang L, Lei Z, Liu X, Liu R, Zhang H. [Association of mutation and methylation in the promoter region of TIF1gamma with non-small cell lung cancer]. *Zhongguo Fei Ai Za Zhi* 2013; **16**: 227–232.
- Fattet L, Ay AS, Bonneau B, Jallades L, Mikaelian I, Treilleux I *et al*. TIF1gamma requires sumoylation to exert its repressive activity on TGFbeta signaling. *J Cell Sci* 2013; **126**: 3713–3723.
- Hesling C, Fattet L, Teyre G, Jury D, Gonzalo P, Lopez J *et al*. Antagonistic regulation of EMT by TIF1gamma and Smad4 in mammary epithelial cells. *EMBO Rep* 2011; **12**: 665–672.
- Gontan C, de Munck A, Vermeij M, Grosveld F, Tibboel D, Rottier R. Sox2 is important for two crucial processes in lung development: branching morphogenesis and epithelial cell differentiation. *Dev Biol* 2008; **317**: 296–309.
- Que J, Luo X, Schwartz RJ, Hogan BL. Multiple roles for Sox2 in the developing and adult mouse trachea. *Development* 2009; **136**: 1899–1907.
- Lefebvre V, Dumitriu B, Penzo-Mendez A, Han Y, Pallavi B. Control of cell fate and differentiation by Sry-related high-mobility-group box (Sox) transcription factors. *Int J Biochem Cell Biol* 2007; **39**: 2195–2214.
- Avilion AA, Nicolis SK, Pevny LH, Perez L, Vivian N, Lovell-Badge R. Multipotent cell lineages in early mouse development depend on SOX2 function. *Genes Dev* 2003; **17**: 126–140.
- Liu K, Lin B, Zhao M, Yang X, Chen M, Gao A *et al*. The multiple roles for Sox2 in stem cell maintenance and tumorigenesis. *Cell Signal* 2013; **25**: 1264–1271.
- Xu N, Papagiannakopoulos T, Pan G, Thomson JA, Kosik KS. MicroRNA-145 regulates OCT4, SOX2, and KLF4 and represses pluripotency in human embryonic stem cells. *Cell* 2009; **137**: 647–658.
- Xu W, Wei Y, Tan Y, Cheng SY, Wu J. [The expression and significance of stem cell transcription factor Sox2 in lung carcinoma]. *Zhongguo Fei Ai Za Zhi* 2013; **16**: 591–595.
- Nakatsugawa M, Takahashi A, Hirohashi Y, Torigoe T, Inoda S, Murase M *et al*. SOX2 is overexpressed in stem-like cells of human lung adenocarcinoma and augments the tumorigenicity. *Lab Invest* 2011; **91**: 1796–1804.
- Justilien V, Walsh MP, Ali SA, Thompson EA, Murray NR, Fields AP. The PRKCI and SOX2 oncogenes are coamplified and cooperate to activate Hedgehog signaling in lung squamous cell carcinoma. *Cancer Cell* 2014; **25**: 139–151.
- Li X, Xu Y, Chen Y, Chen S, Jia X, Sun T *et al*. SOX2 promotes tumor metastasis by stimulating epithelial-to-mesenchymal transition via regulation of WNT/beta-catenin signal network. *Cancer Lett* 2013; **336**: 379–389.
- Han X, Fang X, Lou X, Hua D, Ding W, Foltz G *et al*. Silencing SOX2 induced mesenchymal-epithelial transition and its expression predicts liver and lymph node metastasis of CRC patients. *PLoS One* 2012; **7**: e41335.
- Pirozzi G, Tirino V, Camerlingo R, Franco R, La Rocca A, Liguori E *et al*. Epithelial to mesenchymal transition by TGFbeta-1 induction increases stemness characteristics in primary non small cell lung cancer cell line. *PLoS One* 2011; **6**: e21548.
- Asselin-Paturel C, Echchakir H, Carayol G, Gay F, Opolon P, Grunenwald D *et al*. Quantitative analysis of Th1, Th2 and TGF-beta1 cytokine expression in tumor, TIL and PBL of non-small cell lung cancer patients. *Int J Cancer* 1998; **77**: 7–12.
- Bennett WP, el-Deiry WS, Rush WL, Guinee DG Jr., Freedman AN, Caporaso NE *et al*. p21waf1/cip1 and transforming growth factor beta 1 protein expression correlate with survival in non-small cell lung cancer. *Clin Cancer Res* 1998; **4**: 1499–1506.
- Deckers M, van Dinther M, Buijs J, Que I, Lowik C, van der Pluijm G *et al*. The tumor suppressor Smad4 is required for transforming growth factor beta-induced epithelial to mesenchymal transition and bone metastasis of breast cancer cells. *Cancer Res* 2006; **66**: 2202–2209.
- Akhurst RJ, Balmain A. Genetic events and the role of TGF beta in epithelial tumour progression. *J Pathol* 1999; **187**: 82–90.
- Han G, Lu SL, Li AG, He W, Corless CL, Kulesz-Martin M *et al*. Distinct mechanisms of TGF-beta1-mediated epithelial-to-mesenchymal transition and metastasis during skin carcinogenesis. *J Clin Invest* 2005; **115**: 1714–1723.
- Xue J, Lin X, Chiu WT, Chen YH, Yu G, Liu M *et al*. Sustained activation of SMAD3/SMAD4 by FOXM1 promotes TGF-beta-dependent cancer metastasis. *J Clin Invest* 2014; **124**: 564–579.
- Zhou CH, Ye LP, Ye SX, Li Y, Zhang XY, Xu XY *et al*. Clinical significance of SOX9 in human non-small cell lung cancer progression and overall patient survival. *J Exp Clin Cancer Res* 2012; **31**: 18.
- Szymanowska-Narloch A, Jassem E, Skrzypski M, Muley T, Meister M, Dienemann H *et al*. Molecular profiles of non-small cell lung cancers in cigarette smoking and never-smoking patients. *Adv Med Sci* 2013; **58**: 196–206.
- Fang WT, Fan CC, Li SM, Jang TH, Lin HP, Shih NY *et al*. Downregulation of a putative tumor suppressor BMP4 by SOX2 promotes growth of lung squamous cell carcinoma. *Int J Cancer* 2014; **135**: 809–819.
- Qian Q, Shi X, Lei Z, Zhan L, Liu RY, Zhao J *et al*. Methylated +58CpG site decreases DCN mRNA expression and enhances TGF-beta/Smad signaling in NSCLC cells with high metastatic potential. *Int J Oncol* 2014; **44**: 874–882.

Supplementary Information accompanies this paper on the Oncogene website (<http://www.nature.com/onc>)